Australian Government
Department of Defence
Defence Science and
Technology Organisation

DSTO

Structural Analyses of a Demonstrator Composite Replacement Panel in a F-111C Cold Proof Load Test

Alex B. Harman and
Paul J. Callus

DSTO-TN-0546

Australian Government
Department of Defence
Defence Science and
Technology Organisation

Structural Analyses of a Demonstrator Composite Replacement Panel in a F-111C Cold Proof Load Test

Alex B. Harman and Paul J. Callus

Air Vehicles Division
Platforms Sciences Laboratory

DSTO-TN-0546

ABSTRACT

The Defence Science and Technology Organisation, in collaboration with the Cooperative Research Centre for Advanced Composite Structures, is developing the Composite Replacement Panel Technology (CRPT). The aim of this technology is to replace metallic aircraft structure with that manufactured from advanced composites, thereby reducing support costs and/or increasing capability. The CRPT is being developed through the production of a demonstrator replacement for F-111C Panel 3208, denoted Panel I. It is planned that the design methodology for Panel I (and the analysis described in this report) be validated through the Composite Replacement Panel Strain Survey (CRPSS). In the CRPSS, Panel I will be installed on an F-111C aircraft undergoing a Cold Proof Load Test (CPLT). The CPLT is a static ground test conducted at -40 °C that imparts design limit load to critical airframe structure. This report describes the analysis, based on the F-111 Internal Loads Model Revision 1 (December 2002), and tests that predict positive margins-of-safety and no buckling for Panel I, the fasteners and local sub-structure during CPLT loading. It has been accepted by an Australian Defence Force Authorised Engineering Organisation (AeroStructures®) as satisfactorily addressing the structural requirements for the CRPSS.

Published by

DSTO Platforms Sciences Laboratory
506 Lorimer St
Fishermans Bend, Victoria 3207 Australia

Telephone: (03) 9626 7000
Fax: (03) 9626 7999

AR-013-071
March 2004

APPROVED FOR PUBLIC RELEASE

Structural Analyses of a Demonstrator Composite Replacement Panel in a F-111C Cold Proof Load Test

Executive Summary

DSTO, in collaboration with the Cooperative Research Centre for Advanced Composite Structures (CRC-ACS), is developing the capability to replace metallic aircraft panels with affordable advanced composite panels. This capability is known as the Composite Replacement Panel Technology (CRPT). The replacement panels are expected to be significantly more durable than the existing aluminium panels because composites are resistant to corrosion and fatigue cracking, and the panel will be designed in a configuration to enhance impact resistance. This will reduce substantially the through-life-support cost for such structures. Panels may also incorporate additional functionality such as armour, antenna or low observable coatings to enhance aircraft capability.

Although the research is focused on producing a generic capability suitable for all aircraft, it is being developed through the production and testing of a demonstrator composite replacement panel for the fuselage of the Royal Australian Air Force (RAAF) operated F-111C, specifically F-111 Panel 3208.

It is prohibitively expensive to validate the design of Panel I by conducting a full-scale test with representative loading. Fortunately a low cost alternative is available. F-111 aircraft are subjected to the Cold Proof Load Test (CPLT), a series of static ground tests where the aircraft is cooled to -40 °C and critical parts of the airframe subjected to the design limit load. Moderate loads are transferred into Panel 3208 during the CPLT. Therefore it is intended that Panel I be instrumented and fitted to a F-111C prior to CPLT. The design predictions may then be validated against the observed strains. This test shall be known as the Composite Replacement Panel Strain Survey (CRPSS).

Prior to conducting the CRPSS it is necessary to demonstrate positive margins-of-safety and no buckling in Panel I, the fasteners and local sub-structure, during a CPLT. This report presents the results of an analysis, supported by test, showing that these requirements have been met.

Design data for Panel I was established by test at the coupon and design detail level. The analysis was conducted using the F-111C Aircraft Internal Loads Finite Element Model (ILM) Revision 1 (current in December 2002). Although Revision 2 of the ILM was released in October 2003 the analysis was not repeated because it was judged that the results would not change significantly with the revised ILM.

The relatively coarse mesh ILM was used to provide the boundary conditions for fine mesh sub-models of Panel 3208, Panel I and the local sub-structure. Analyses were performed for metallic and composite panels, with and without thermal effects

This report has been reviewed by an ADF approved Authorised Engineering Organisation (AEO) (AeroStructures®). The AEO has accepted that the scope, depth and methods of testing and analysis described in this report are sufficient to demonstrate that the structural aspects of the CRPSS have been addressed satisfactorily.

Authors

Alex B. Harman
Air Vehicles Division

Alex Harman is a Professional Officer at DSTO. He holds a B.Eng (Hons.) in Aerospace Engineering from RMIT and is currently a graduate member of both the Institution of Engineers and the Royal Aeronautical Society. He joined DSTO in 1999 and has performed dynamic loads analyses for the F/A-18, structural integrity analyses for the F-111, composites and metallic finite element analyses and testing, bonded joint design and composite design. He is currently working with the Composites and Bonded Repair Functional Area in the Air Vehicles Division (AVD).

Paul J. Callus
Air Vehicles Division

Dr Paul Callus gained his PhD, in the area of fracture toughness testing of thermal spray coatings, from Monash University in 1993. He worked with CSIRO for four years using ceramic processing techniques to develop electrode coatings for solid oxide fuel cells. He then spent two years at RMIT investigating failure progression in textile composites. He is currently a Senior Research Scientist in the Composites and Bonded Structures Functional Area of the AVD. His work includes the development of composite replacement panels, the certification of composite structure and developing the AVD capability to support future aircraft.

Contents

Nomenclature

Acronym	Description
ACID	Analysis Coordinate System Identification
ADF	Australian Defence Force
AEO	Authorised Engineering Organisation
BVID	Barely Visible Impact Damage
CAI	Compression After Impact
CPLT	Cold Proof Load Test
CRC-ACS	Cooperative Research Centre for Advanced Composite Structures
CLT	Classical Laminate Theory
CTA	Cold Temperature Ambient
CTD	Cold Temperature Dry
CTE	Coefficient of Thermal Expansion
CRPSS	Composite Replacement Panel Strain Survey
CRPT	Composite Replacement Panel Technology
DLL	Design Limit Load
DSTO	Defence Science and Technology Organisation
ETW	Elevated Temperature Wet
FEA	Finite Element Analyses
FEM	Finite Element Model
FR	Failure Ratio
GCID	Global Coordinate System Identification
GCS	Global Coordinate System
ID	Identification
ILM	F-111C Internal Loads Finite Element Model
ILMr1	Version of the ILM current on 2 December 2002
ILMr2i2	Version of the ILM released on 21 October 2003
LHS	Left Hand Side
Lockheed	Lockheed Martin Tactical Aircraft Systems
MDF	Medium Density Fibreboard
MOS	Margin of Safety
OEM	Original Equipment Manufacturer (formerly General Dynamics now Lockheed Martin Tactical Aircraft Systems)
Panel I	Composite Replacement Panel for Panel 3208
Panel 3208	Right Hand Side Panel – F-111 Part Number 12B-3913
Panel 3108	Left Hand Side Panel – F-111 Part Number 12B-3913
PWD	Planned Withdrawal Date
RAAF	Royal Australian Air Force
RHS	Right Hand Side
RTA	Room Temperature Ambient
RTD	Room Temperature Dry
SAI	Shear After Impact
SOP	Sole Operator Program (refer to reference 1)

1. Introduction

1.1 Overview

Old components in aging military aircraft commonly suffer from several types of degradation including corrosion, cracking and, in adhesively bonded structures, disbonding. Honeycomb panels are often costly airframe components to support. Disbonding and corrosion caused by moisture ingress, following the breakdown of edge seals, are major problems. Panels in older aircraft are particularly prone to these problems since they were bonded using inferior pre-bonding surface treatments and contain corrosion susceptible cores. In addition, the thin-skin construction of honeycomb panels makes them prone to impact damage.

One option for fleet managers when support costs become excessive or replacements are unavailable is to substitute the existing component with one made from a more durable material, possibly in a more robust configuration. A collaborative program between the Defence Science and Technology Organisation (DSTO) and the Cooperative Research Centre for Advanced Composite Structures (CRC-ACS) is developing the capability to replace aging metallic aircraft panels with affordable advanced composite panels [1]. This is the so-called Composite Replacement Panel Technology (CRPT). It is being developed through the production of a demonstrator panel (Panel I) for the fuselage of the Royal Australian Air Force (RAAF) operated F-111C, specifically F-111 Panel 3208.

The CRPT also offers the potential to enhance aircraft capability. Individual panels could contain low observable coatings, embedded sensors (for structural health monitoring or individual aircraft tracking), conformal antennae, armour or piezoelectric patches (for buffet load alleviation). The outer profile of the panels may also be modified, within aerodynamic and sub-structure constraints, to reduce further aircraft signature. Multiple panels may be replaced by a single replacement to eliminate edge gaps. The low density of composite materials and improved panel configuration mean that these capabilities could be added with little, or no, weight penalty.

One step toward airworthiness certification of the CRPT is validation of the capability to predict strain within composite replacement panels and the aircraft sub-structure. The Composite Replacement Panel Strain Survey (CRPSS) shall be conducted to obtain this validation. Panel I shall be installed on a suitable aircraft, then the aircraft subjected to loads at non-ambient temperature while the strain in Panel I and the local sub-structure are measured. These shall be compared with strains predicted by finite element analysis (FEA).

The Cold Proof Load Test (CPLT) represents a low cost (relative to flight test or full-scale test with representative loading) method of achieving the desired conditions. The CPLT is a proof test designed to load critical D6ac steel components of the F-111 airframe to their Design Limit Load (DLL). The critical crack size required to cause catastrophic failure in D6ac steel falls with temperature. The CPLT is therefore conducted at -40 °C (-40 °F) so that, if the D6ac components survive the CPLT then the cracks within them must be sufficiently small that they will not grow to a critical length prior to the next CPLT.

The CRPSS was originally to be conducted in conjunction with another test known as the F-111C Fuselage Strain Survey. In this Survey 60 % CPLT loads were applied to a F-111C aircraft at ambient temperature. It was shown [2], through FEA, that Panel I did not fail or buckle, nor did the fasteners fail, in the ambient temperature 60 % CPLT. The plan to include the CRPSS as part

of the F-111C Fuselage Strain Survey has been superseded by one to conduct the CRPSS during a full CPLT. This report extends the work of [2] and shows predictions, through analysis supported by test, that during a full CPLT (i) Panel I, the fasteners and surrounding sub-structure will not fail, and (ii) Panel I and the surrounding sub-structure will not buckle.

Design data for Panel I was established by test at the coupon and design detail level. The analysis was conducted using the F-111C Aircraft Internal Loads Finite Element Model (ILM) Revision 1 (current in December 2002). Although Revision 2 of the ILM was released in October 2003 the analysis was not repeated because it was judged that the results would not change significantly with the revised ILM.

AeroStructures® has reviewed this report in its capacity as an ADF approved Authorised Engineering Organisation (AEO). The AEO has accepted [3] that the scope, depth and methods of testing and analysis described in this report are sufficient to meet the recommendations of Advisory Circular 20-107A [4] as applied to the CRPSS. AC 20-107A is an acceptable means for composite aircraft structure to demonstrate compliance with FAR 25 [5]. Therefore this report demonstrates that the structural aspects of the CRPSS have been addressed satisfactorily.

1.2 Replacement Panel Design

1.2.1 Replacement Panel Demonstrator Selection

F-111 Panel 3208 (Part Number 12B-3913) was selected as the demonstrator for the first phase of the replacement panel work program. This panel is located on the right hand side (RHS) of the aircraft on the external surface of the nacelle inlet. Its counterpart, Panel 3108, on the left hand side (LHS) of the aircraft is shown in Figure 1.

In this report the demonstrator composite replacement for Panel 3208 will be referred to as Panel I. This will be used to distinguish it from the original metallic honeycomb panel, which is referred to as Panel 3208.

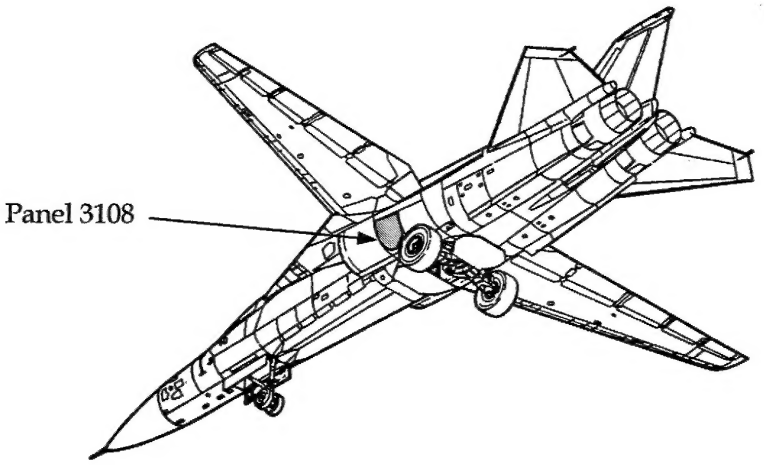

Figure 1 F-111 aircraft showing Panel 3108. Panel 3208 is located in the identical position on the aircraft RHS

Panel 3208 was one of several panels that satisfied the selection requirements for demonstration of the generic CRPT. The criteria for selection of the demonstrator were that it be:

- primary structure rigidly fixed to airframe and sufficiently highly loaded so that structural strength issues had to be addressed,
- moderately large, approximately 1 m x 1 m, to represent a manufacturing challenge but not so large that it was un-representative of the panels likely to require replacement,
- curved, so that even simple external loading will produce complex loading within the panel, thus presenting a design and manufacturing challenge,
- mechanically fastened, representing a joint design challenge and to ease replacement during the evaluation stage,
- available as spares for reference during design and manufacture development.

1.2.2 Replacement Panel Design Requirements

The key design requirements for the CRPT were to:

- establish the critical loads and load cases,
- design a composite panel to match the strength and stiffness of the existing panel with due regard to orthotropism, relatively low bearing strength and low coefficient of thermal expansion (CTE) of composites,
- develop low cost manufacturing processes suitable for small panel numbers,
- devise rapid low cost certification procedures that require minimal testing.

1.2.3 Reverse Engineering of the Panel

The reverse engineering approach to panel design is shown diagrammatically in Figure 2. The first step was to determine all geometric and material parameters likely to have an impact on the maximum loads the panel could support in operation. In the case of Panel I, the geometric parameters were determined via measurement of the original panel. The material properties were obtained from the original aircraft manufacturer (OEM). The next step was to determine the stiffness and strength of the existing panel in all critical modes from these material and geometry parameters. These could be either in-plane or out-of-plane loading or a combination thereof. It was found, from the OEM stress notes, that the critical modes for Panel 3208 were axial compression and shear.

Once individual modes were determined a load envelope for the metallic panel was plotted. A panel of equivalent stiffness in all modes (axial, shear, bending, pressure) was chosen from a set of standard composite panel solutions. The load envelope for this panel was then superimposed on the metallic panel load envelope. If the load envelope for the metallic panel was not fully covered by that of the composite replacement panel, then the shear and/or axial stiffness of the composite replacement must be increased. At this point another design was chosen from the set of standard composite replacement panel solutions. This was an iterative procedure and was stopped once the load envelope of the composite replacement panel covered the entire load envelope of the existing panel. Within this iterative procedure the effect of differences, in panel stiffness and mismatch in CTE on the surrounding sub-structure, were also determined.

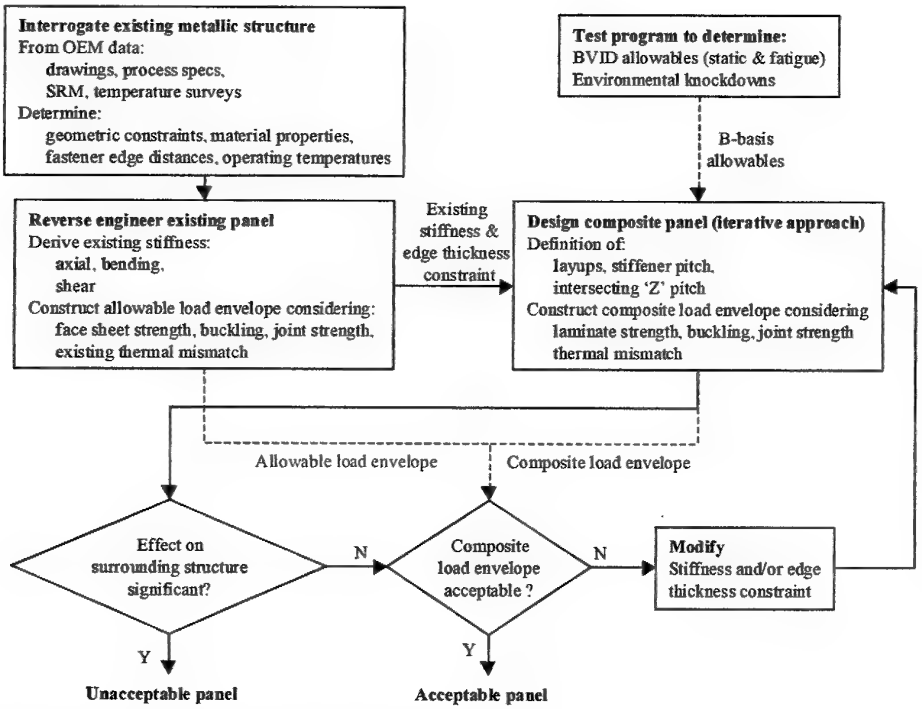

Figure 2 Reverse engineering approach to panel design

1.3 Structural Analyses

1.3.1 Available Design Data

The ADF became the sole operator of the F-111 in May 1998 and instigated the Sole Operator Program (SOP) to ensure the aircraft could be supported through to its planned-withdrawal-date (PWD) of 2020 [9]. Although the PWD has recently been revised to 2010-2012, much of the work in the SOP has been completed. As a part of the SOP, the OEM design data relevant to the composite replacement panel work was acquired. The original General Dynamics (GD) stress/design reports were used to determine the panel and fastener loads, margins of safety, properties and design allowables. This data was generated in the early 1960's and is based on many approximate, and probably very conservative, assumptions. However, it constituted the certification basis for the aircraft and so was considered valid for use in the demonstrator program.

This data would not have been available in a true reverse engineering situation. Nevertheless, it was decided to take advantage of all available data to facilitate the identification of the pitfalls and difficulties likely to be encountered had a reverse engineering route been taken. This would accelerate the learning curve for developing a true reverse engineering capability and reduce the time from design to production for the demonstrator panel.

A full-scale finite element model of the F-111C (known as the ILM and described in Section 1.4) was used to evaluate the stresses/strains in the replacement panel and its effect on the local sub-structure when the aircraft is subjected to a CPLT. The findings of these analyses are the subject of this report.

1.3.2 Direct Measurement of Panel Strains

Three options were available to confirm the design stresses in Panel I and surrounding sub-structure. The first two options involved measuring the strain distribution within the structure for Panel I and the original bonded panel during an instrumented flight, or ground, test. However the costly nature of these, in terms both time and money, prevented them from becoming feasible. Fortunately, a third option was available due to the unusual structural integrity management approach employed for F-111 aircraft. Direct measurement of strains was possible from aircraft undergoing the CPLT.

The CPLT is a static ground test conducted on F-111 aircraft where critical parts of the airframe are subjected to Design Limit Load (DLL) at -40 °C. The CPLT has a special role in the F-111 safety-by-inspection program. It targets the D6ac steel components in the structure by capitalising on the low temperature embrittlement of steels. These components are otherwise difficult to inspect because of limited access and/or because D6ac has a very short critical crack length. The CPLT loading configuration is designed to subject the aircraft to loading levels above those likely to occur in flight, effectively providing a proof test of the D6ac components.

The CPLT consists of four proof test conditions applied in the following sequence:

1. CPLT I -2.40g at 56° wing sweep
2. CPLT II +7.33g at 56° wing sweep
3. CPLT III -3.00g at 26° wing sweep
4. CPLT IV +7.33g at 26° wing sweep

Panel 3208 is fastened to a number of D6ac components and therefore experiences moderate loading during the CPLT. Thus, the CPLT provides an excellent, low-risk, opportunity to demonstrate Panel I and validate some of the assumptions used in its design.

1.4 Finite Element Modelling

FEA provides the means to accurately predict the stresses and strains in complex structure subjected to complex loading. In this case, FEA was used to determine the margins-of-safety for all critical failure modes in each of the CPLT loadcases. The critical modes of failure for Panel I in the CPLT are:

- panel strength,
- sub-structure strength,
- fastener strength,
- sub-structure stability,
- panel stability.

The F-111C aircraft internal loads finite element model (ILM) was developed to accurately predict the internal load distribution for any given CPLT or flight condition. This model was developed under contract by Lockheed Martin Tactical Aircraft Systems (Lockheed) through the F-111 SOP in cooperation with Australian industry and DSTO engineers. It provided the ideal baseline from which to develop fine grid models of Panel I. A description of the ILM is provided in Section 3.3.

Fine grid sub-models were developed to accurately measure stresses and strains within the local panel region. In total, four sub-models were created. Two were created to measure the effect of replacing the original panel with a composite panel. Two additional sub-models, with an identical mesh to the first two, were created to account for the effect of temperature. These sub-models are listed as follows:

- original metallic panel (Panel 3208),
- original metallic panel (Panel 3208) with the addition of thermal properties,
- composite replacement panel (Panel I),
- composite replacement panel (Panel I) with the addition of thermal properties.

The original panel sub-model is described in Section 3.3.3 and the composite replacement panel sub-model is described in Section 3.4.

The only difference between the first and second sub-model in each set were modifications made to the element material properties in order to include the coefficient of thermal expansion (CTE) and a reference temperature. In this case the reference temperature, which was the temperature at which the aircraft was built, has been assumed to be 20 °C (68 °F). The aircraft was assumed to have zero thermal stress at this temperature.

The analyses conducted with these models predicted that the structural integrity of the panel, surrounding structure and the fasteners, shall be maintained during CPLT loading. They also predicted that the onset of buckling would not occur at a lower load than that applied for each of the CPLT cases. The results of these analyses are provided in Section 4.

1.5 Risks

The analyses presented in this report are based on the first revision of the ILM (ILMr1). This was up-to-date in accordance with the concurrent version control software [6, 7] as of 2 December 2002. This model was not correlated with experimental data from the F-111C Fuselage Strain Survey. Results from this survey have been incorporated into the ILM and a second revision, know as F111C Revision 2 Internal Load Model (ILMr2i2), released on 21 October 2003. The analysis conducted for this report was not repeated using ILMr2i2 for the reasons explained in Section 3.3.2.

As a fully correlated version of the ILM was not used in this analysis there is a risk that some of the margins-of-safety (MOS) predicted in this report are negative and that Panel I, or the aircraft, may be damaged during a CPLT where Panel I is installed. It is judged that this risk is extremely low for the following four reasons:

1. the comparison described in Section 3.3.2 showed that there was little difference in the predictions of displacement and stress, for the structure assessed in this report, between ILMr1 and ILMr2i2,

2. the joints in the ILM are excessively stiff (Section 3.3.5 describes one example) and more load is transferred through the ILM than in reality. Thus the predictions made by the ILM, and in this report, should be conservative,

3. in this report both the metal (Panel 3208) and composite (Panel I) panels were modelled and compared. In general the MOS with Panel I installed were not degraded from those

with the existing metal Panel 3208 installed. Since the latter clearly survives the CPLT, then it is expected that Panel I too will survive,

4. of all the MOS predicted in this report, only a small number were negative. These were explained as being modelling artefacts or not directly influencing the structural integrity of Panel I or the aircraft.

2. Panel Construction

2.1 Original Panel 3208

Panel 3208 is fastened to the aircraft sub-structure, (Figure 3) via countersunk screws around the periphery (Figure 4) and is fabricated by metal to metal bonding with the construction shown in Figure 5.

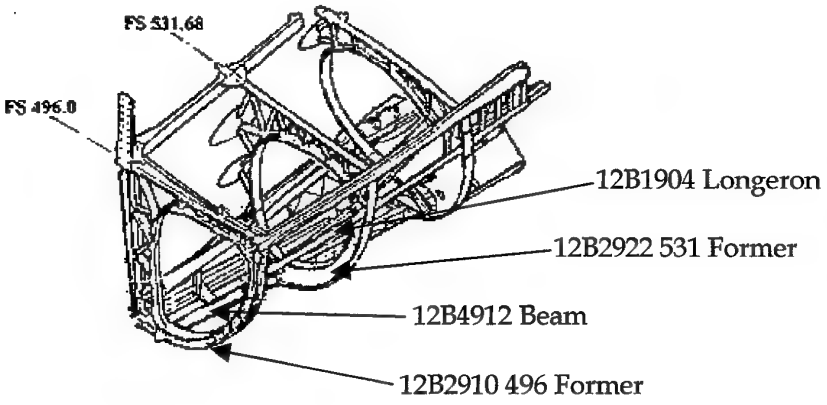

Figure 3 Panel 3108 sub-structure. The sub-structure for Panel 3208 is a mirror image of this about the longitudinal axis of the aircraft

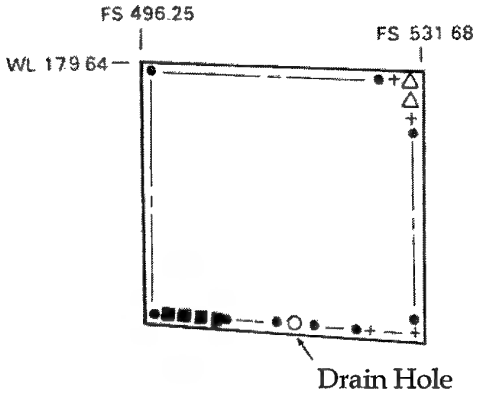

Fastener Type	Quantity
△ NAS1154V11	2
+ NAS1154V8	8
• NAS1153V5	116
■ C082-5-8	4

Figure 4 Countersunk screws used to attach (LH) panel to aircraft

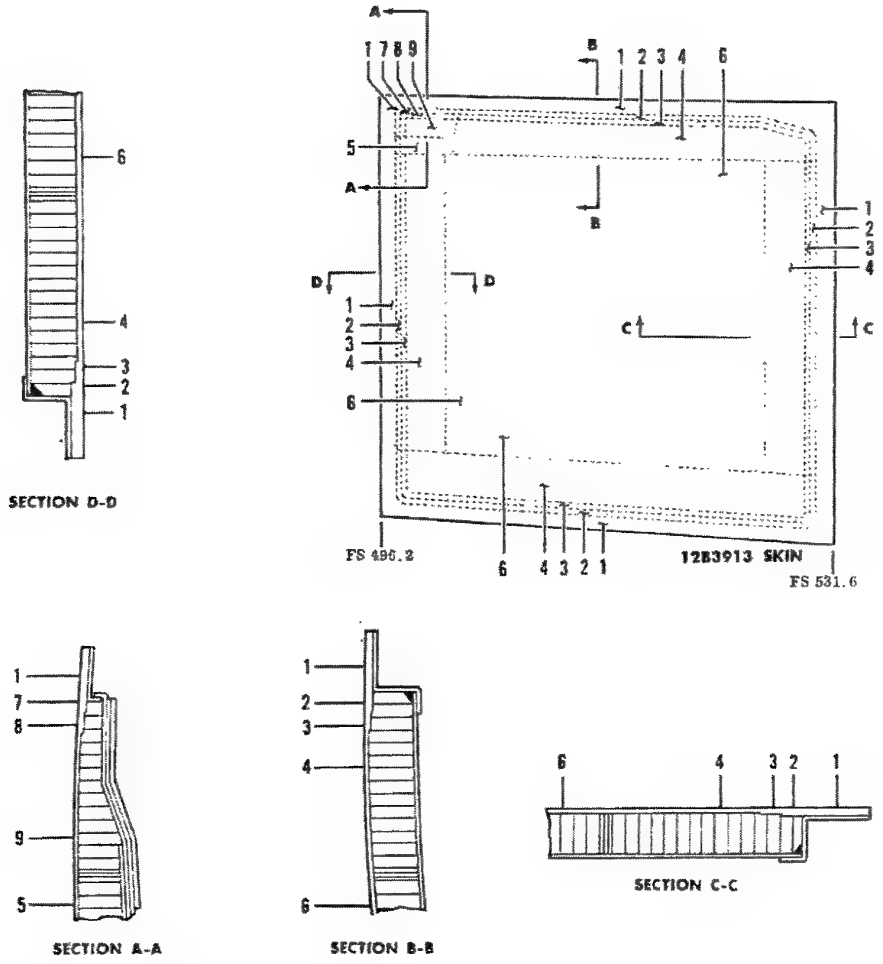

Standard Panel Construction	Gauge (inches)/Material	Zones
External Skin	0.120/2024-T81	1,2,7
	0.071/2024-T81	3,8
	0.032/2024-T81	4,5,6,9
Core	1/8-5052-0.002-8.1	2,3,4,5
	1/8-5052-0.0015-6.1	7 THRU 9
	1/8-5052-0.001-4.5	6
Internal Skin	0.020/2024-T81	2 THRU 6
Edge Member	0.012/2024-T81	1,2
	GLASS FABRIC, 8-PLY	5,7,8,9

Figure 5 Fabrication details of metallic Panel 3208

2.2 Panel I

Section 2.2 provides a summary of the manufacture details for Panel I that were given in reference [8].

2.2.1 Configuration

Panel I, as shown in Figure 6, consisted of a skin stiffened with twelve hat sections and a single intersecting "Z" section through the centre, all manufactured from carbon fibre fabric/epoxy prepreg. The periphery of the panel that contacts the aircraft sub-structure had a layer of fibreglass cloth on the surface to prevent electrical contact, and thus galvanic corrosion, between the carbon/epoxy composite and the aluminium/steel sub-structure. All fasteners through the carbon were titanium or cres steel. Lightning protection was provided by a tissue of aluminium mesh covering the outside surface of Panel I. Film adhesive was used to bond the stiffeners and lightning mesh to the skin. The entire panel assembly was co-cured in two stages.

The overall panel geometry is shown in Figure 7 and Figure 8, while lay-up and stiffener geometry is detailed in Figure 9 and Figure 10. Some of the important details contained in these drawings are shown in Table 1.

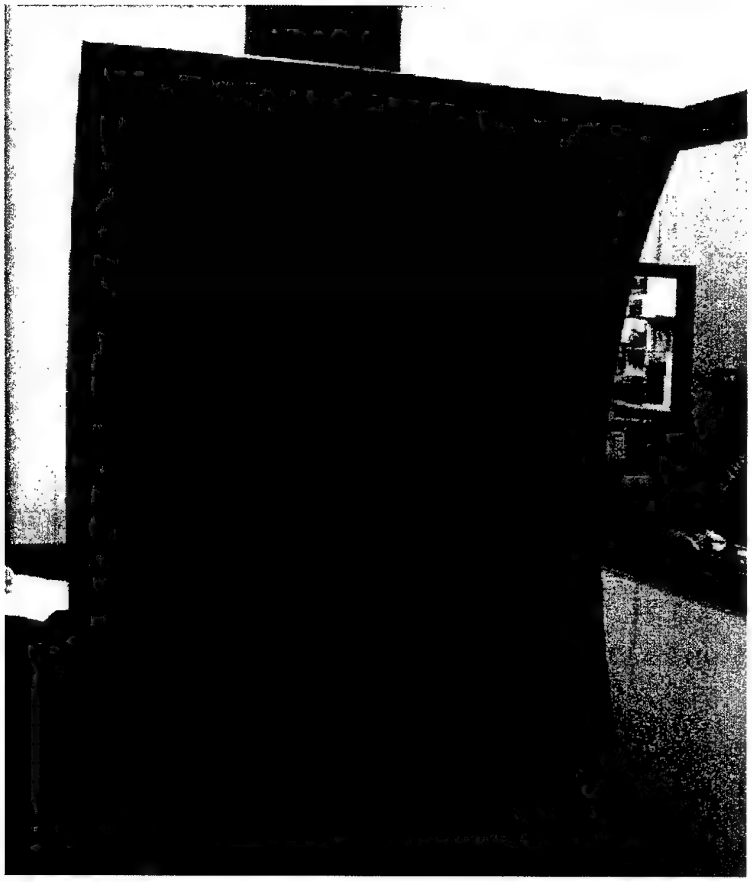

Figure 6 Photograph of the as-manufactured Panel I, prior to trimming and drilling

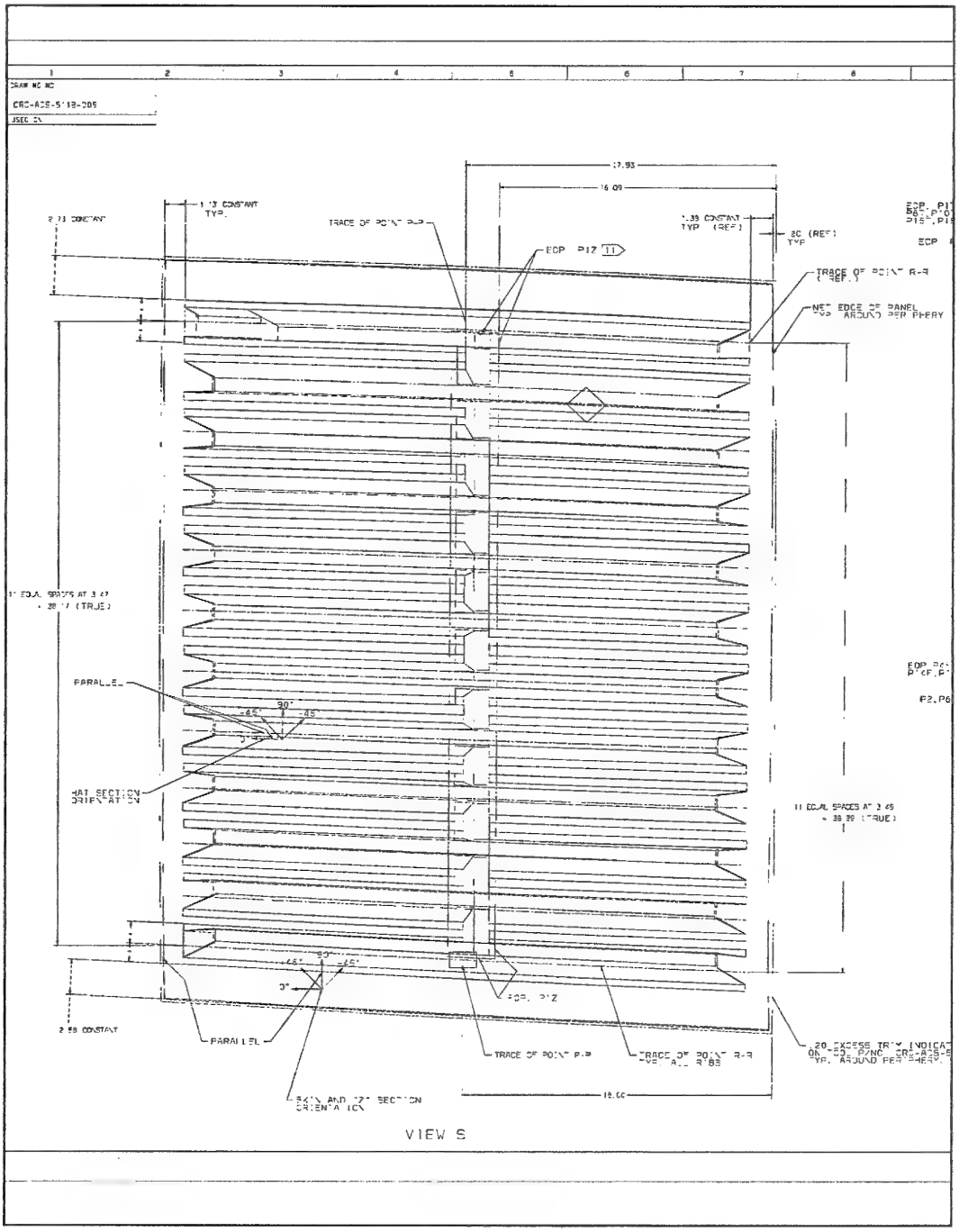

Figure 7 Carbon replacement panel (DWG CRC-ACS-511b-009, sheet 3, A1-L8)

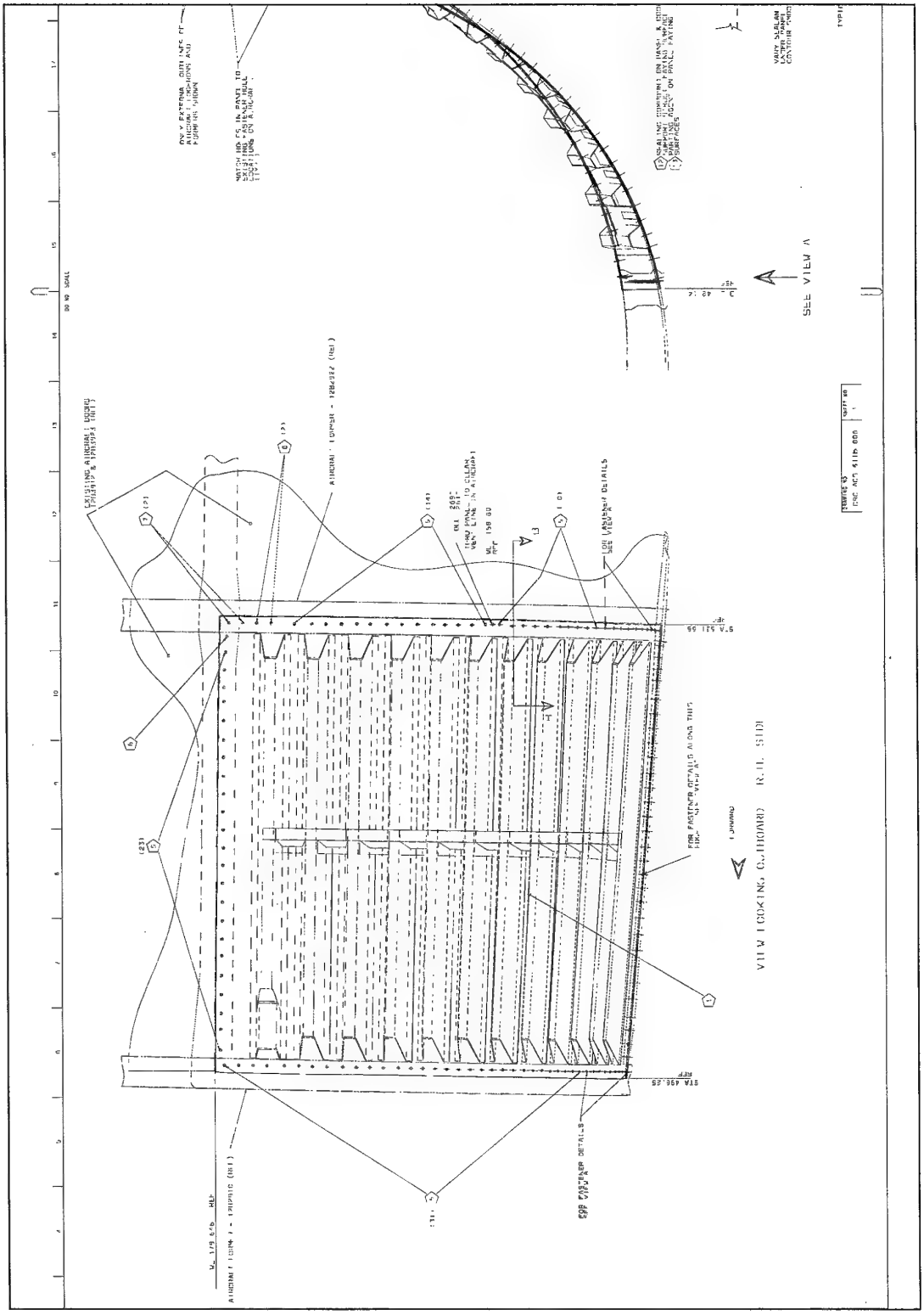

Figure 8 Carbon replacement panel (DWG CRC-ACS-511b-009, sheet 1, A1-L17)

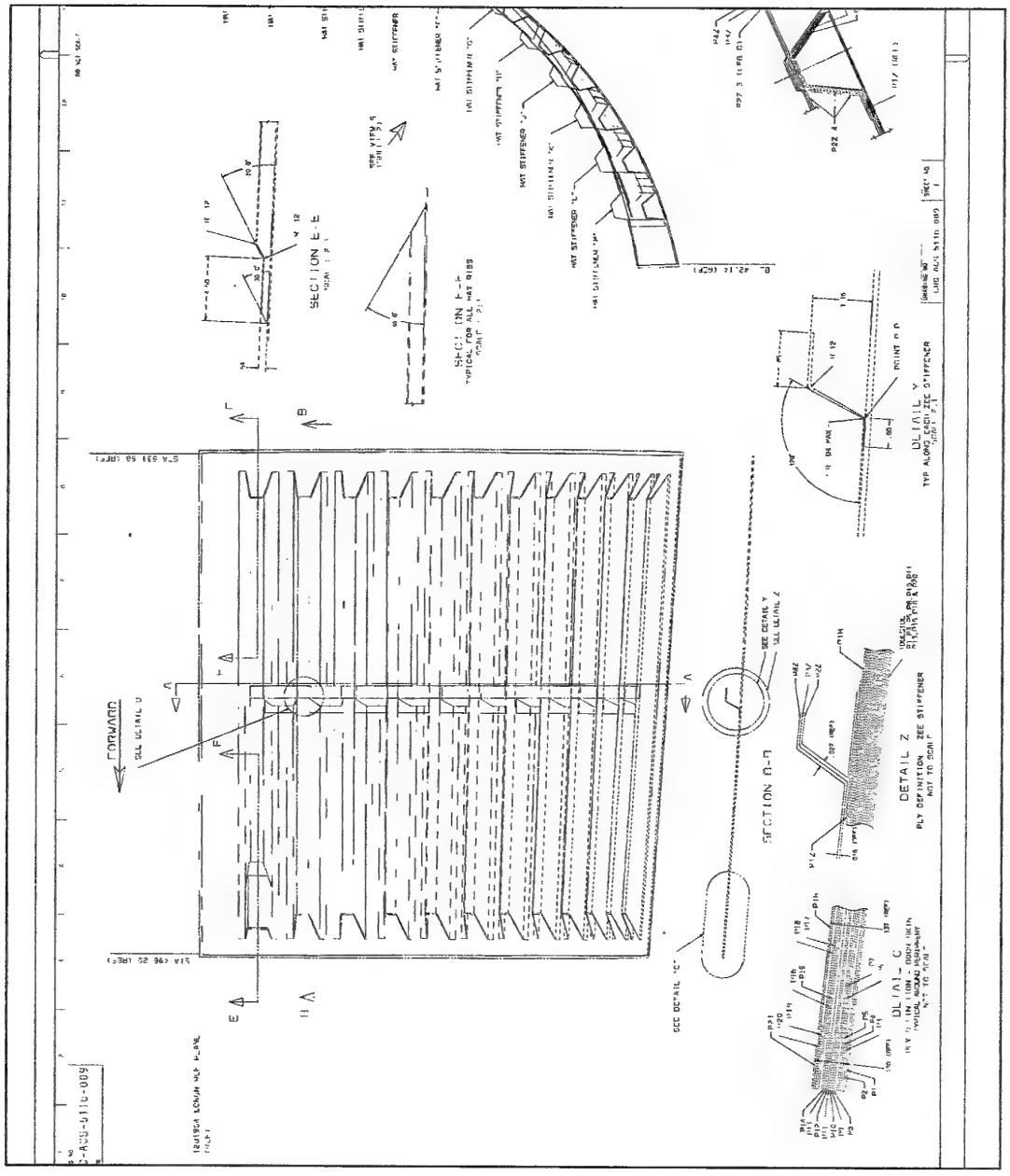

Figure 9 Carbon replacement panel (DWG CRC-ACS-511b-009, sheet 2, A1-L12)

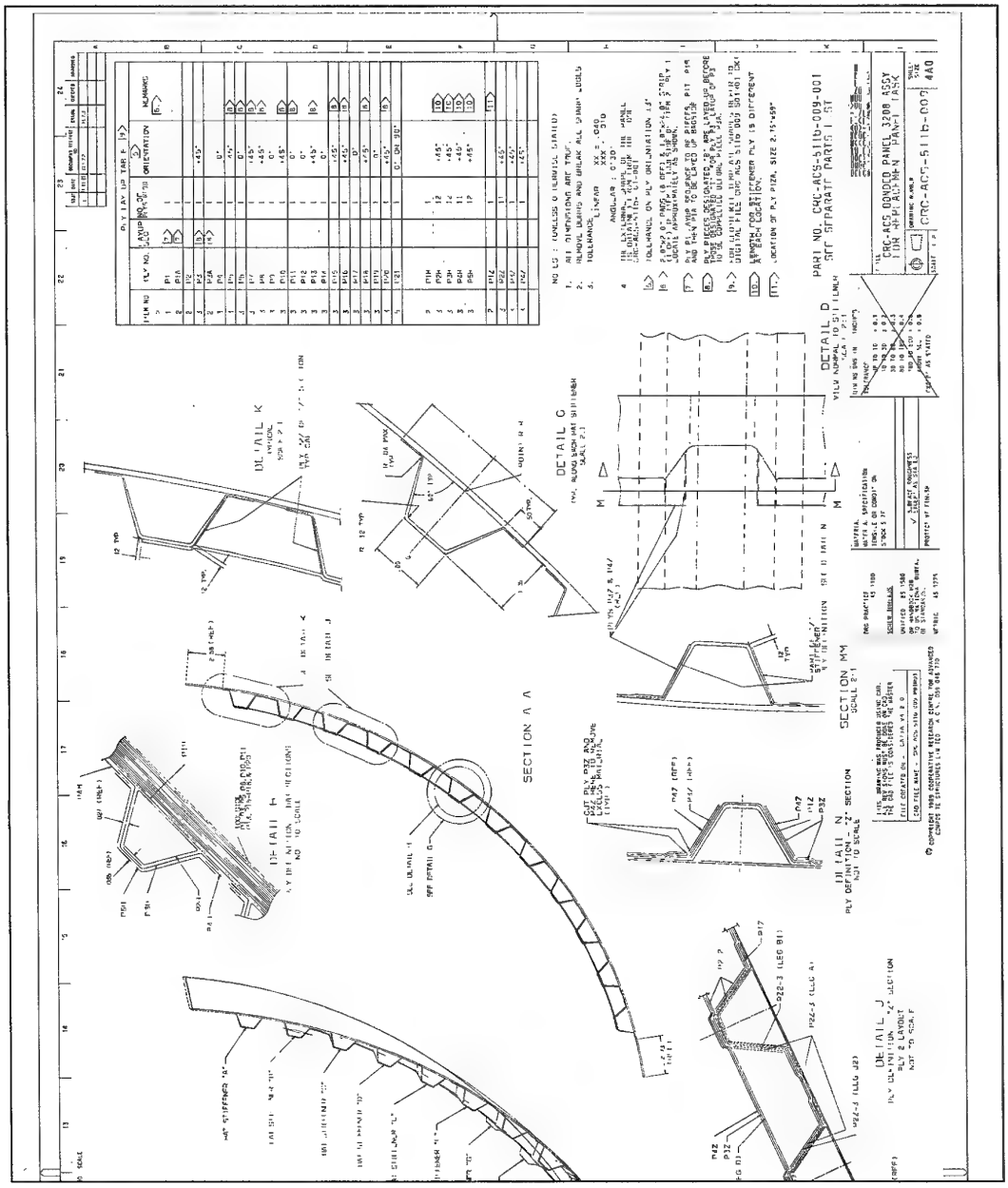

Figure 10 Carbon replacement panel (DWG CRC-ACS-511b-009, sheet 2, L13-L24)

Table 1 Construction details for Panel I

Item	Detail	Quantity
Skin		
Lay-up	General	$[45_2\ 0\ 45_3\ 0\ 45_3\ 0\ 45_2]$
	Under hat stiffeners	$[45_2\ 0\ 45_3\ 0\ 45_3\ 0\ 45_2 45]$
	Panel edge	$[(45\ 0)_{4s}\ 0]$ (inner 0° ply was glass fabric for electrical isolation)
Top-hat stiffeners		
Lay-up	Caps	$[45_4]$
	Webs & flanges	$[45_3]$
Pitch	-	88.4 mm (3.48″)
Run-out angle	-	30°
Height	-	29.5 mm (1.16″) except locally at FS 496 and WL179.6 where the height reduced to 13.0 mm (0.51″)
Z-stiffeners		
Lay-up	Caps, webs & flanges	$[45_3]$
	Height	29.5 mm (1.16″)
General		
Ply drops		5.1 mm (0.2″) intervals

2.2.2 Materials

A summary of all the materials used to fabricate the composite replacement panel is shown in Table 2. The carbon prepreg was supplied by the Advanced Composite Group (UK) while Hawker de Havilland supplied the fibreglass and aluminium mesh.

2.2.3 Cure

Panel I underwent a two-stage cure cycle. Initially, the panel was cured for 8 hours at 80 °C under vacuum (-14 psi), with heating and cooling rates of 3 °C min^{-1}. This cure

Table 2 Materials used in Panel I

Material	Designation
Carbon fibre prepreg	ACG MTM49-3/CFO403-55%FV-199 2x2 TWILL
Fibreglass cloth	Style 120
Film adhesive	ACG XLTA246/PK13-185
Aluminium mesh	ASTROSEAL ALUMESH AL-016

cycle was performed with the panel laid up on a female tool fabricated from medium density fibreboard (MDF) wood. The stiffener sections were supported and consolidated with silicon and gelflex mandrels. After curing the panel was broken off the tool.

A freestanding post-cure, consisting of 2 hours at 175 °C was performed. The ramp rate was 5 °C min^{-1} from room temperature to 80 °C, then 0.33 °C min^{-1} from 80 to 175 °C. The cooling rate was 3 °C min^{-1}. The mandrels used to form the stiffeners were removed from the fully cured part after cooling.

Temperature recording equipment was used in the oven to ensure that the nominal thermal profiles were followed during the cure and post-cure cycles.

3. Finite Element Model Description and Assumptions

3.1 General

Finite element models of the panel and surrounding sub-structure were developed in order to accurately predict in-plane stresses and strains, fastener loads and stability modes in the panel region for the CPLT load cases. The ILM was used to predict these results in conjunction with a series of sub-models. This section describes these models and explains the assumptions made in their creation. In a broad sense, the ILM was used to predict the grid point displacements and rotations for the entire aircraft during CPLT loading. The ILM output results were then input into a more refined sub-model of the panel and surrounding structure to more accurately predict the stresses, strains and stability modes. This technique is described in Section 3.2.

Various assumptions are required when solving practical problems with a finite element representation. These assumptions determine the validity of a model for a given output. A summary of the assumptions made during the construction of the ILM are provided in Section 3.3. A summary of the assumptions made in creating the original metallic panel sub-models and the composite replacement panel sub-models are provided in Section 3.3.3 and Section 3.4 respectively.

Various modifications were made to the ILM in order to enable its use in this application. These included the addition of capability to measure the thermal residual internal loads distribution and also the modification of element properties in order to determine the internal load distribution for the composite replacement panel. These modifications are described in Section 3.5.

As mentioned previously, there were effectively four versions of the ILM and four sub-models used for the analyses. A test matrix has been provided in Section 3.6 in order to show how each of the models was used to generate the results.

3.2 Sub-Modelling Technique

The sub-models were designed to allow the transfer of the ILM internal load distribution into the panel models during CPLT loading. The sub-model boundary was selected to extend one to two panel widths from the panel edge in order to minimise the influence that the sub-model edge may have on the stress distribution close to the panel. This was possible for every edge of the panel except for the edge adjacent to the STA 496 Former. The inlet shroud on the opposite side of the former was not modelled in ILMr1, thus the sub-model was terminated at the edge of the 496 Former.

3.2.1 Methodology

A displacement control method was used to transfer internal loads from the ILM to the sub-model. The grid point translations and rotations obtained from the ILM were applied to the sub-model at the boundary nodes. By forcing these nodes to deform in this manner, the CPLT internal loads were transferred into the sub-model. Thus, the ILM was only required to generate the entire F-111 internal loads distribution for each of the CPLT loadcases once. The internal loads could then be used as often as required throughout the sub-model development and verification phases. This methodology is shown in Figure 11.

The CPLT is conducted at –40 °C and thermal effects were expected to be significant. Therefore the approach summarised below was developed where both mechanical and thermal loads could be applied to the sub-model. Validation of this process is described in Appendix A. The essential steps in this process were to:

- perform the analysis on the global model including all mechanical and thermal loads. This model must include a representation of the composite replacement panel,
- generate a displacement field from these results,
- apply the displacement field around the boundary of the sub-model (apply to two rows of nodes). The more detailed sub-model includes the carbon composite panel and the surrounding structure,
- apply the thermal load to the sub-model,
- run the sub-model analysis.

3.2.2 Boundary Definition

The sub-models were all bounded in exactly the same manner. Therefore, the same grid points define the sub-model boundary for each of the sub-models. Consideration

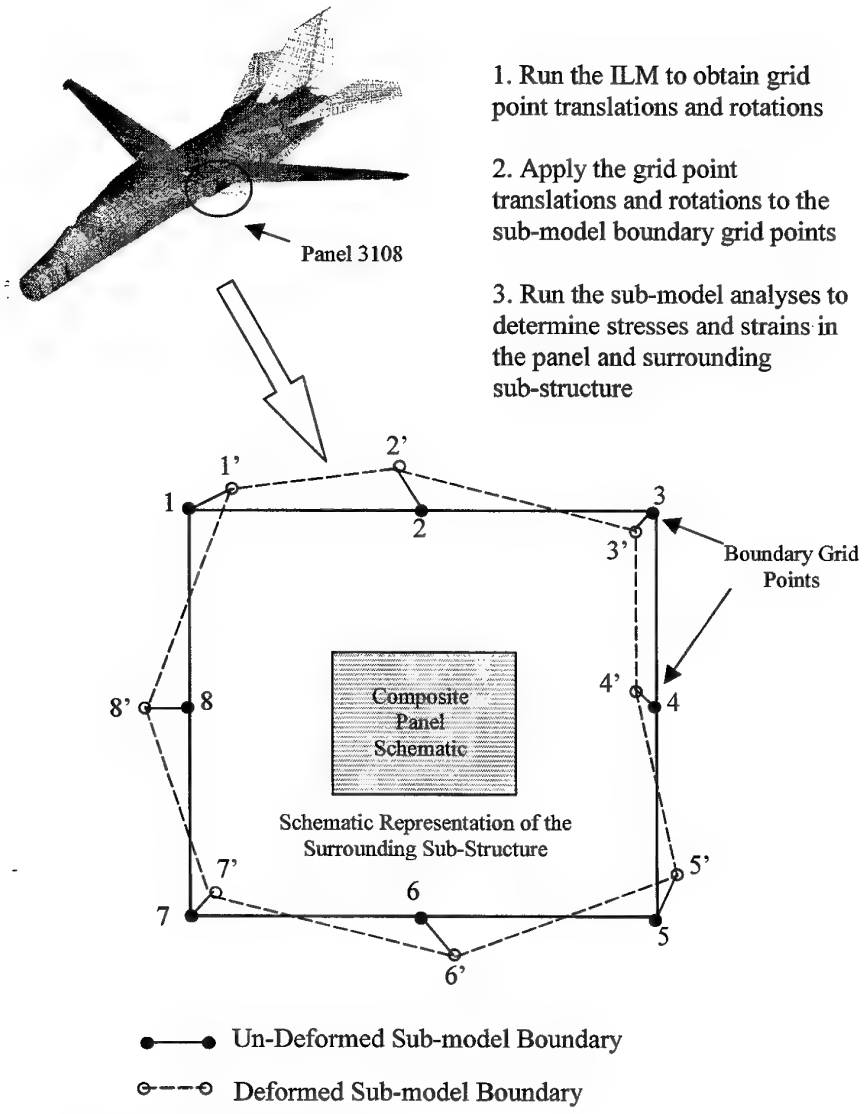

Figure 11 Sub-modelling methodology

was given to both strength and stability of the panel and surrounding structure when the boundary was defined. Components that were located at the sub-model edge were cut through locations approximately one to two panel widths beyond the panel edge. In so doing, care was taken to ensure that the cuts were made as far as possible away from structural joints or areas of structural complexity. However, in some cases this was unavoidable. The sub-model itself and its boundary are shown in Figure 12. The components that were cut are shown in Figure 13 and Figure 14 and a description of these components is provided in Table 3. A list of the sub-model boundary nodes and their location is provided in Appendix B.

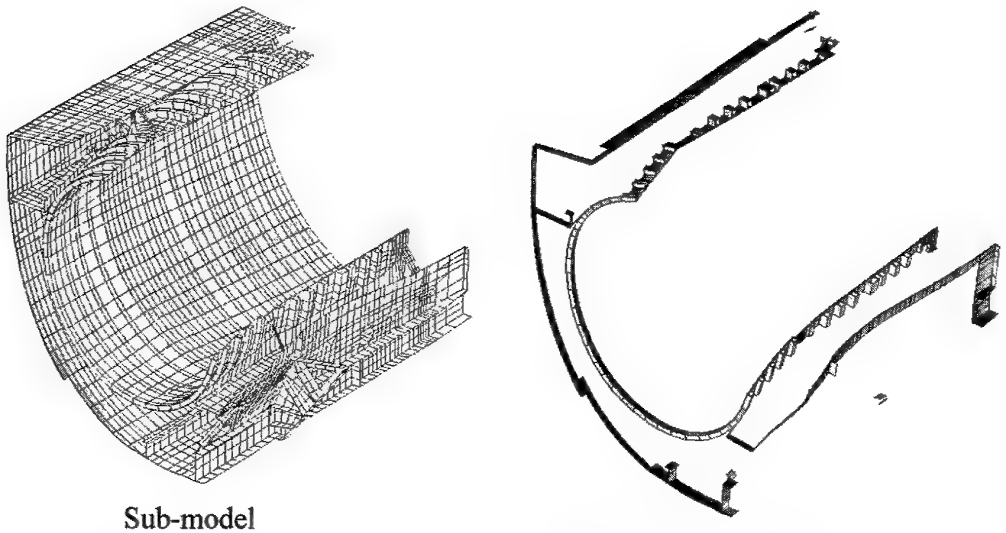

Figure 12 Sub-model and sub-model boundary (Note that Panel I is obscured)

3.3 Internal Loads Model

3.3.1 Finite Element Mesh

The ILM, shown in Figure 15, was a three dimensional representation of a RAAF F-111C aircraft. It contained structural components such as longerons, bulkheads, skins, panels and other miscellaneous structure. The model was intended to provide the internal structural loads for future fine grid finite element models. As such, the mesh detail was intentionally coarse and only sufficient to provide representative load transfer. Refinement of the mesh was required for any analysis that requires stress and strain output from the model.

In many cases structure of no structural significance has been left out of the model. In other cases, dummy structure has been included at locations where loads are applied in order to facilitate an accurate load introduction mechanism.

The ILM is comprised predominantly of quadrilateral and triangular shell elements, and where required rod, beam and three-dimensional solid elements. For a description of how these element types have been utilised in this model refer to reference [10]. The model consists of 315500 grid points, 393600 elements, resulting in approximately 1870000 degrees of freedom.

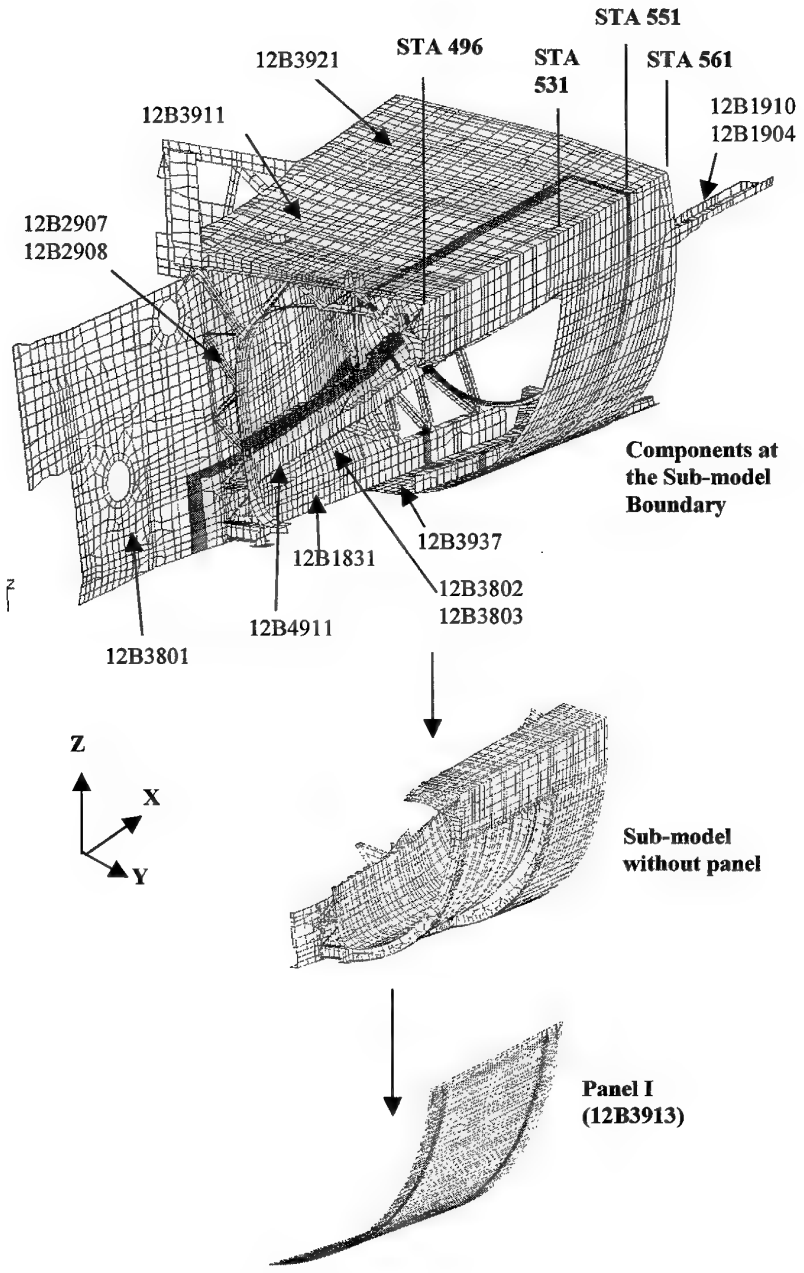

Figure 13 Sub-model boundary components (Isometric view from FWD)

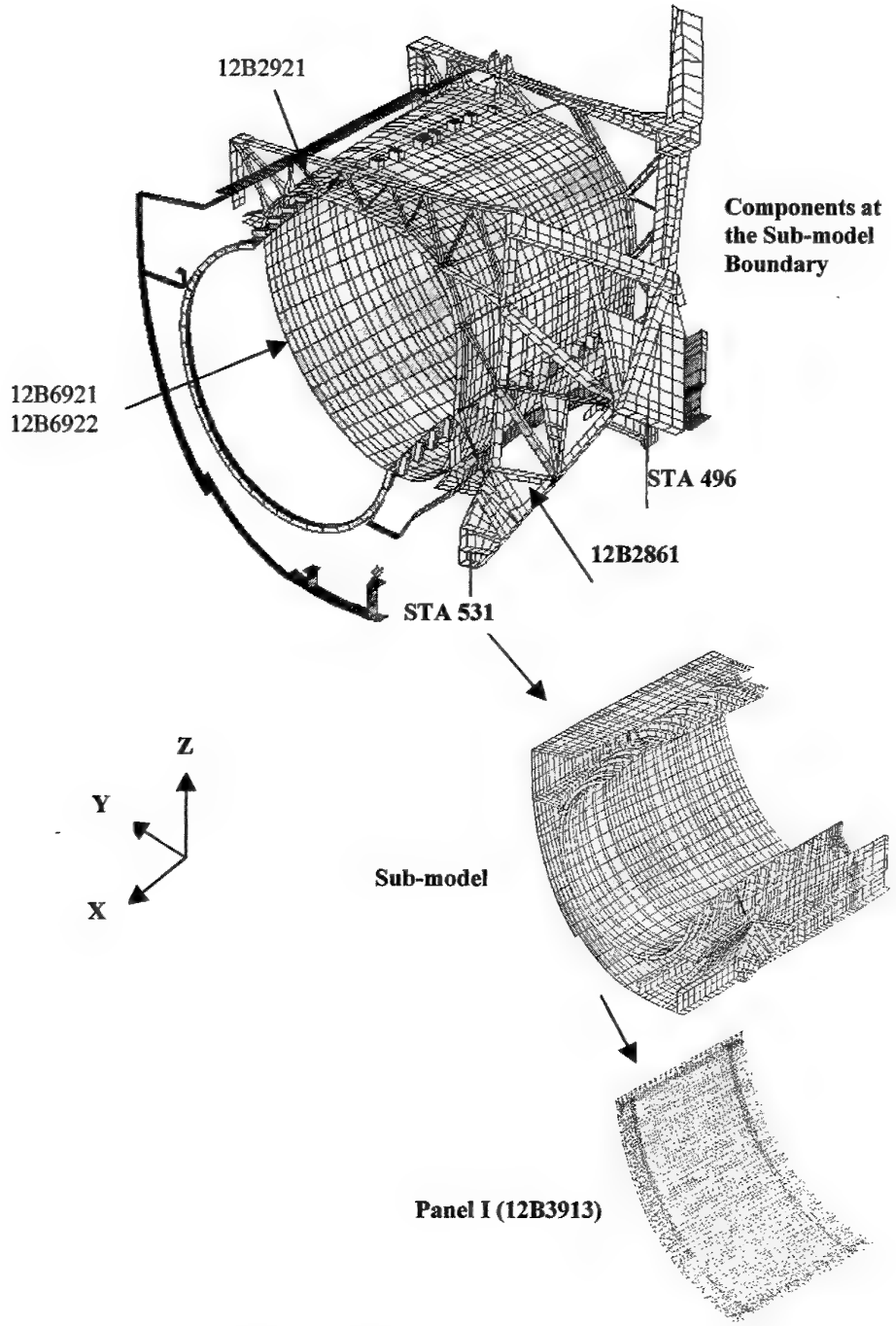

Figure 14 Sub-model boundary components (Isometric view from AFT)

Table 3 Cut components at the sub-model boundary

Item	Part ID	Description
1	12B1831	Longeron at approximately BL32 and WL150 that extends from STA 459 to STA 570
2	12B1904	Longeron at the top of Panel 3208/3108 that extends from STA 496 to STA 591
3	12B1910	Longeron running parallel and connected to 12B1904 that extends from STA 496 to STA 593
4	12B2861	Bulkhead positioned at STA 531
5	12B2907	STA 496 former component
6	12B2908	STA 496 former component
7	12B2921	STA 531 former component
8	12B3801	Fuselage skin that extends from STA 448 to STA 570
9	12B3802	Fuselage skin adjoined to the 12B1831 longeron that extends from STA 500 to the main landing gear
10	12B3803	Fuselage skin adjoined to 12B3802 that extends from STA 496 to the main landing gear
11	12B3911	Underwing nacelle skin that extends from STA 496 to STA 531
12	12B3912	Nacelle cover that extends from STA 496 to STA 562
13	12B3921	Underwing nacelle skin that extends from STA 531 to STA 562
14	12B3923	Outboard nacelle skin that extends from STA 531 to STA 572
15	12B3937	Nacelle cover that extends from STA 496 to STA 610
16	12B4911	Lower beam that extends from STA 496 to STA 572
17	12B4922	Lower beam that extends from STA 531 to STA 593
18	12B6921	Engine inlet duct skin that extends from STA 496 to STA 531
19	12B6922	Engine inlet duct assembly stiffeners

3.3.2 Validation Activities

The ILM used for the analysis in this report was up to date in accordance with the concurrent version control software [6, 7] as of 2 December 2002 (ILMr1). The F-111C Fuselage Strain Survey was conducted in the period July to October 2002. In that program a RAAF F-111C (A8-144) was instrumented with approximately 470 strain gauges and a number of strain surveys, including a full CPLT, were conducted. At the time of performing the analyses and the drafting of this report (January to April 2003), the ILM had not been correlated with this experimental data. The first phase of correlation activities was completed and a revised version, known as the F111C Revision 2 Internal Load Model (ILMr2i2), released on 21 October 2003. It is expected that further revisions will be made in the future.

The effect of this revision was established by comparing selected predictions from both models. As shown in Table 4, the predicted peak displacements were all well within

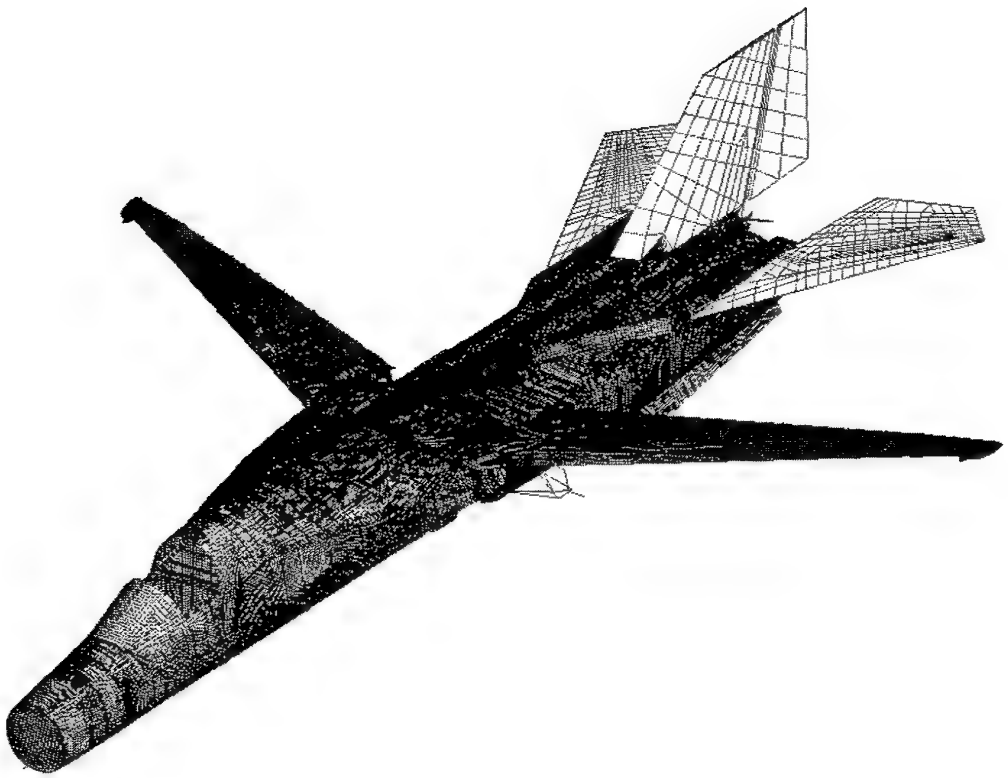

Figure 15 F-111C Internal Loads Finite Element Model. Panel 3108 is highlighted

5% and typically closer than 1.5%. This indicates that the displacement predictions, that were used as boundary conditions for the sub-models, were expected to be very close for both ILMr1 and ILMr2i2. Most peak stress predictions were well within 10 % and the distribution of stresses was very similar for both models. It is most likely that the three outliers shown in Table 4 were artefacts caused by the relatively coarse mesh used in the ILM. As stated in Section 3.3.1, the ILM was too coarse for detailed stress and strain analysis. It was therefore concluded that ILMr2i2 did not alter displacement and stress predictions, for Panel 3208 and the local sub-structure, sufficiently to require that the analysis conducted with ILMr1 be repeated.

3.3.3 Original Panel Sub-Model

A sub-model of Panel 3208 was created in order to determine stresses and strains. The sub-model provided a more detailed representation of the original panel than the ILM and as such could more accurately model the stress distribution. The sub-model was created by refining the ILM. The main focus was on reducing the element size and increasing the accuracy of the panel edge joint modelling.

Table 4 Selected predictions from ILMr1 and ILMr2i2

Quantity	Part Number	CPLT	Peak	ILMr1	ILMr2i2	Difference	
						Absolute	(%)
Magnitude of displacement (mm)	12B3913	III	Max	15.0	14.9	-0.1	-0.7
			Min	6.83	6.80	-0.03	-0.4
		IV	Max	30.2	30.6	0.4	1.3
			Min	13.6	13.9	0.3	2.2
	12B2908 and 12B2909	III	Max	17.2	17.2	0.0	0.0
			Min	12.1	11.6	-0.5	-4.1
		IV	Max	35.0	35.4	0.4	1.1
			Min	23.2	23.4	0.2	0.9
	12B2922	III	Max	10.6	10.3	-0.3	-2.8
			Min	6.70	6.66	-0.04	-0.6
		IV	Max	21.1	21.4	0.3	1.4
			Min	13.3	13.6	0.3	2.3
Von Mises stress (psi)	12B3913	III	Max	8050	8080	30	0.4
			Min	542	705	163	30.1
		IV	Max	19000	19400	400	2.1
			Min	1320	1420	100	7.6
x-direction stress (psi)		III	Max	5290	4730	-560	-10.6
			Min	-2150	-3100	-950	-44.2
		IV	Max	5320	5600	280	5.3
			Min	-12700	-12700	0	0.0
xy-direction stress (psi)		III	Max	3780	4050	270	7.1
			Min	-3760	-4030	-270	-7.2
		IV	Max	8860	9140	280	3.2
			Min	-8900	-9180	-280	-3.1
						Average	5.8

3.3.4 Panel Mesh

The size of each element within the panel was reduced by an order of magnitude through the refinement process. As such the number of elements within the panel rose from 548 to 5285. The original mesh and the refined mesh are shown in Figure 16. Whilst this was still a fairly crude representation of the honeycomb core panel, it provided sufficient mesh density for stress prediction.

3.3.5 Panel Edge Joint

The ILM used an overlapping element method to transfer load from the panel into the adjacent frame structure. This resulted in a very stiff connection. In reality the panel was joined to the sub-structure via a single row of fasteners around the panel edge. Each of these fasteners was thus a pin connection.

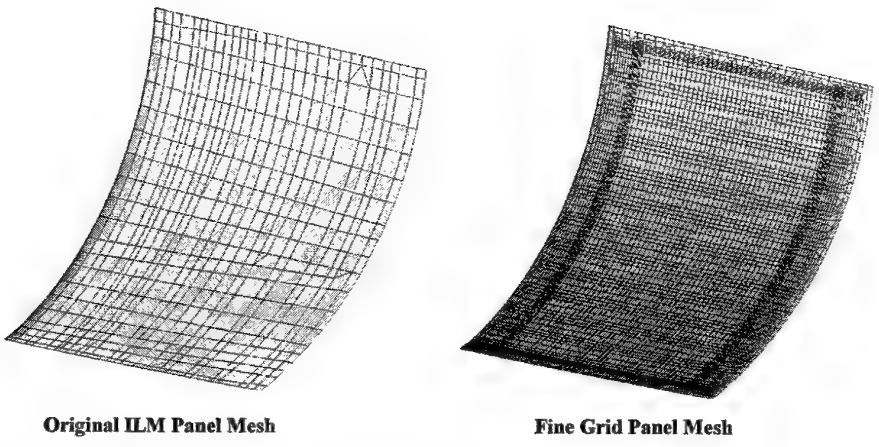

Figure 16 Original ILM panel mesh and the fine grid panel mesh

The assumption made when using element overlap was that the combined effect of all fasteners fitted along the panel edge provided a clamped edge connection. This assumption can lead to an over estimate of the load transfer into the panel and an inaccurate load transfer distribution along the panel edge.

To more accurately represent the joint, grid points were created at each of the fastener locations on both the panel edge and the sub-structure frame. These grid points were equivalenced at the fastener locations in order to simulate a fastener connection. That is, a single node was created at the connection point that replaced the previous two nodes on both structures. This represents the point of contact and allows load to transfer at this location. Figure 17 show the connection modelled using the ILM methodology and the connection modelled using the refined approach. Whilst the refined approach effectively clamped the edge joint in the same manner as modelled previously, the distribution of load entering the panel at the fastener locations was more representative of reality. Therefore, a conservative yet more representative estimate of the fastener load distribution during loading was expected.

3.3.6 Material and Property Definition

The material properties used for the sub-model were all obtained from the ILM. As there were no major changes made to the ILM mesh outside of Panel 3108/3208, no further description is provided for these components. Material properties for these components can all be found in reference [10].

Since modifications were required for the mesh refinement of the panel, the material properties needed to be re-applied. The property sets were distributed throughout the panel in a pattern that was equivalent to that used in the ILM. The material property

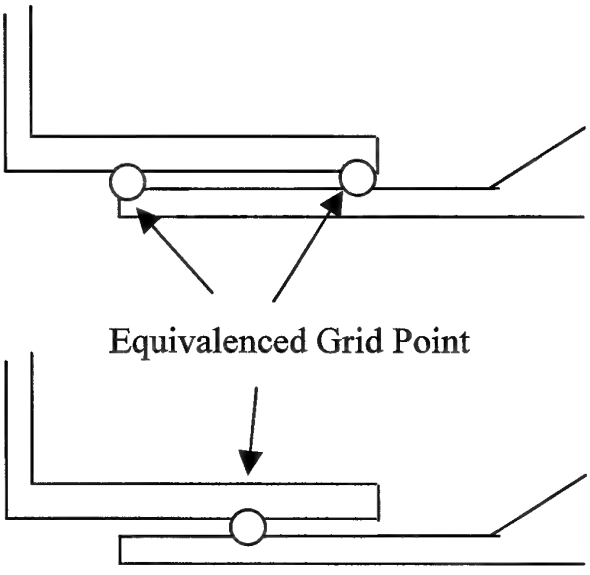

Original ILM Joint
Note: Grid points are equivalenced at random locations along the panel edge

Refined ILM Joint
Note: Grid points are equivalenced at fastener positions

Figure 17 Joint modelling methodology

distribution for both the ILM panel and the refined panel can be seen in Figure 18. A description of each of the property sets used is provided in Table 5. The material and property set values can be found in reference [10].

3.4 Replacement Panel Sub-Model

A sub-model of Panel I and its surrounding structure was created in order to measure the stresses and strains in the region. The sub-model provides a fine grid representation of the composite panel and as such can accurately measure the stress distribution in the region.

3.4.1 Panel Mesh

As described in Section 2, Panel I comprised a skin, reinforced edges, and was stiffened across its length and breadth with top hat and "Z" stiffeners. All geometric features of the replacement panel were modelled using quadrilateral shell elements. The panel mesh can be seen in Figure 19.

3.4.2 Panel Edge Joint

Modelling of the edge joint was performed in the same way as that done for the original panel sub-model. Refer to Section 3.3.5 for a description of this method.

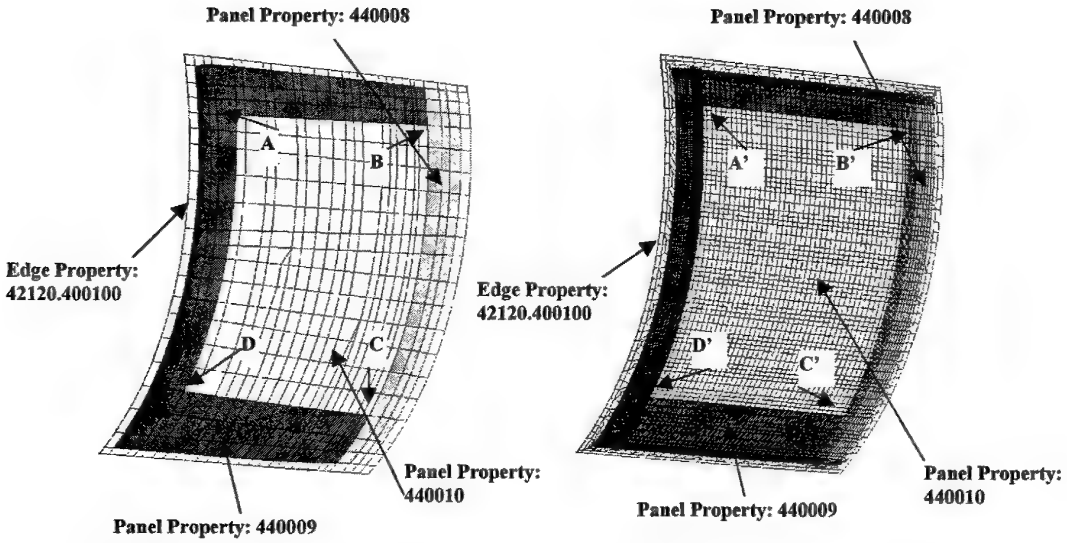

Node Location A: (525,-70,173)
Node Location B: (501,-70,173)
Node Location C: (501,-50,150)
Node Location D: (525,-50,150)

Node Location A': (527,-70,175)
Node Location B': (501,-71,175)
Node Location C': (501,-50,151)
Node Location D': (527,-50,149)

Note: All node locations are in the F-111C Global Coordinate System (GCS)

(a) (b)

Figure 18 Metallic panel property assignment in the (a) ILM and (b) refined model

Table 5 Property set description

Property Set	Description
42120.400100	Isotropic edge panel set. Defined using coordinate system 400100
440008	Isotropic honeycomb sandwich panel set. In-plane shear material ID = 400044 (Values in reference [10]).
440009	Isotropic honeycomb sandwich panel set. In-plane shear material ID = 400034 (Values in reference [10]).
440010	Isotropic honeycomb sandwich panel set. In-plane shear material ID = 400024 (Values in reference [10]).

3.4.3 Material and Property Definition

The composite material properties were input on a ply-by-ply basis for each of the elements within the panel model. The overall laminate behaviour was extrapolated from these laminae properties using classical laminate theory (CLT). CLT is a feature within the PATRAN/NASTRAN software suite that allows the user to both define the properties and then obtain the ply stresses and ply strains within a loaded structure.

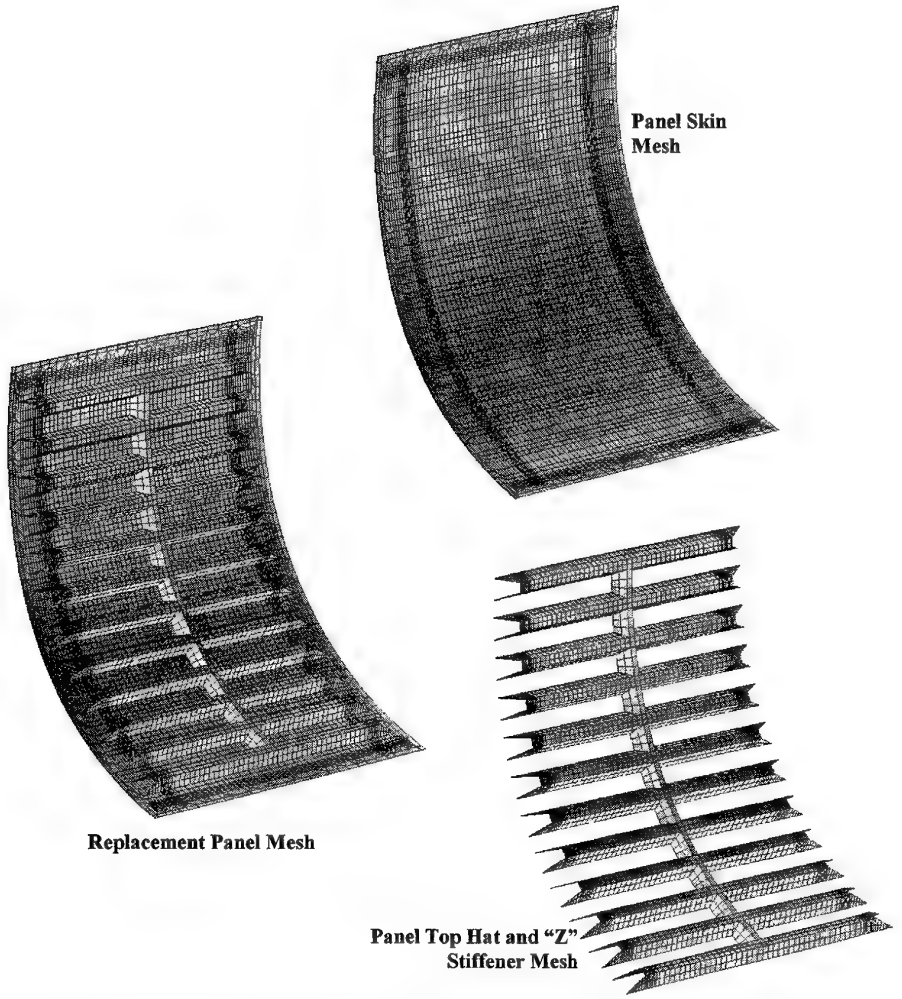

Figure 19 Replacement panel mesh showing the skin and stiffeners

As described in Section 2, Panel I was built up using mainly plies of carbon fibre fabric that were pre-impregnated with epoxy resin (prepreg). Various other materials were also used in the construction, but as they do not add a significant strength or stability benefit they were not included in the model. The laminae properties used for modelling the fabric prepregs were obtained by test and are shown in Table 6. The ply lay-up for each part of the panel was provided in Section 2.

The data shown in Table 6 is for the XMTM49-3 in the Room Temperature Dry (RTD) condition. This was used in the FE models because it is expected that these properties will not be significantly different in the Cold temperature Dry (CTD) conditions of the CPLT. The following evidence supports this argument:

Table 6 Carbon fibre fabric prepreg laminae properties

Property	Used	Reference
Elastic Modulus 11, E_{11} (psi)	8.77E6	11[1]
Elastic Modulus 22, E_{22} (psi)	8.77E6	[2]
Poisson Ratio 12, ν_{12}	0.06	12
Shear Modulus 12, G_{12} (psi)	5.70E5	11
Shear Modulus 23, G_{23} (psi)	5.70E5	11
Shear Modulus 13, G_{13} (psi)	5.70E5	11
CTE_{11} ($°F^{-1}$)	1.66E-6	13[3]
CTE_{22} ($°F^{-1}$)	1.66E-6	13[3]

Notes:

[1] Use average of RT tension and compression modulus

[2] Assume $E_{22} = E_{11}$

[3] Used average of measured values: CTE_{11} = 1.551E-6 $°F^{-1}$ and CTE_{22} = 1.764E-6 $°F^{-1}$

1. the tensile modulus of the fabric was the only elastic property that has been measured in the CTD condition. Reference [11] shows that $E_{11(CTD)} = 9.11 \times 10^6$ psi and $E_{11(RTD)} = 9.04 \times 10^6$ psi, a difference of only 0.77 %,

2. MIL-HDBK-17-2F [14] contains data for 22 carbon/epoxy composite systems at both the room temperature ambient (RTA) and cold temperature ambient (CTA = -54 °C) conditions. The relevant data for these systems is reproduced in Appendix B. Although XMTM49-3 undergoes a two-stage oven cure, it is an epoxy resin and final cure is conducted at the usual 177 °C, therefore it is expected that it will behave similarly to the materials described in Appendix C. For all of the data shown in Appendix B, the average elastic properties in the CTD condition were 1.095 that of the same property in the RTD condition.

3.5 Internal Loads Model Modifications

3.5.1 Transition Mesh

The analyses required refinement of the finite element mesh in the panel region. This region included the panel itself and a transition region. The transition region allowed the fine mesh models of the panels to be inserted directly into the sub-model of the surrounding structure. It extended from the panel edge for approximately three element lengths. The components that adjoin directly to the panel are shown in Figure 20. Also shown are the elements used to form the transition region.

Care was taken to ensure that the aspect ratio of all new elements were close to one. This ensured the mathematical integrity of the finite element model.

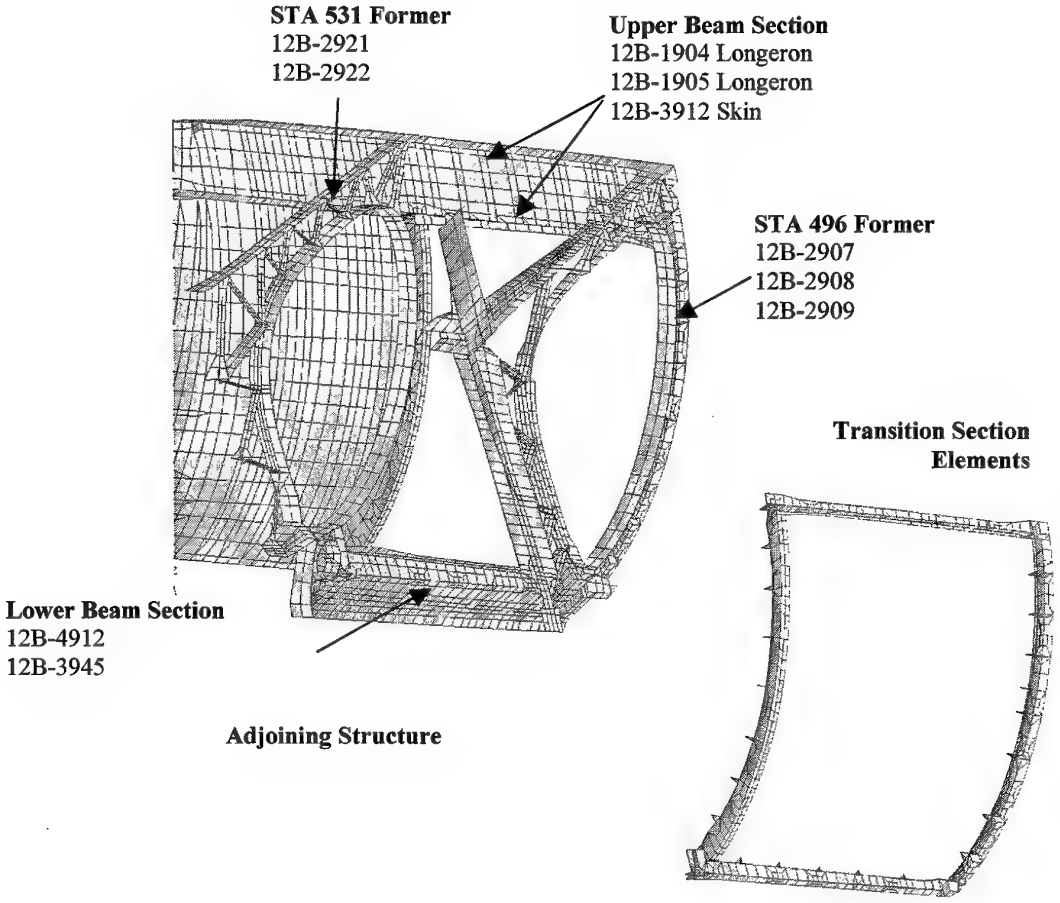

Figure 20 Components adjoining to Panel 3208 (Panel not shown) and the transition section elements

3.5.2 Thermal Stresses

The CPLT is conducted at -40 °C, therefore thermal stresses are introduced into the structure prior to any applied loading. This is due to differences in the CTE of the materials used to construct the F-111. The CTE of the materials used in the panel region and also the replacement panel CTE are provided in Table 7.

The lower the CTE of a material then the lower the amount that the material expands or contracts when the operating temperature changes from the reference temperature (which is usually room temperature). If two components made from materials with different CTE are connected, then there will be a force transfer when a temperature change is applied. In these cases, one component will try to restrain the other. Modifications were made to the

Table 7 CTEs for Panel I/Panel 3208 and adjoining structure

Part ID	Material	CTE ($°F^{-1}$)
12B4912 (Lower Beam)	D6ac Steel	6.2E-6
12B2921/12B2922 (STA 531 Former)	Aluminium 2024-T851	1.3E-5
12B1904 (Upper Longeron)	Aluminium 2024-T851	1.3E-5
12B2907/12B2908/12B2909 (STA 496 Former)	D6ac Steel	6.2E-6
Original Panel Skin	Aluminium 2024-T851	1.3E-5
Panel I	Refer to Table 6	

ILM to include the CTE in the material definitions. At present this modification has not been validated.

3.5.3 Equivalent Panel

The first part of the analysis required calculation, in the ILM, of the boundary node displacements that would be used as inputs for the sub-models. This was readily achieved for the metallic panel by simply running the ILM. An equivalent panel had to be developed to account for the different materials/configuration of Panel I. In this equivalent panel, the fine grid detail of the composite model was "collapsed" into a form that could be inserted into the ILM without requiring modification of the mesh.

An equivalent property set was created through modification to the fine grid replacement panel model. The effectiveness of the equivalent model was verified through a comparison of the panel edge displacements under compression and shear. The procedure used was:

1. to remove the stiffener mesh from the model of Panel I, leaving only the skin elements,

2. add extra plies to the central part of the skin mesh to account for the missing stiffeners,

3. convert the panel property definition into a form that included specific laminate stiffness values defining the linear anisotropic behaviour of the panel. These values were calculated from the ply lay-up and laminae property definitions of the equivalent panel.

   This conversion process was conducted using PATRAN. In this instance, the edge and the central region of the panel (Figure 21) were of interest. The outputs for each region was a PSHELL card that referenced three MAT2 cards. The PSHELL card defined the equivalent panel thickness and the distances from the neutral axis to the panel surface. The three MAT2 cards defined matrices that described the bending properties, transverse shear properties and the membrane-bending coupling properties of the panel respectively. The details of, and associated

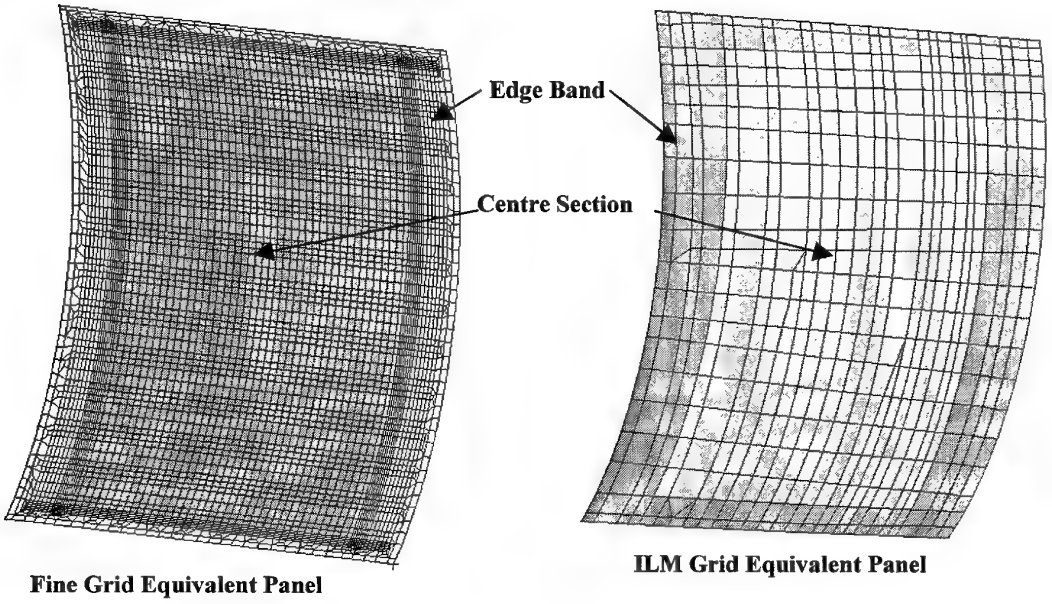

Figure 21 Equivalent replacement panel used for within the ILM

PSHELL and MAT2 cards for, the edge band and central region are shown in Appendix D,

4. verify that the equivalent panel edge displacements were identical to the fine grid replacement panel model under simple loading. The two panels were both loaded in compression and shear,

5. verify that the equivalent panel edge displaced identically to the fine grid replacement panel model under complex loading. The panels were both subjected to CPLT loading after being inserted into identical F-111 sub-models,

6. assign the property sets to the ILM elements (Figure 21).

3.6 Finite Element Analyses Test Matrix

Linear static and buckling finite element analyses were performed to verify the modelling techniques used and to obtain the margins-of- safety (MOS). As is described in Section 3.2, a sub-modelling technique was used to facilitate the efficient processing of all of the analyses runs required. The test matrix shown in Table 8 describes of all the finite element analyses runs that were performed.

4. Finite Element Analyses Results and Review

4.1 General

In Section 4 the analyses results from all sub-models, both with and without the effect of temperature, are provided and interpreted. The cases covered are:

- panel strength,
- sub-structure strength,
- fastener strength,
- sub-structure stability,
- panel stability.

4.2 Internal Loads Model Results

The ILM was used to generate grid point translations and rotations for each of the boundary nodes during CPLT loading. Four separate versions of the ILM were used to account for the different panels used and the thermal effects. 16 sets of grid point translation and rotations results were generated from the four ILM versions to account for each of the four CPLT load cases. These sets were input into the respective submodels as per the test matrix provided in Table 8.

4.3 Panel I Design Allowables

The design allowables for Panel I were derived from a series of tests designed to investigate the critical features of the full-scale panel. These test specimens were representative of the construction of Panel I, but also contained barely visible impact damage (BVID). This is the maximum damage size that may be present in Panel I during the CPLT. Tests were conducted at the coupon level in the RTD, elevated temperature wet (ETW) and CTD condition, and the design detail level in the RTD condition.

4.3.1 Coupons

4.3.1.1 Bearing allowables

Coupon level tests were conducted to establish the allowable joint strength of the notched laminate. These tests are described in full in reference [15] and summarised in this section.

With reference to Figure 22, the coupon was fabricated to represent the edge-band lay-up configuration of Panel I. The hole size and countersink dimensions and tolerances are the same as those in the metal panel for each fastener size used. MIL-HDBK-5F was used to determine the ultimate strength using the secondary modulus method. Table 9

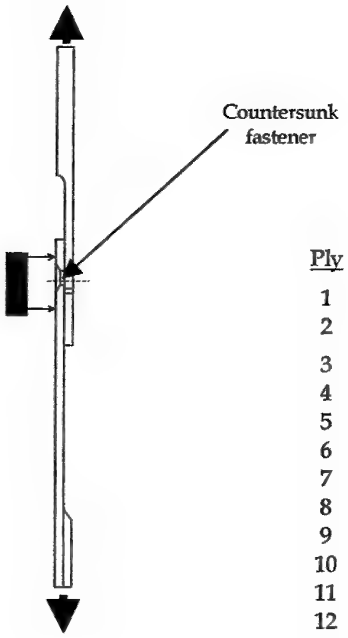

Ply	Material
1	Aluminium Mesh
2	Film Adhesive
3	Carbon Fabric
4	Carbon Fabric
5	Carbon Fabric
6	Carbon Fabric
7	Carbon Fabric
8	Carbon Fabric
9	Carbon Fabric
10	Carbon Fabric
11	Carbon Fabric
12	Carbon Fabric
13	Carbon Fabric
14	Carbon Fabric
15	Carbon Fabric
16	Carbon Fabric
17	Carbon Fabric
18	Carbon Fabric

Figure 22 Fastener joint strength test configuration and coupon lay-up

summarises the results derived for allowable joint strengths under elevated temperature wet (ETW) conditions.

No additional knockdown was applied to the bearing allowables to account for the -40 °C conditions in the CPLT because the measured ETW bearing allowables were expected to be very conservative. It is widely accepted that ETW conditions are critical for carbon/epoxy composites and that the ETW properties are typically substantially inferior to those at the CTD condition. It is argued that if the analysis, using the ETW joint allowables, predicts that the joints will not fail then it can be safely assumed that they will easily survive the CPLT.

4.3.1.2 Environmental knockdown factor

The design detail tests (Section 4.3.2) were conducted in the RTD condition. The allowables generated by these tests were factored by a CTD Knockdown Factor, as defined in Equation 1, to account for the CTD conditions in the CPLT.

Table 9 Summary of joint strength test results

Specimen	Joint Strength lbf (kN) Wet, 194 °F (90 °C)		
	ϕ 3/16 Titanium	ϕ 1/4 Titanium	ϕ 5/16 Steel
1	1956 (8.7)	2136 (9.5)	3316 (14.8)
2	1956 (8.7)	2653 (11.8)	3473 (15.5)
3	1911 (8.5)	2720 (12.1)	3867 (17.2)
4	2056 (9.1)	2608 (11.6)	3462 (15.4)
5	2012 (9.0)	2675 (11.9)	3507 (15.6)
6	1832 (8.2)	2720 (12.1)	3687 (16.4)
7	1877 (8.4)	2664 (11.85)	3619 (16.1)
8	-	-	3912 (17.4)
B-Basis value	1843 (8.2)	2450 (10.9)	3080 (13.7)
Weibull/Kolmogorov-Smirnov			

Equation 1

$$\text{CTD Knockdown Factor} = \frac{\text{property in CTD condition}}{\text{property in RTD condition}}$$

Three sets of tests were conducted on the XMTM49-3 fabric in the CTD condition [11]. The relevant data from these tests and the corresponding CTD Knockdown Factors are shown in Table 10. The critical CTD Knockdown Factor for XMTM49-3 fabric was selected as 0.904.

It is argued that this is conservative because the average of the ten strength based factors shown in Appendix B was 1.027, and only one discrete factor was lower than the selected 0.904 (0.890 for longitudinal tensile strength).

The selected CTD Knockdown Factor was applied to the critical allowable from the design detail tests (-4175 με from CAI tests (Table 11)) to produce a final design allowable of -3774 με.

Table 10 Data from tests conducted under RTD and CTD condition on XMTM49-3 fabric

Property	RTD	CTD	CTD Knockdown
Ultimate tensile strain (με)	13689	12380	0.904
Tensile strength (MPa)	878	801	0.912
Interlaminar shear strength (2003 test) (MPa)	55.3	60.8	1.099

4.3.2 Design Details

Two types of design detail specimens were tested, compression-after-impact (CAI) and shear-after-impact (SAI). These tests are reported fully in reference [16] and summarised in Section 4.3.2.

A drawing of the CAI specimen is shown in Figure 23. The details of the SAI specimens were identical, except that the skin was 25 mm wider around the periphery (total specimen size was 330 x 330 mm) to facilitate gripping in the test fixture. The specimens were loaded as indicated in Figure 24.

All specimens were impacted at critical locations (A and B in Figure 25) with sufficient energy to cause barely visible impact damage (BVID) at location B or stiffener flange disbonding at location A. Impacting was applied from the tool-side utilising a 5.6 kg (12.35 lb) mass with a 16 mm (0.63") diameter hemispherical steel tip. These locations were selected as critical because failure in large panels typically initiates from separation of the stiffener flange and skin near the end of the stiffener runout. Testing with BVID at these sites would verify the damage tolerance of the structure.

4.3.2.1 Compression-after-impact testing

Table 11 summarises the results derived from the CAI sub-component tests. A statistical analysis program based on the Weibull distribution was used to determine the B-basis allowable. The data from Specimen 1 was omitted from the calculation because the impact energy at location A was much lower than that of the remaining five specimens and the failure strain was correspondingly (artificially) high.

4.3.2.2 Shear-after-impact testing

Table 12 summarises the results derived for the SAI sub-component tests. A statistical analysis program based on the Weibull distribution was used to determine the B-basis allowable. Specimen 2 was omitted from the calculation of the B-basis value because the film adhesive used to co-cure the hat and intersecting "Z" section had passed its expiry date, leading to an artificially low strain-to-failure.

4.4 Panel Stiffness

The mechanical behaviour of Panel I was designed to match as closely as possible the behaviour of Panel 3208. However, the compromises inevitable from constructing the panel from a different material with a different construction have meant that differences will exist in the in-plane shear and axial stiffness properties.

The edge deflection during CPLT loading has been used to compare the relative stiffness differences between the metallic and composite panels. Plots of the panel edge displacement, at room temperature, have been generated for all CPLT loading cases. These

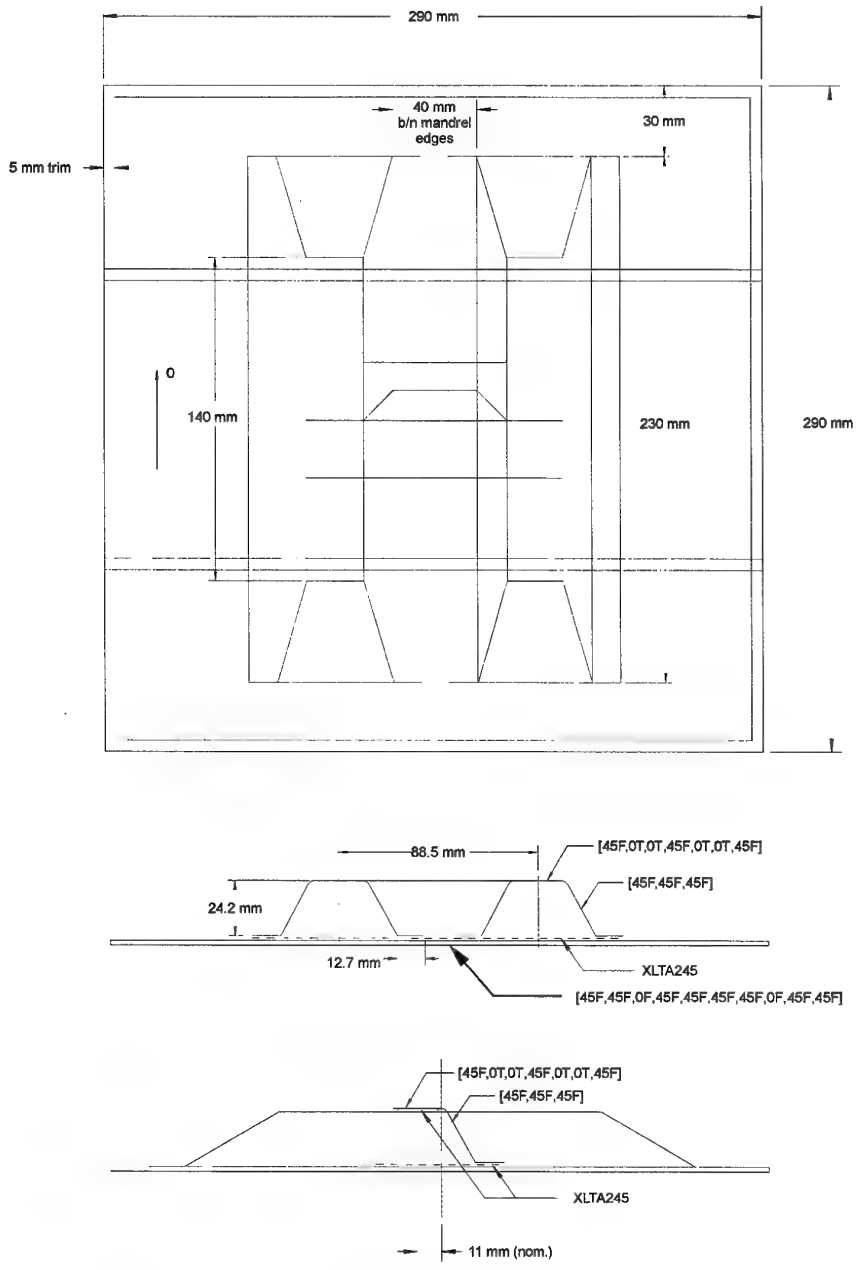

Figure 23 Compression-after-impact (CAI) specimen configuration

plots are provided in Figure 26 to Figure 29. There was almost negligible difference between the edge displacements of Panel 3208 and Panel I for all CPLT loadcases at this temperature. It was therefore concluded that the effect of Panel I, in terms of edge displacement, was not significant.

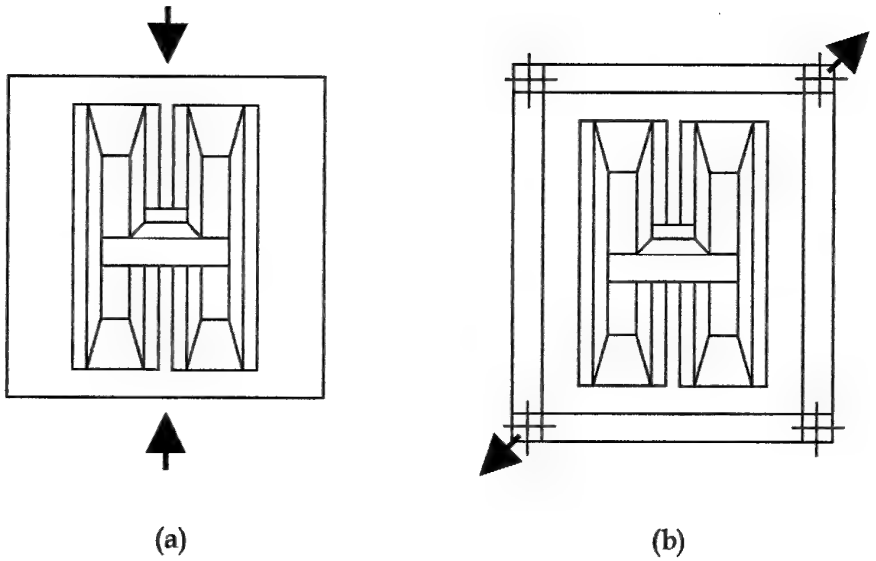

Figure 24 Direction of loading for (a) CAI and (b) SAI, sub-component specimens

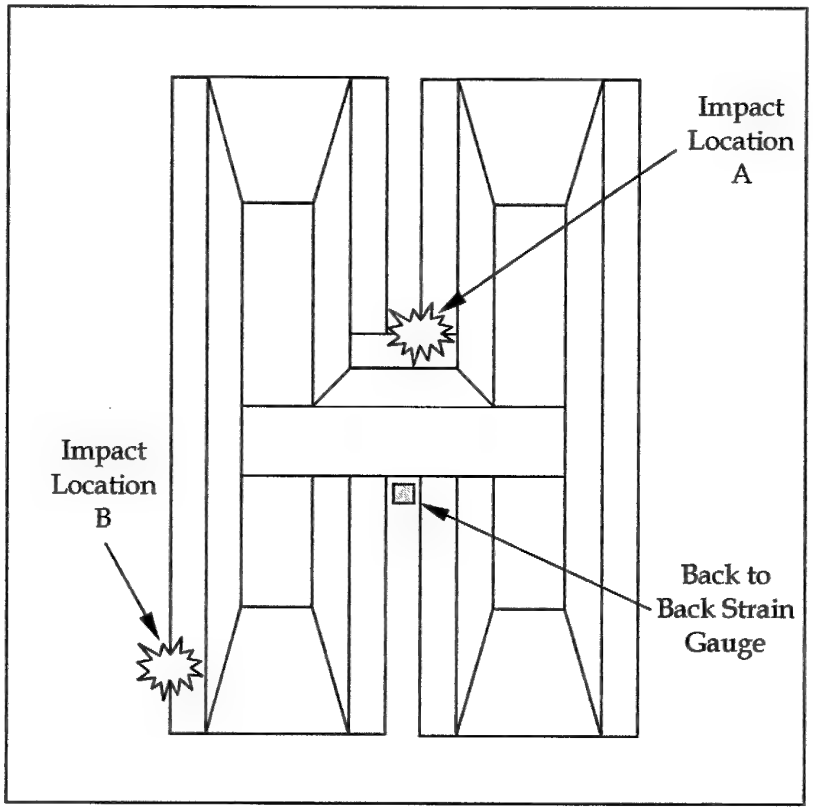

Figure 25 Impact sites for CAI and SAI sub-component specimens

Table 11 Summary of CAI test results

Specimen	Location A		Location B		Average 0° Failure Strain (με)
	Impact Energy (in-lb)	Dent Depth (inch)	Impact Energy (in-lb)	Dent Depth (inch)	
1	124	0.024	443	0.040	-6893
2	219	0.075	316	0.025	-5227
3	243	0.100	316	0.030	-4754
4	195	0.022	316	0.032	-5065
5	209	0.029	316	0.028	-5464
6	175	0.016	443	0.040	-5472
B-Basis value (Weibull/Kolmogorov-Smirnov)					-4175

Table 12 Summary of SAI test results

Specimen	Location A		Location B		Average 45° Failure Strain (με)
	Impact Energy (in-lb)	Dent Depth (inch)	Impact Energy (in-lb)	Dent Depth (inch)	
1	209	0.026	316	0.078	-4522
2	209	0.032	316	0.073	-3934
3	209	0.030	316	0.032	-4662
4	209	0.028	316	0.085	-4699
5	209	0.026	316	0.122	-4566
6	209	0.026	316	0.050	-4430
B-Basis value (Weibull/Kolmogorov-Smirnov)					-4207

Figure 30 to Figure 33 shows the magnitude of displacements in the panels during CPLT loading. Note that the scale for the metal and composite panel in each figure are identical, permitting direct comparison, however the scales on each figure vary because of the large difference in displacements in each of the CPLT loadcases. Again, it is clear that there was almost negligible difference between the panel displacements of metallic Panel 3208 and composite Panel I for each loadcase. It was therefore concluded that the effect of Panel I, in terms of panel displacement, was not significant.

4.5 Panel Strength

The panel strength was determined using the maximum strain failure criteria. The maximum allowable compressive strain of 3774 με (Section 4.3.1.2) was used for MOS calculations. A NASTRAN linear static analysis (SOL 101) was used to perform the analyses and produce the ply-by-ply failure ratios. The failure ratio (FR) and MOS were given by Equation 2 and Equation 3 respectively.

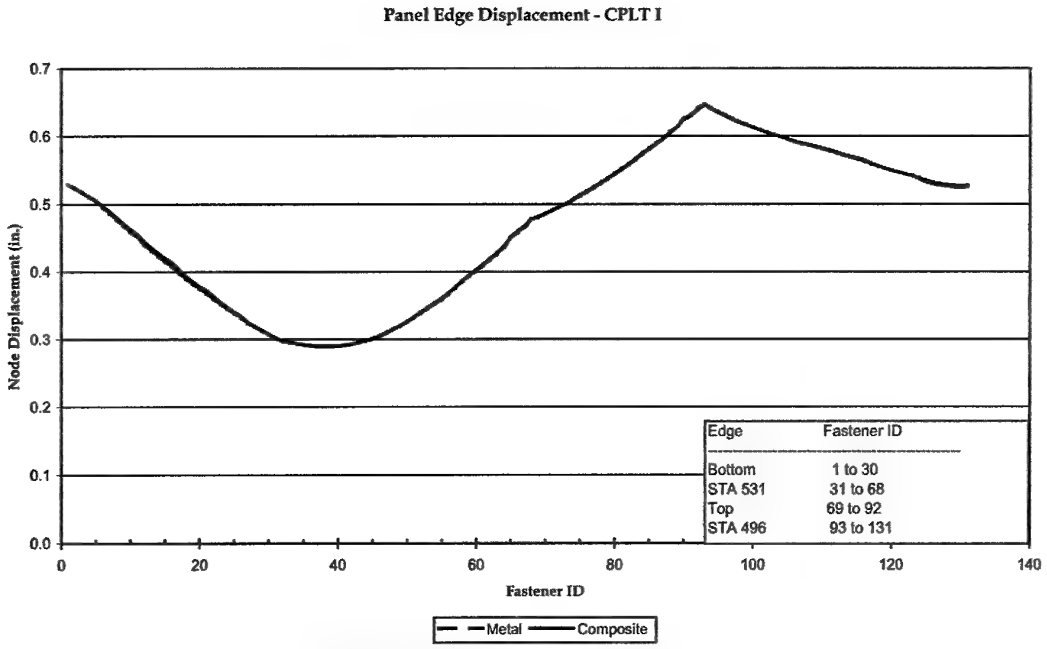

Figure 26 CPLT I panel edge displacement at 20 °C (68 °F)

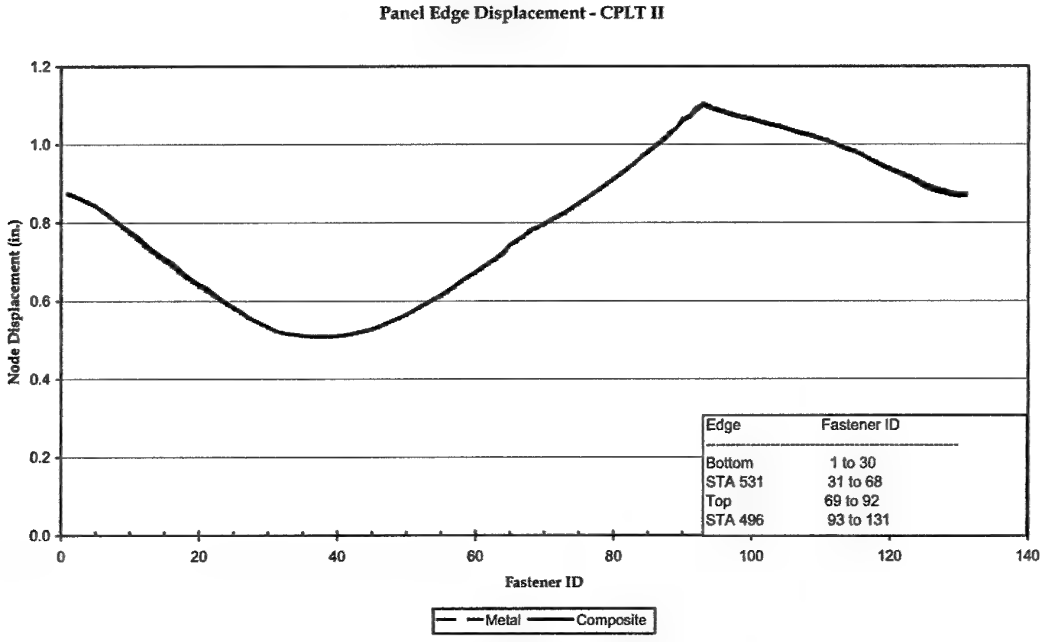

Figure 27 CPLT II panel edge displacements at 20 °C (68 °F)

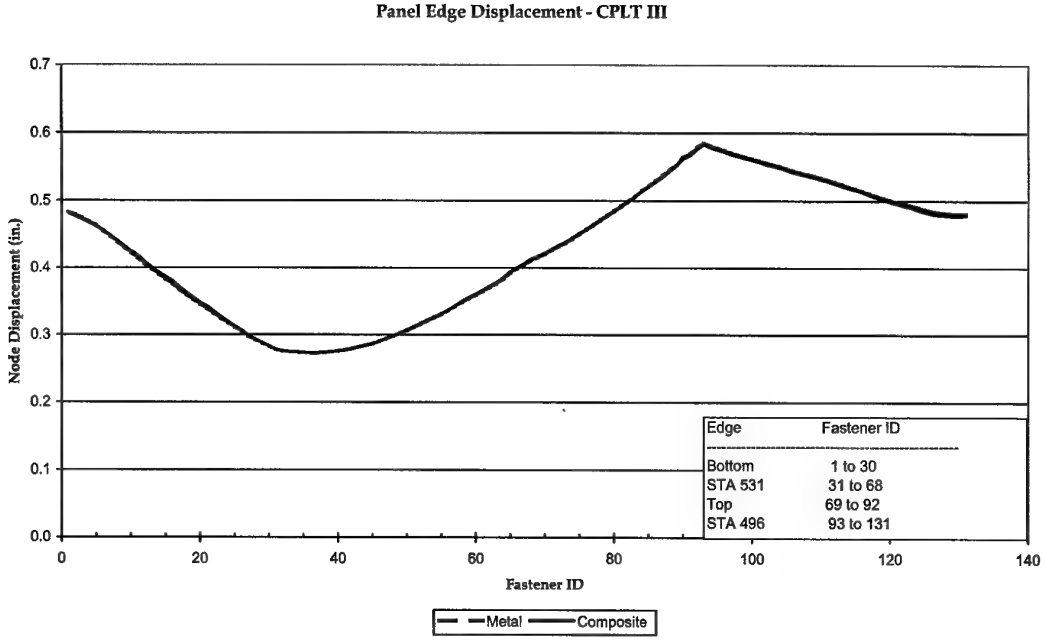

Figure 28 CPLT III panel edge displacements at 20 °C (68 °F)

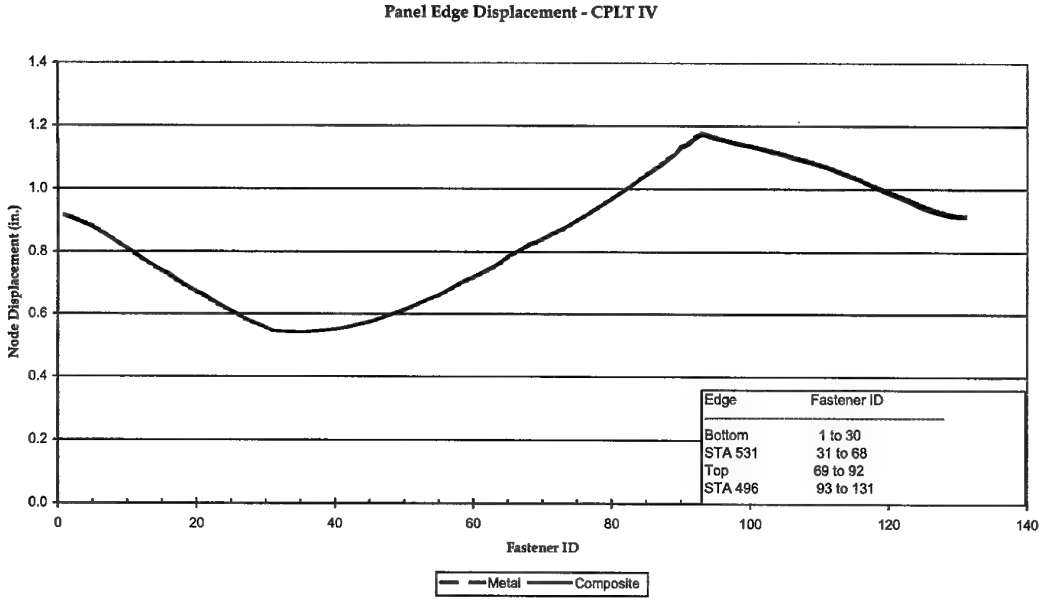

Figure 29 CPLT IV panel edge displacements at 20 °C (68 °F)

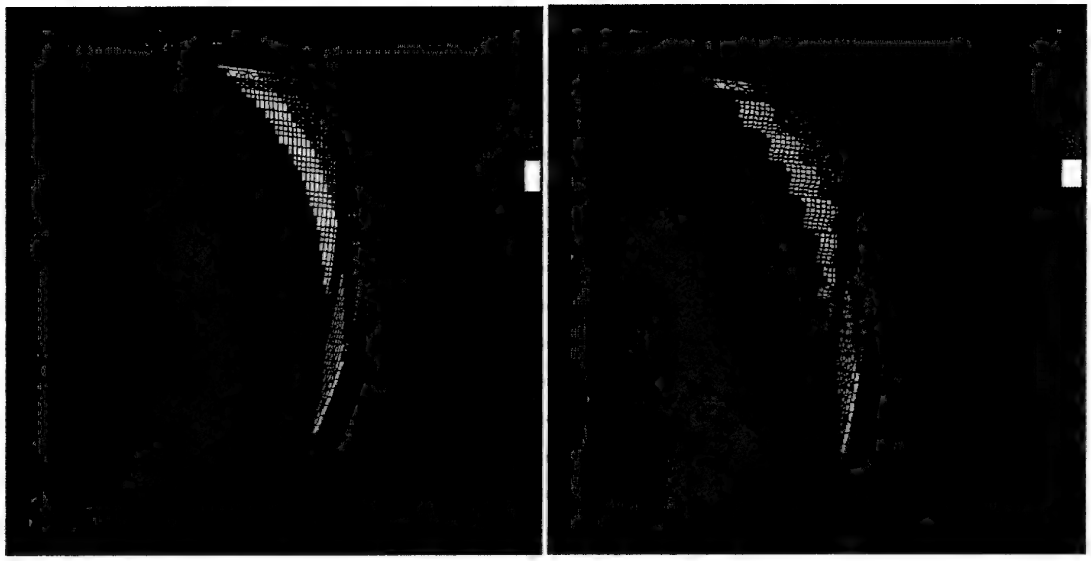

Metallic Panel Composite Panel

Figure 30 Panel displacement during CPLT I. The same colour scale is used for Figs 30-33

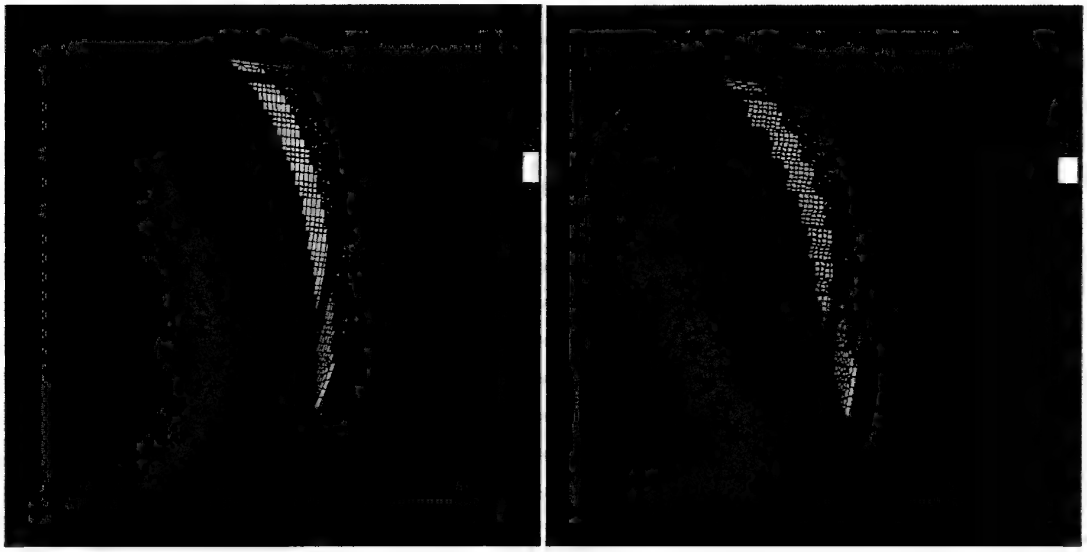

Metallic Panel Composite Panel

Figure 31 Panel displacements during CPLT II. The same colour scale is used for Figs 30-33

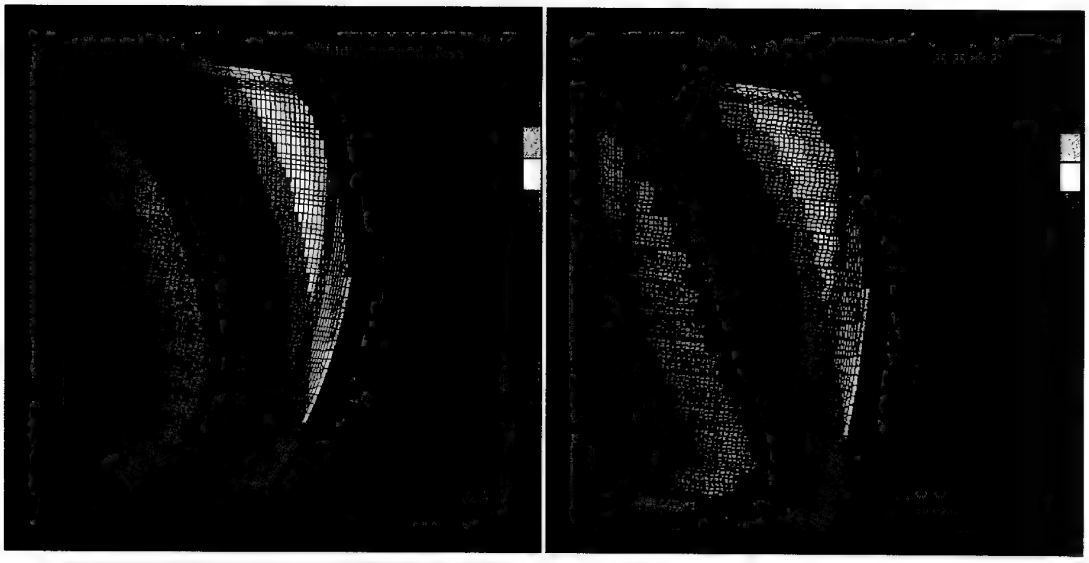

Metallic Panel Composite Panel

Figure 32 Panel displacements during CPLT III. The same colour scale is used for Figs 30-33

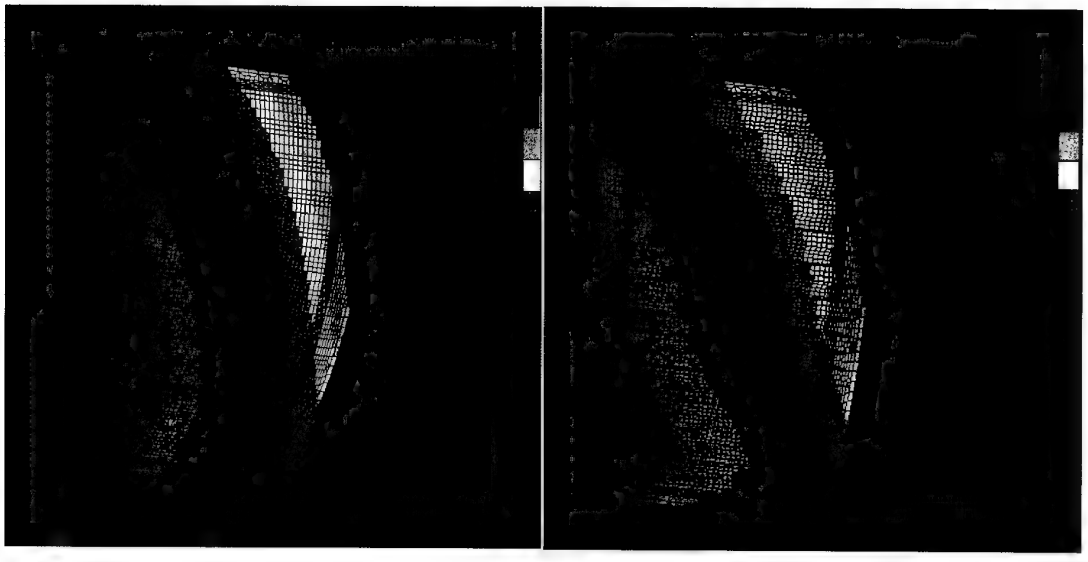

Metallic Panel Composite Panel

Figure 33 Panel displacements during CPLT IV. The same colour scale is used for Figs 30-33

Equation 2

$$FR = \frac{\varepsilon_{applied}}{\varepsilon_{allow}}$$

Equation 3

$$MOS = \frac{1}{FR} - 1$$

Where:

$\varepsilon_{applied}$ = Maximum ply strain under applied load

ε_{allow} = Allowable ply strain before first ply failure (= 3774 με)

As the thermal effects will influence the distribution of strains in the panel, plots showing the MOS distribution have been generated for each of the CPLT loadcases (CPLT I-IV) both with and without the temperature effects modelled. These plots are shown in Figure 34 to Figure 37. Note that the scale in each of these plots is the same with the margin of safety ranging from 0 (red) to 15 (blue). The minimum margin of safety and the element in which this occurs have been summarised in Table 13. Figure 38 indicates the location of the elements with the critical (minimum) MOS. In the worst case (CPLT II) the applied strain was still predicted as only 63 % of the allowable strain. These results show that the entire panel was predicted to have a large margin of safety for all CPLT loadcases.

4.6 Strength of the Surrounding Sub-Structure

The design of Panel I cannot match the stiffness of Panel 3208 in all directions and loading modes, therefore the transfer of load through the region was expected to change. To determine the effect of this change, the stresses in the surrounding structure during CPLT loading for Panel 3208 were compared with those for Panel I. As temperature will contribute to the load transfer pattern in the region, this was considered in the assessment also.

The surrounding structure that was considered is shown in Table 14. The yield stress for D6ac steel was obtained from reference [17] and Al 2024-T851 from reference [18].

Table 13 The critical MOS for Panel I

	Without Thermal Effects		With Thermal Effects	
Loadcase	MOS	Element	MOS	Element
CPLT I	1.72	1955977	1.24	1956079
CPLT II	0.60	1956079	0.58	1955977
CPLT III	3.74	1956079	1.95	1950950
CPLT IV	1.21	1956079	0.96	1955934

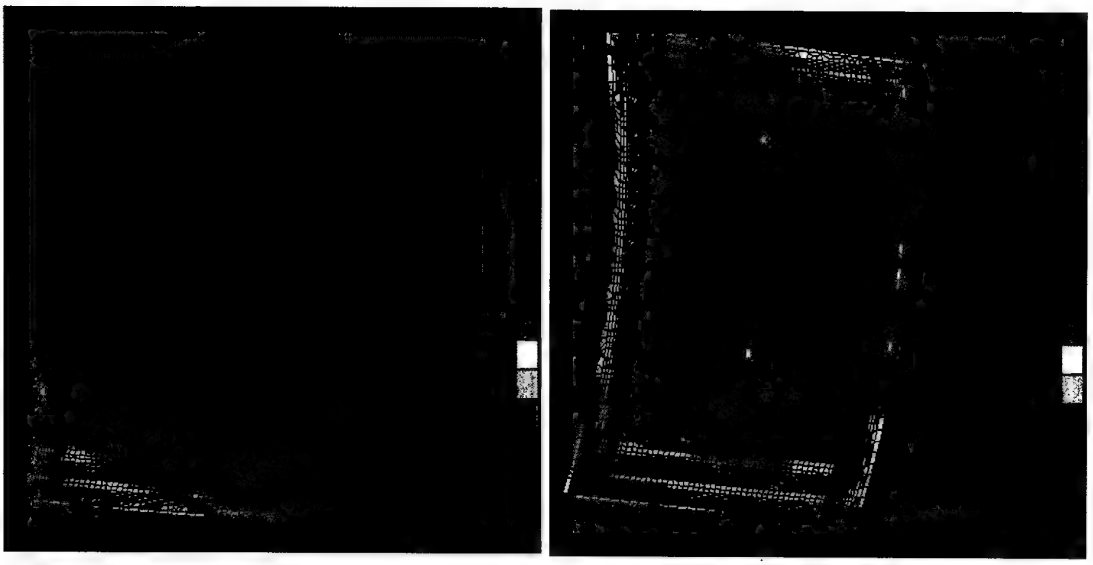

No Thermal Effects Thermal Effects Included

Figure 34 CPLT I MOS for Panel I. The same colour scale is used for Figs 34-37

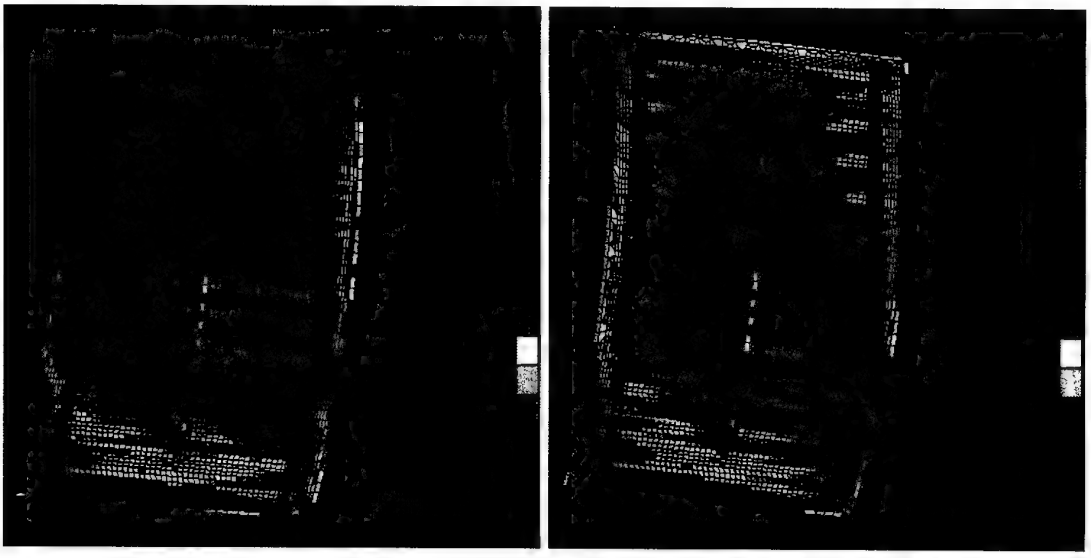

No Thermal Effects Thermal Effects Included

Figure 35 CPLT II MOS for Panel I. The same colour scale is used for Figs 34-37

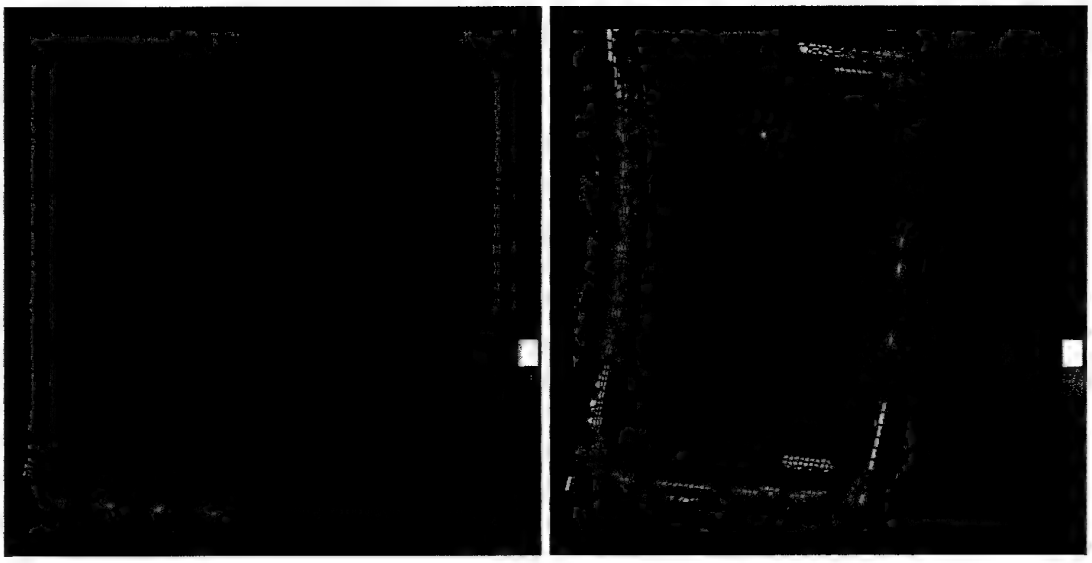

No Thermal Effects Thermal Effects Included

Figure 36 CPLT III MOS for Panel I. The same colour scale is used for Figs 34-37

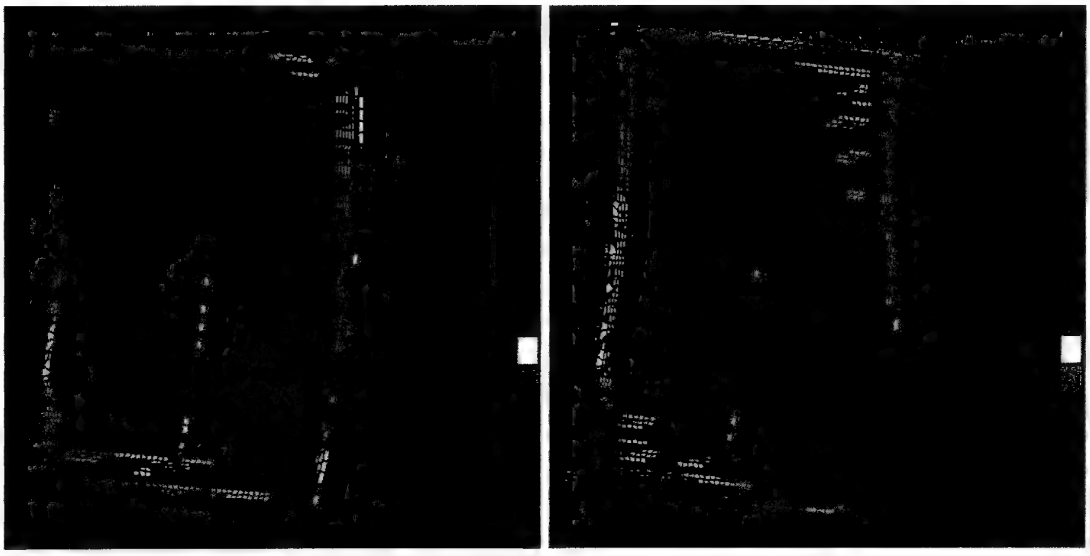

No Thermal Effects Thermal Effects Included

Figure 37 CPLT IV MOS for Panel I. The same colour scale is used for Figs 34-37

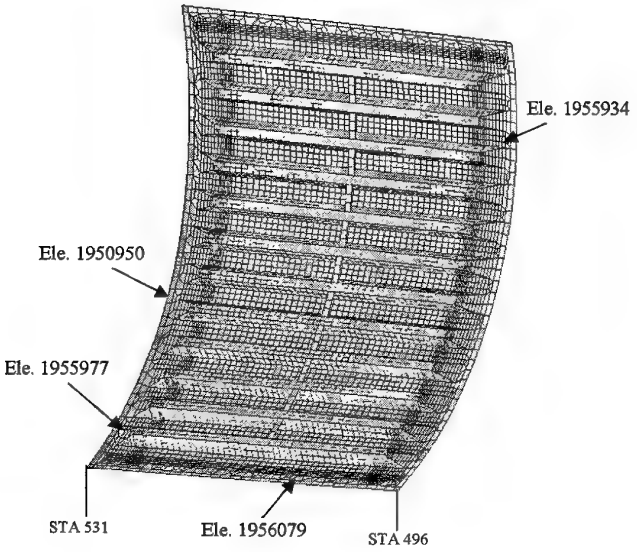

Figure 38 The Panel I fine mesh and elements with the critical MOS

Table 14 Sub-structure adjacent to Panel 3208/Panel I considered in strength analyses

Panel Edge	Component Part ID	Component Description	Component Material	Material Yield Stress (ksi)
Lower	12B-4912	Beam	D6AC 220-240	190
	12B-3945	Skin	17-7 PH Stainless Steel	190
STA 531	12B-2921	Former	Al 2024-T851	58
	12B-2922	Former	Al 2024-T851	58
Upper	12B-1904	Longeron	Al 2024-T851	58
	12B-1905	Longeron	Al 2024-T851	58
	12B-3912	Skin	Al 2024-T851	58
STA 496	12B-2907	Former	D6AC 220-240	190
	12B-2908	Former	D6AC 220-240	190
	12B-2909	Former	D6AC 220-240	190

Plots of the critical MOS for the surrounding sub-structure with Panel 3208 and Panel I, both with and without temperature effects, subjected to CPLT I-IV loading are provided in Figure 39 to Figure 42. The following may be concluded from these results:

1. the surrounding structure was not predicted to yield when either Panel 3208 or Panel I were installed,

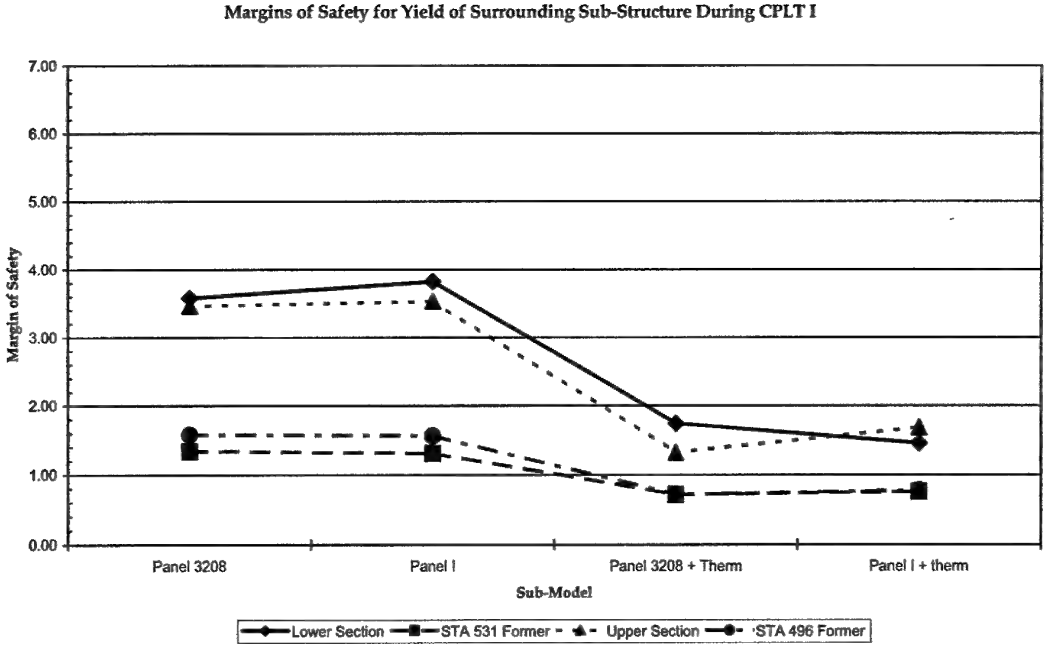

Figure 39 Yield MOS for the surrounding sub-structure during CPLT I

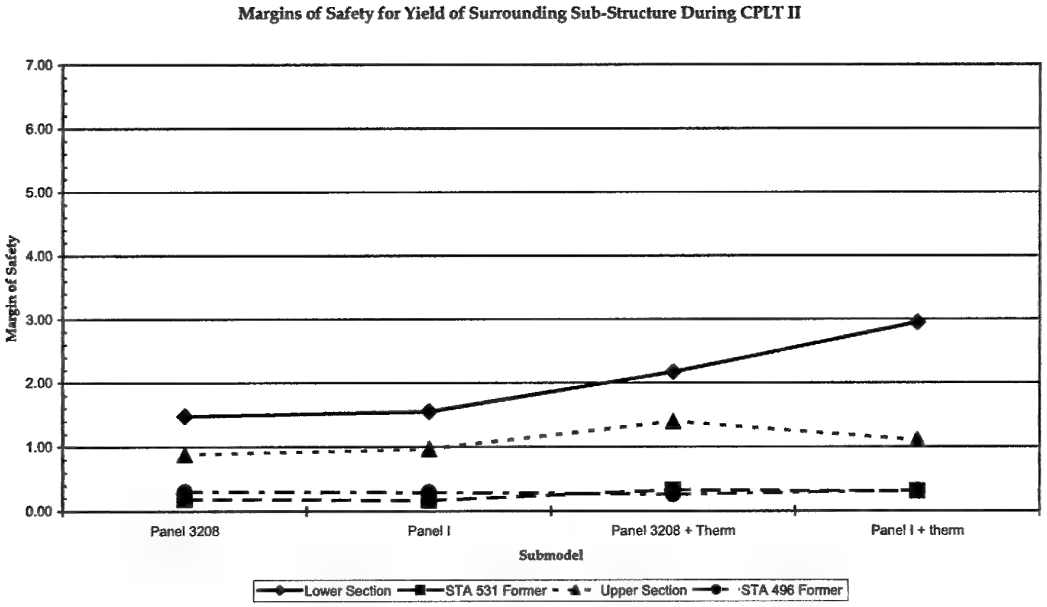

Figure 40 Yield MOS for the surrounding sub-structure during CPLT II

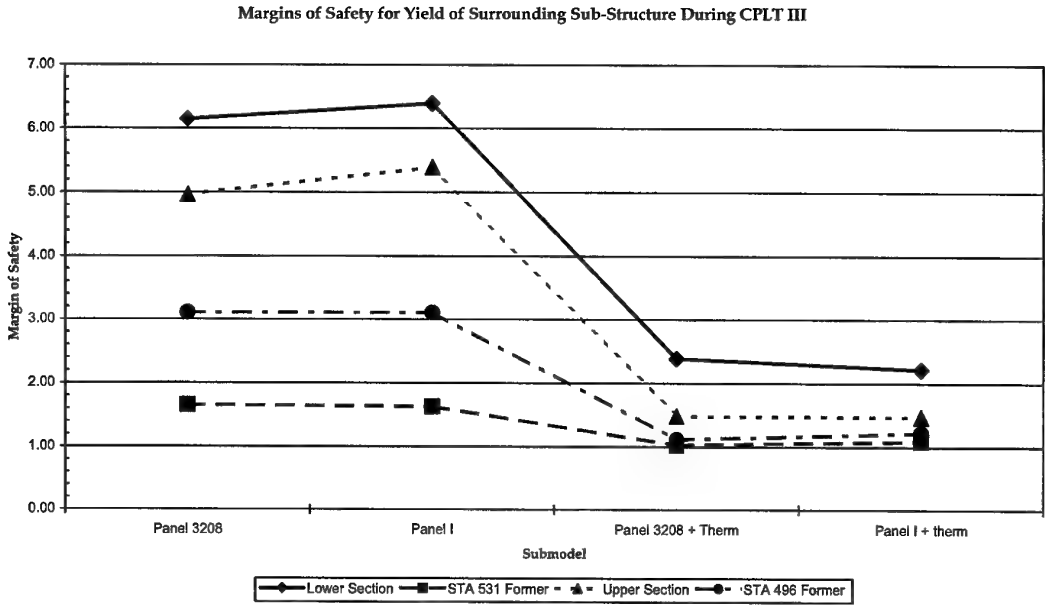

Figure 41 Yield MOS for the surrounding sub-structure during CPLT III

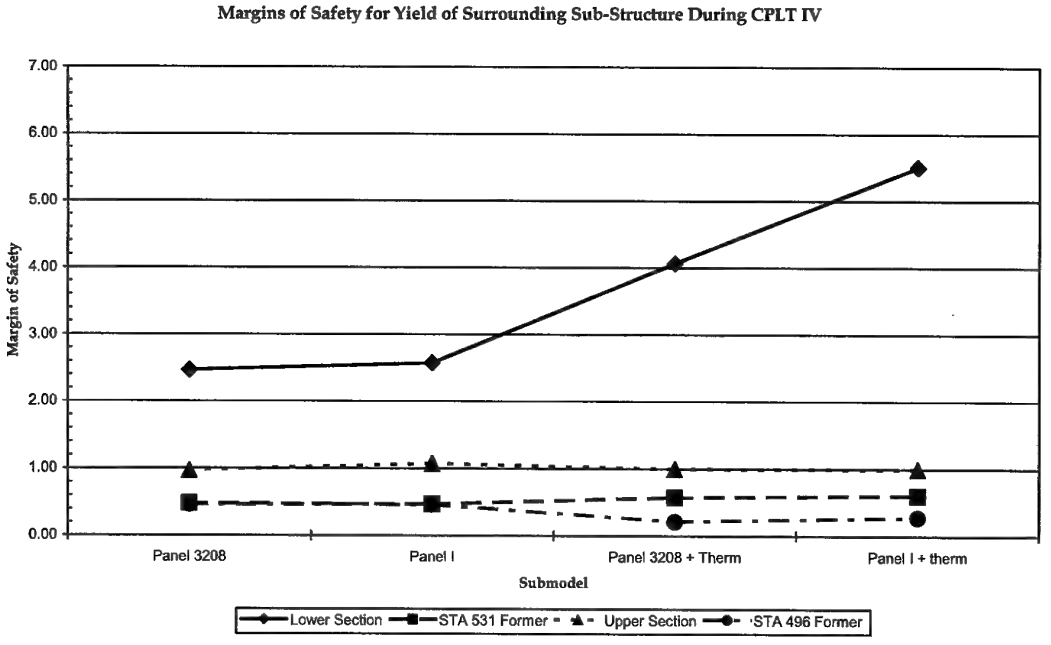

Figure 42 Yield MOS for the surrounding sub-structure during CPLT IV

2. in cases where the stresses were close to yield (low MOS), the effect of replacing Panel 3208 with Panel I was predicted to be negligible,

3. in areas where the stresses were close to yield (and in the majority of other areas) the effect of dropping the temperature to -40 °C on the MOS was predicted to be the same for Panel 3208 and Panel I,

4. in some areas where the stresses were not close to yield (lower section in CPLT I and CPLT III, upper section in CPLT III), the MOS in the surrounding sub-structure was predicted to be degraded. However, as the MOS were very high (1.5 to 4), these were not expected to adversely impact the structural integrity of these components.

4.7 Fastener Strength

The panel edge fasteners were required to have sufficient strength to transfer load to and from the panel into the surrounding sub-structure. Two methods exist for the prediction of the fastener load MOS.

The OEM calculations were based on an allowable edge load for each of the four panel edges. The applied edge load was compared against this allowable to determine the edge MOS. An alternate method utilised individual fastener allowable loads, which were compared with the applied fastener load distribution around the panel to yield a MOS for each fastener. Both methods have advantages and disadvantages and both have been used in this work.

As the load distribution around the panel edge will depend on the temperature, the MOS have been generated both with and without the effect of temperature included. As explained in Section 4.3.1.2, no knock-down factor was applied to the ETW edge joint allowables. The edge allowables were determined by multiplying the OEM fastener allowables [19] with the number of fasteners and are shown in Table 15.

Table 15 Fastener and panel edge allowable loads

Fastener ϕ (in.)	Fastener allowable (lb) from ref. [19]	Fastener quantity			
		Bottom edge	STA 531 edge	Upper edge	STA 496 edge
3/16	1843	21	33	23.5	38.5
1/4	2450	4.5	4	1.5	0
5/16	3080	4	0	0	0
Allowable edge load (lb)		62048	70619	46986	70956
Edge length (in)		35.43	45.00	35.43	45.00
Allowable edge load (lb/in)		1751	1569	1326	1577

The MOS for each of the four panel edges and for each sub-model and CPLT loadcases are shown in Figure 43 to Figure 46. The fastener load distributions are shown in Figure 47 to Figure 50 and the individual fastener MOS distributions in Figure 51 to Figure 54.

It can be concluded from these results that:

1. the MOS for all edges was predicted to be very high, even the STA 531 edge where Fastener 32 was located,

2. the MOS for most fasteners was predicted to be very high,

3. a negative margin of safety (-0.13) was predicted for Fastener 32 of Panel 3208 during CPLT I when thermal effects were considered. This fastener was located at the lower part of the STA 531 edge. This supports earlier statements that the ILM is conservative. Obviously the fasteners survive the CPLT when Panel 3208 is installed, yet the version of the ILM used in this work predicted a negative MOS. The MOS for the same fastener with Panel I in place was +0.73,

4. in general, the load distribution on Panel I fasteners was predicted to be more "peaky" than that for Panel 3208. Loads on the corner fasteners tended to be higher and loads in the middle of the edges tended to be lower, than their metal counterpart. This should not impact structural integrity because these peaks were predicted to be still well below the design allowable for the fasteners,

5. the fasteners attaching Panel I to the surrounding sub-structure were all predicted to have sufficient margins of safety.

4.8 Panel Stability

4.8.1 Sub-structure

Analyses were conducted to determine whether the surrounding sub-structure would buckle during the CRPSS. The existing sub-model was used for this analysis. It was recognised that the ILM mesh was relatively coarse and not suitable for detailed buckling analysis. Therefore any predictions regarding the stability of the surrounding sub-structure were treated with caution.

The mesh in the remainder of the sub-model would need to be refined by approximately the same amount as that for Panel 3208 and Panel I if conclusive stability results for the sub-structure were to be obtained. This refinement was not performed because it was judged that, because of the arguments presented in the remainder of Section 4.8.1, the sub-structure would not buckle during the CRPSS. The additional confidence that a more

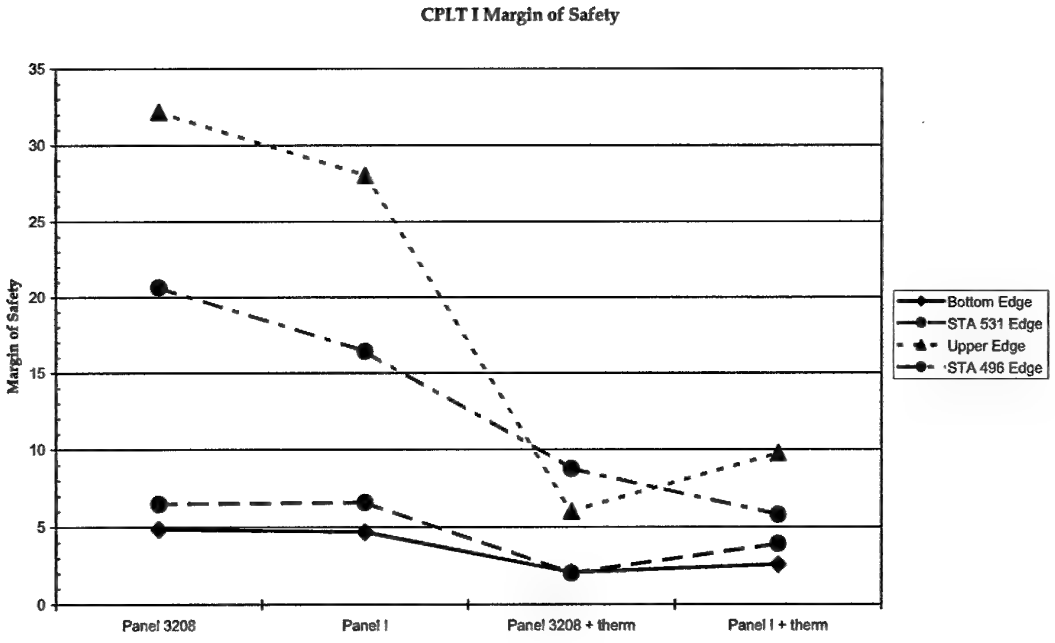

Figure 43 CPLT I edge MOS

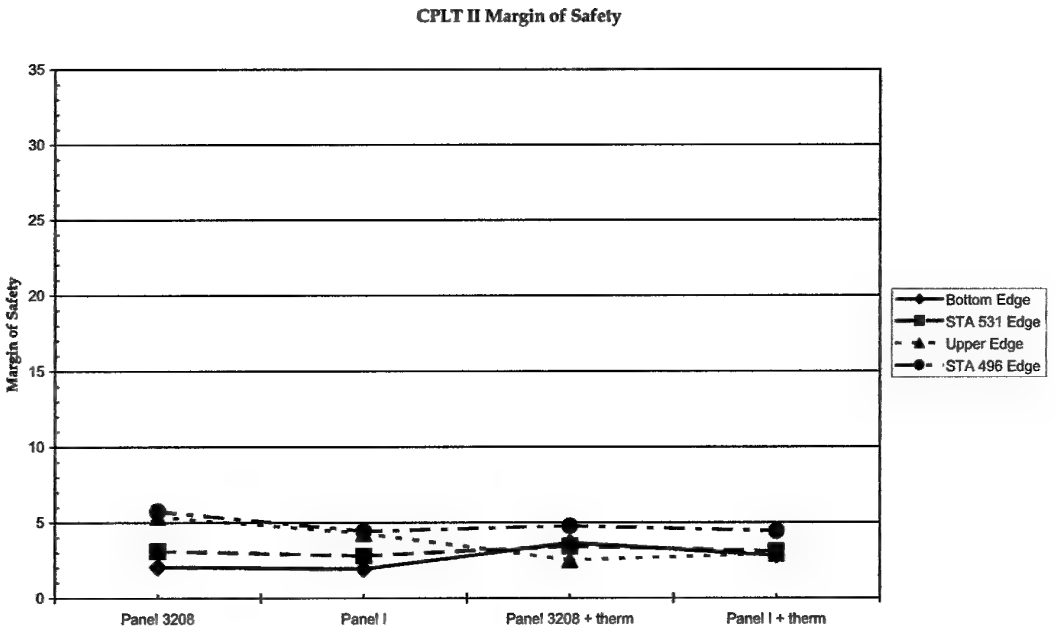

Figure 44 CPLT II edge MOS

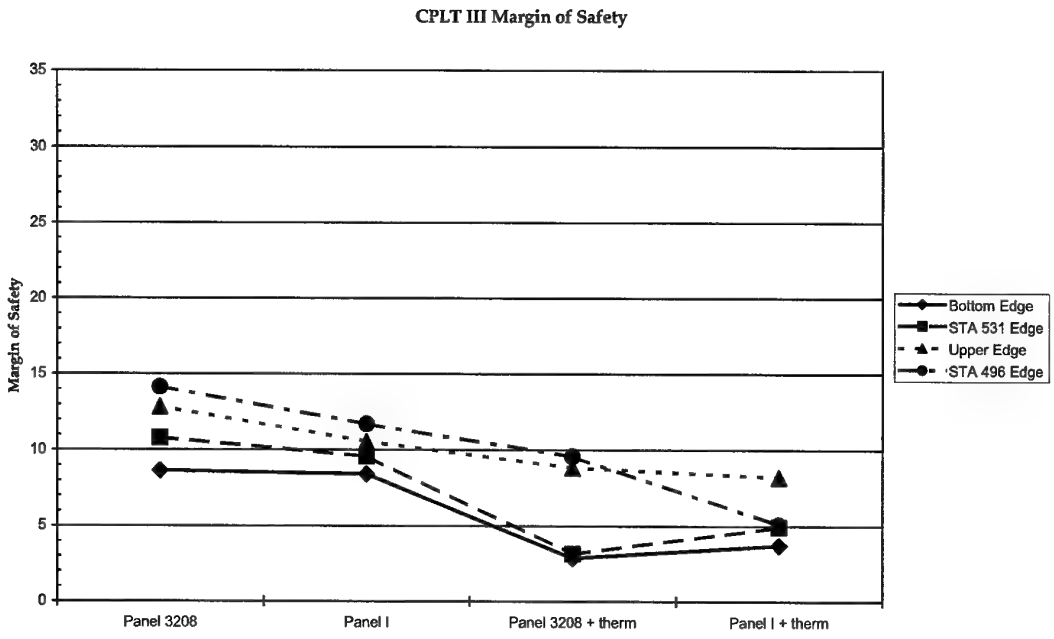

Figure 45 CPLT III edge MOS

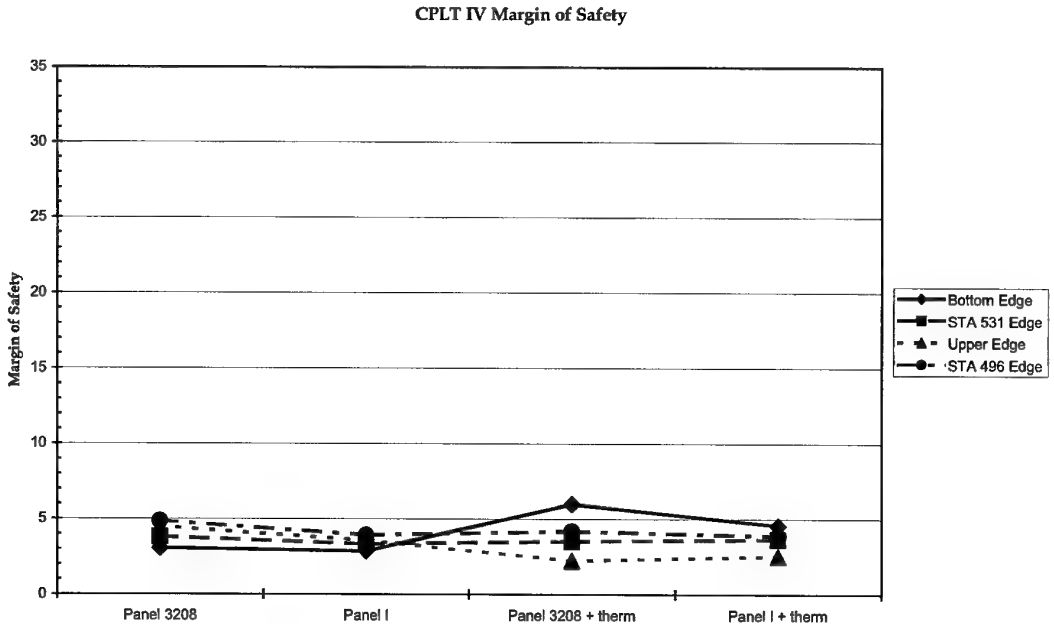

Figure 46 CPLT IV edge MOS

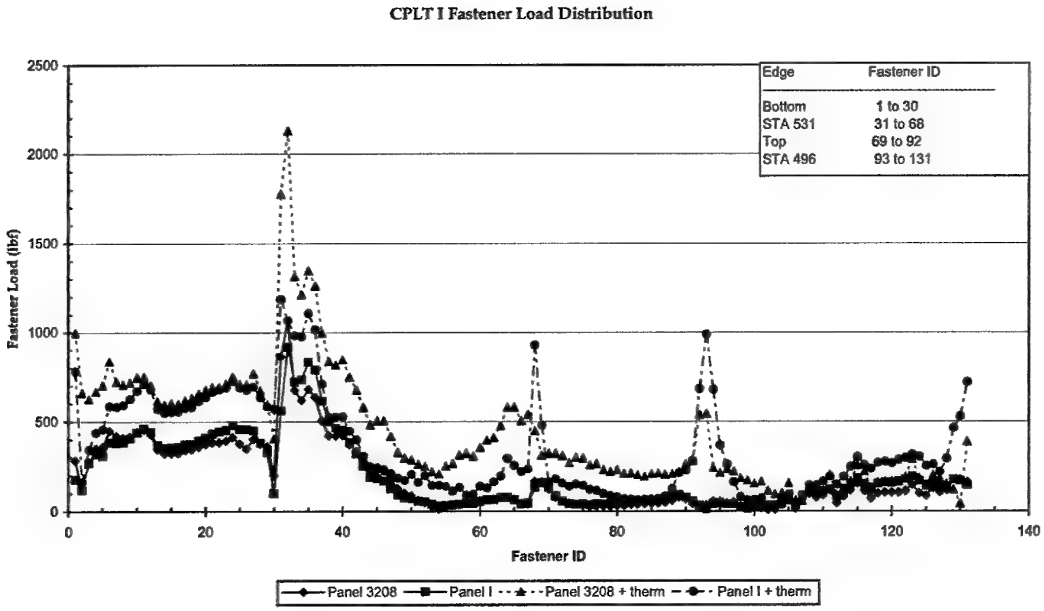

Figure 47 CPLT I fastener load distribution

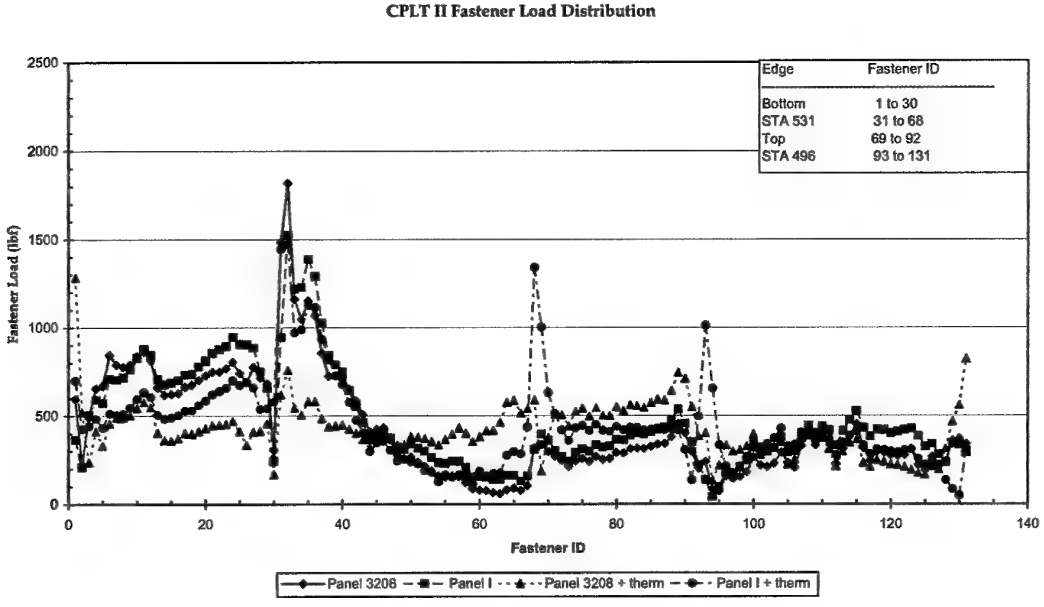

Figure 48 CPLT II fastener load distribution

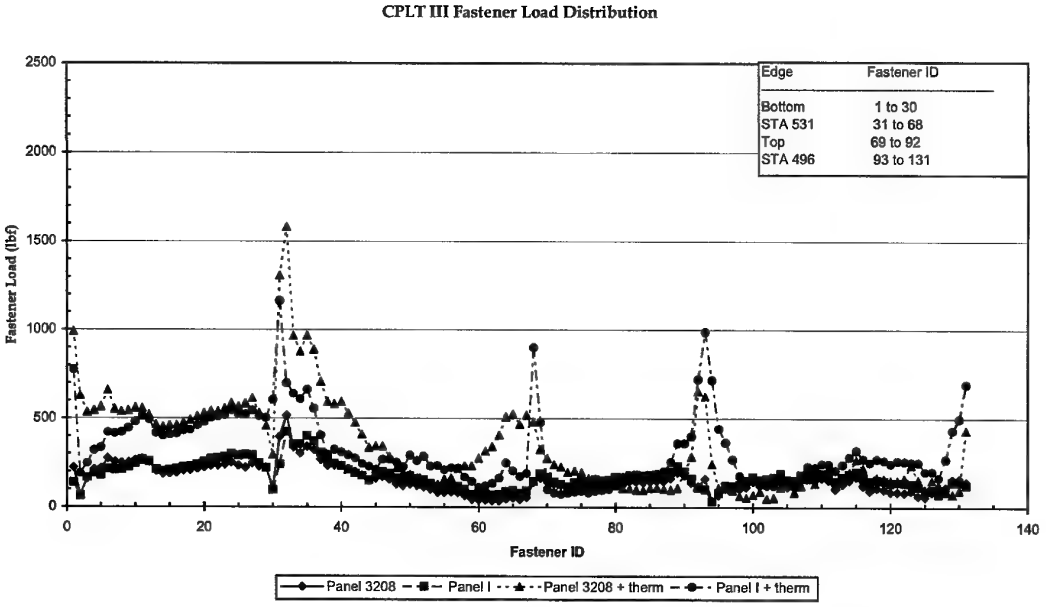

Figure 49 CPLT III fastener load distribution

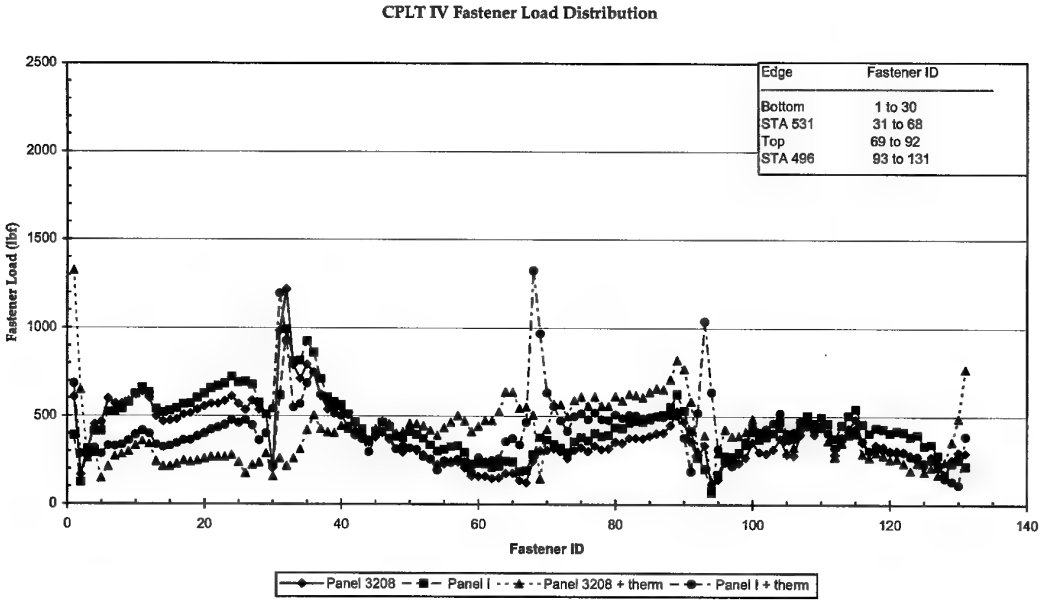

Figure 50 CPLT IV fastener load distribution

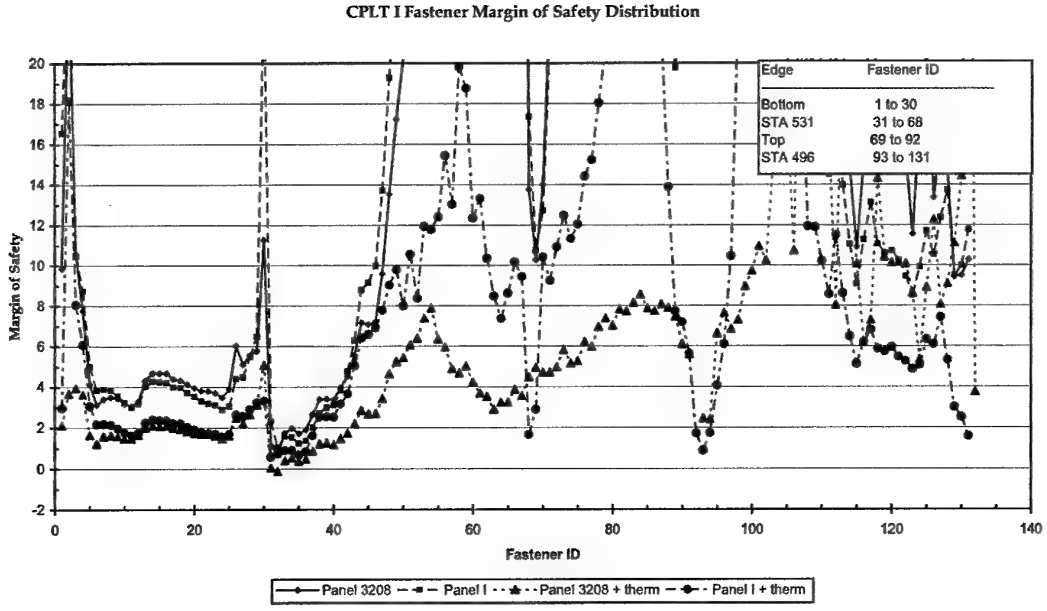

Figure 51 CPLT I fastener MOS distribution

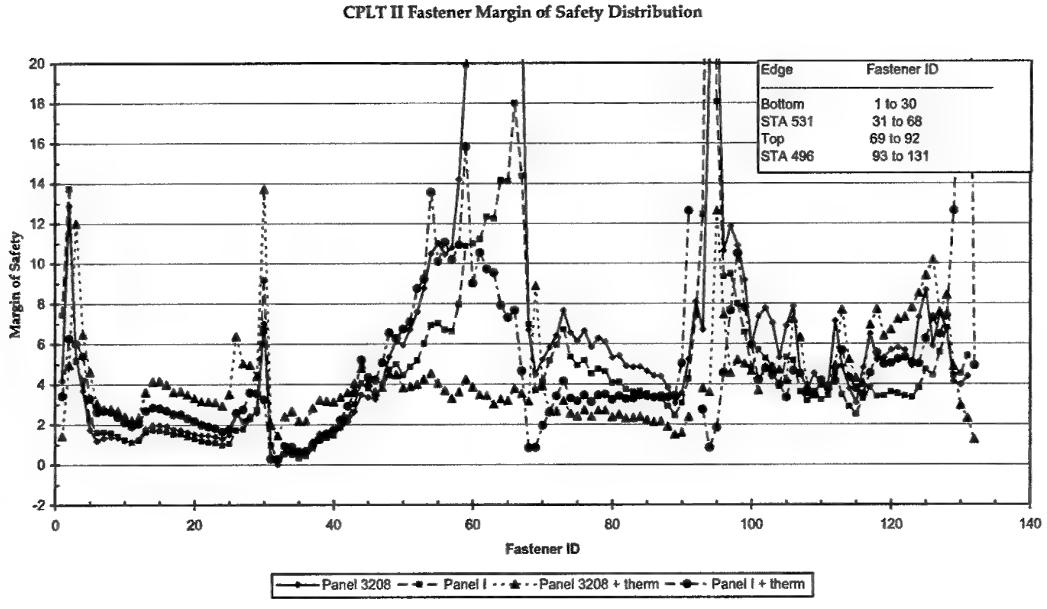

Figure 52 CPLT II fastener MOS distribution

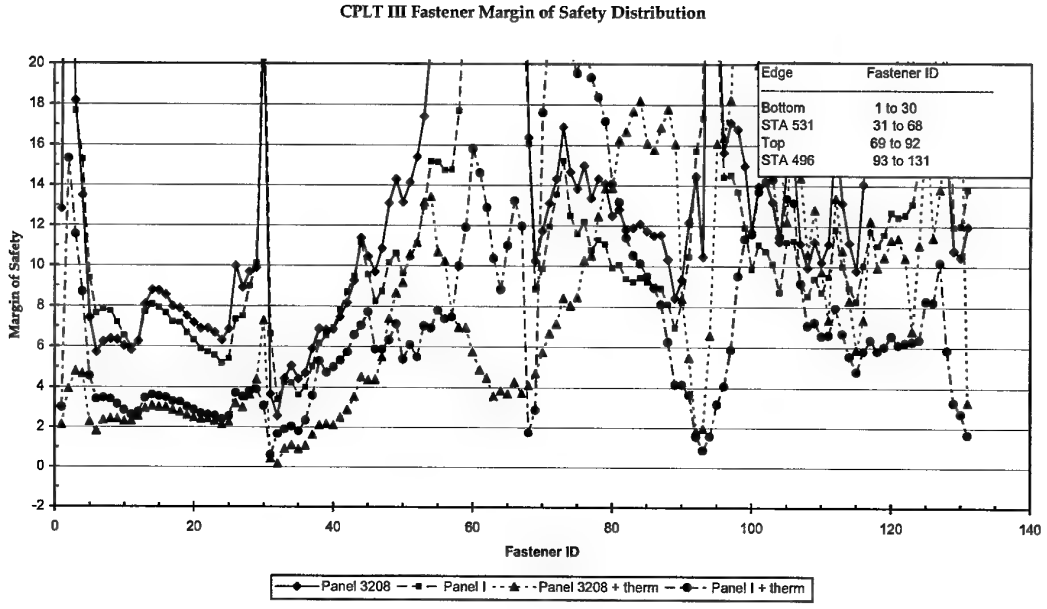

Figure 53 CPLT III fastener MOS distribution

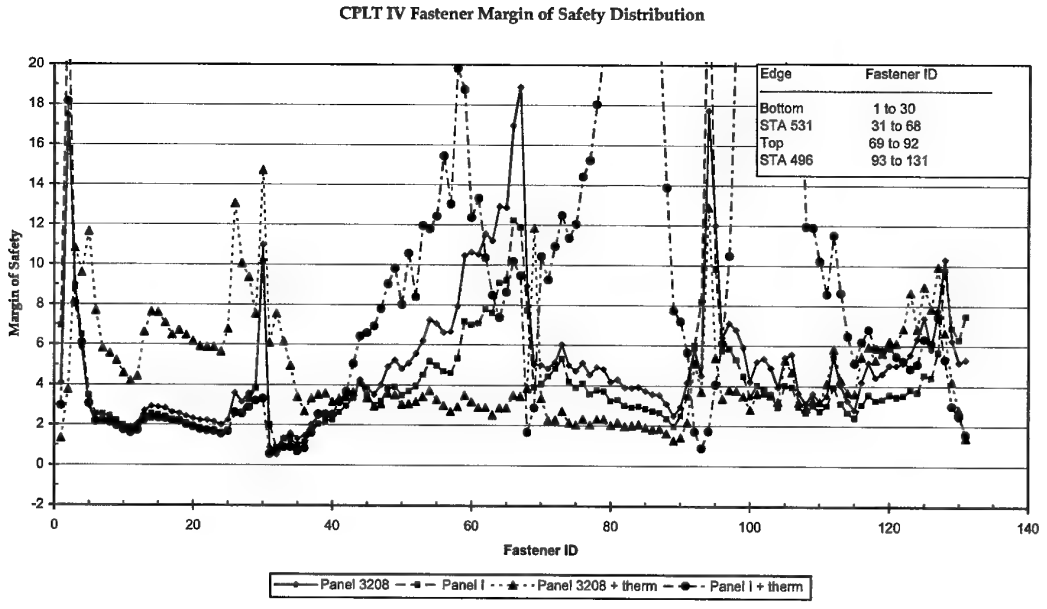

Figure 54 CPLT IV fastener MOS distribution

accurate sub-model would provide was not sufficient to justify the substantial cost and time delay in performing the refinement.

The first argument was qualitative and based on the observation that the load distribution through the surrounding sub-structure was not significantly different when either Panel 3208 or Panel I were installed (Section 4.4). Given that the real structure does not buckle during the CPLT then it can be expected that, likewise, the sub-structure would not buckle with Panel I installed during the CRPSS.

The second argument refers to an analysis of the instabilities predicted in the sub-model, at –40 °C, with both Panel 3208 and Panel I installed. The observations from this analysis are described in the following four paragraphs.

The results of the buckling analysis are summarised in Table 16. The eigenvalue for each buckling mode is the factor that the applied load must be multiplied to produce that buckling mode. A value less than 1.00 indicates that the buckling mode would occur at the analysis load. All eigenvalues up to 1.20 are reported, or the first eigenvalue if there were none below 1.20. The displacement corresponding to that buckling mode is also stated, as is the location of the buckled element. Each mode was categorised in accordance with the definitions provided at the foot of Table 16.

In all cases except one (Cat. = 3 in Table 16), the buckling modes in the sub-structure with Panel I installed were associated with an equivalent buckling mode in the sub-structure with Panel 3208 installed (Cat. = 1 and 4). The eigenvalues for these Cat. = 1 and 4 modes with Panel I installed were always larger that the associated mode with Panel 3208 installed. In addition there were some buckling modes predicted with Panel 3208 installed that were not predicted with Panel I installed (Cat. = 2). Both of these issues suggest increased stability with Panel I installed.

In only one case was a buckling mode predicted with Panel I installed for which there was no direct association with a Panel 3208 buckling mode (Cat = 3 in Table 16). It is likely (given the weight of evidence that suggests no buckling was predicted in the sub-structure), although it cannot be shown conclusively, that this difference in behaviour between the models was the result of the coarse ILM mesh and not a real prediction of buckling in the sub-structure during the CRPSS.

The final observation regarding Table 16 was that the real sub-structure survives CPLT loading without buckling, despite the large number of instabilities that were predicted by the sub-model with Panel 3208 installed. Obviously the prediction of instabilities in the sub-structure, with Panel 3208 installed, must therefore be conservative. Table 16 suggests that the sub-structure with Panel I installed was more stable than that with Panel 3208, further increasing confidence that the sub-structure will not buckle during the CRPSS.

Table 16 Comparison of the predicted eigenvalues for the sub-model, with Panel 3208 and Panel I installed, at CPLT temperature (-40 °C)

Mode		Eigenvalue		Max. Deflection (")		Buckled element		Cat.[2]
3208	I	3208	I	3208	I	No.	Part No.[1]	
CPLT I								
1	1	0.751	0.783	6.85E-1	6.86E-1	462477	12B1910-57 (upper longeron)	1
CPLT II								
1	1	0.280	0.340	6.11E-1	6.12E-1	463527	12B4912 (lower beam)	1
2	2	0.325	0.401	2.84E-1	2.37E-1	2009978	12B4912 (transition)	1
3		0.407		8.16E-1		463534	12B4912	2
4	3	0.433	0.506	1.00E0	7.33E-1	463449	"	1
	4		0.528		9.36E-1	463520	"	2
5	5	0.478	0.581	7.93E-1	5.15E-1	463541	"	1
6	6	0.543	0.661	7.89E-1	8.05E-1	463443	"	1
7		0.587		8.20E-1		463449	"	1
	7		0.724		5.88E-1	462236	12B1910-53 (Upper longeron)	3
8	8	0.631	0.747	2.80E-1	2.93E-1	2009973	12B4912 (transition)	1
9	9	0.739	0.783	5.13E-1	1.00E0	463449	12B4912	1
	10		0.784		3.76E-1	2007264	Panel I – S1 (lower)	5
	11		0.822		5.05E-1	2007254	Panel I – S2	5
10	12	0.835	0.843	6.60E-1	6.65E-1	462477	12B1910-57	1
	13		0.892		3.68E-1	2007244	Panel I – S2	5
11		0.941		5.03E-1		463548	12B4912	2
	14		0.947		7.63E-1	463449	"	4
	15		0.956		5.06E-1	2007274	Panel I - S1	5
	16		1.014		5.04E-1	2007234	Panel I – S3	5
	17		1.032		3.70E-1	2007992	Panel I – S11	5
12		1.066		5.75E-1		462236	12B1910-53	2
	18		1.068		4.92E-1	2008002	Panel I – S10	5
	19		1.072		3.72E-1	2008032	Panel I – S9	5
	20		1.077		4.84E-1	2007064	Panel I – S11	5
	21		1.096		3.74E-1	2007074	"	5
	22		1.102		3.95E-1	2007054	Panel I – S12 (upper)	5
	23		1.108		4.93E-1	2008022	Panel I – S9	5
	24		1.112		3.01E-1	2007265	Panel I – S1	5
	25		1.115		4.00E-1	2007972	Panel I – S12	5
	26		1.134		3.49E-1	2008012	Panel I – S10	5
	27		1.143		4.02E-1	2007255	Panel I – S2	5
13		1.147		8.10E-1		2009972	12B4912	2
	28		1.185		4.91E-1	2007094	Panel I – S10	5
CPLT III								
1	1	0.753	0.785	6.93E-1	6.94E-1	462477	12B1910-57	1

...continued

...continued

Table 16 Comparison of the predicted eigenvalues for the sub-model, with Panel 3208 and Panel I installed, at CPLT temperature (-40 °C)

Mode		Eigenvalue		Max. Deflection (")		Buckled element		Cat.[2]
3208	I	3208	I	3208	I	No.	Part No.[1]	
CPLT IV								
1	1	0.435	0.607	6.07E-1	6.08E-1	463527	12B4912	1
2		0.511		2.74E-1		2009978	"	2
	2		0.719		2.36E-1	2009979	"	4
3		0.638		8.08E-1		463534	"	2
4		0.668		1.00E0		463449	"	2
5		0.744		7.58E-1		463541	"	2
6	3	0.770	0.778	6.59E-1	6.63E-1	462477	12B1910-57	1
	4		0.789		5.85E-1	462236	"	4
7		0.847		7.31E-1		463443	12B4912	2
8	5	0.920	0.905	6.04E-1	7.71E-1	463449	"	1
	6		0.947		9.96E-1	463520	"	4
9		0.974		3.33E-1		463443	"	2
	7		0.977		3.71E-1	2007992	Panel I - S11	5
	8		0.991		3.75E-1	2007264	Panel I - S1	5
	9		1.023		4.00E-1	2007972	Panel I - S12	5
	10		1.024		4.93E-1	2008002	Panel I - S10	5
	11		1.036		5.00E-1	463541	12B4912	4
	12		1.051		5.04E-1	2007254	Panel I - S2	5
	13		1.053		3.72E-1	2008032	Panel I - S9	5
	14		1.090		4.94E-1	2008022	"	5
	15		1.092		3.50E-1	2008012	Panel I - S10	5
	16		1.117		4.79E-1	2007064	Panel I - S11	5
10		1.137		5.70E-1		462236	12B1910-53	2
	17		1.137		3.75E-1	2007074	Panel I - S11	5
	18		1.146		3.68E-1	2007244	Panel I - S2	5
	19		1.148		3.95E-1	2007054	Panel I - S12	5
11		1.166		5.15E-1		463527	12B4912	2
	20		1.190		7.56E-1	463443	"	4
	21		1.196		5.05E-1	2007274	Panel I - S1	5

Notes

[1] The nn on parts labelled "Panel I - Snn" indicates the stiffener number on Panel I. Stiffener 1 was the upper stiffener and 12 the bottom.

[2] Cat. = 1 Identical element predicted to buckle with both Panel 3208 and Panel I installed

Cat. = 2 Element predicted to buckle with Panel 3208 installed but not Panel I (i.e. sub-model is more stable with Panel I than Panel 3208)

Cat. = 3 Element predicted to buckle with Panel I installed but not Panel 3208 (i.e. sub-model is more stable with Panel 3208 than Panel I)

Cat. = 4 Element predicted with Panel I installed but not Panel 3208. Likely that this mode is the same as that predicted for a nearby element with Panel 3208 installed

Cat. = 5 Element located in the runout of a stiffener web in Panel I is predicted to buckle. Cannot be compared with case for Panel 3208. See Section 4.8.2 for discussion.

4.8.2 Panel I

Buckling predictions for Panel I during the CPLT were made using the sub-model. These predictions were considered reasonable because the mesh was sufficiently fine (approximately one order of magnitude finer than the remainder of the ILM).

The results of the stability analysis on Panel I are reported in Table 17 and Table 18. Details are given for the most highly buckled element in the sub-model and Panel at each of the buckling modes. In all room temperature modes, modes [1-9, 12, 14] for CPLT II at -40 °C and modes [1-6, 11, 20] for CPLT IV at -40 °C), the critical element was located in the sub-structure. The Panel (3208 or I) was predicted to deflect simply because it was fastened to the sub-structure. These modes were ignored because the buckling modes were not associated with Panel I and, as stated in Section 4.8.1, the accuracy of buckling predictions in the ILM mesh was not reliable.

The remaining eigenvalues that were below 1.00 were the higher modes in CPLT II and CPLT IV at -40 °C. Here the webs at the end of stiffener runouts were predicted to become locally unstable. Buckling of stiffener run-outs has been reported during the proof-of-structure testing of a large curved composite panel with features identical to that of Panel I [20]. In that case the buckling did not limit the load carrying capability of the specimen and failure occurred at the impact sites remote from these buckles. It was therefore concluded that these local effects will not adversely impact the structural integrity of Panel I or the surrounding sub-structure.

4.9 Strain Prediction

The aircraft on which the CRPSS will be conducted shall be instrumented with strain gauges on both Panel I and the local sub-structure. The location of these gauges has yet to be finalised, but will probably be a selection from the positions used on the F-111C Fuselage Strain Survey. This will facilitate additional correlation between the models.

The strains at the proposed strain gauge locations on Panel I were predicted in the previous report [2]. This prediction was made, despite the recognition that the ILM was uncorrelated, largely to demonstrate that the strains in Panel I would be low during the 60 % room temperature CPLT, emphasising the ample MOS for that test. No predictions were made for the sub-structure because only the Panel 3208 boundary conditions, and not the full ILM, were available to the authors at that time.

Although the full ILM has been available and was used for the work described in this report, it was decided not to perform a strain prediction at the time of writing this report. The timing of the CRPSS is uncertain and it is possible that ILM will be revised further prior to analysis of the data from the CRPSS. It is considered more worthwhile to await the CRPSS and compare the strain gauge results to predictions using the revision of the ILM current at the time of that analysis.

Table 17 Comparison of instabilities predicted in the sub-model and Panel I at room temperature

Mode	Eigen-value	Part number containing buckled element	Element number		Max deflection (")	
			Sub-model	Panel I	Sub-model	Panel I
CPLT I						
1	4.033	12B3802 (skin on 12B1831 longeron)	470100	2000316	1.18E+0	9.63E-4
CPLT II						
1	0.242	12B4912 (lower beam)	463527	2000308	6.19E-1	3.87E-3
2	0.291	12B4912 (transition mesh)	2009979	2000305	2.38E-1	1.22E-3
3	0.363	12B4912	463449	2000305	7.94E-1	5.58E-3
4	0.378	"	463520	2000309	9.99E-1	8.39E-3
5	0.416	"	463541	2000303	4.98E-1	3.98E-3
6	0.474	"	463443	2000304	8.51E-1	8.46E-3
7	0.539	12B4912 (transition mesh)	2009973	2000308	3.01E-1	2.30E-3
8	0.560	12B4912	463449	2000308	9.39E-1	1.10E-3
9	0.682	"	463449	2000308	7.32E-1	9.42E-3
10	0.894	"	463548	2000399	4.08E-1	4.24E-3
11	1.092	12B1910-53 (upper longeron)	462236	2000361	5.99E-1	6.21E-3
12	1.112	12B4912 (transition mesh)	2009972	2000402	8.82E-1	9.22E-3
13	1.180	12B3202	470105	2005268	1.16E+0	4.02E-3
CPLT III						
1	3.491	12B3202	470101	2000316	1.18E+0	1.16E-3
CPLT IV						
1	0.353	12B4912	463527	2000308	6.19E-1	3.88E-3
2	0.427	12B4912 (transition mesh)	2009979	2000305	2.50E-1	1.34E-3
3	0.530	12B4912	463449	2000309	8.54E-1	5.79E-3
4	0.553	"	463520	2000309	1.00E+0	8.15E-3
5	0.607	"	463541	2000303	4.85E-1	3.83E-3
6	0.695	"	463443	2000304	8.42E-1	8.37E-3
7	0.784	12B4912 (transition mesh)	2009973	2000300	3.17E-1	2.50E-3
8	0.827	12B4912	463449	2000308	9.27E-1	1.09E-3
9	1.009	"	463449	2000308	7.64E-1	9.91E-3

5. AEO acceptance

This report has been reviewed by an ADF recognised Authorised Engineering Organisation (AEO) for the design of composite airframe structure, AeroStructures®. The AEO has accepted [3] that the scope, depth and methods of testing and analysis described in this report are sufficient to meet the recommendations of Advisory Circular 20-107A [4]

Table 18 Comparison of instabilities predicted in the sub-model and Panel I at –40 °C

Mode	Eigen -value	Part number containing buckled element	Element number		Max. Defection (")	
			Sub-model	Panel I	Sub-model	Panel I
CPLT I						
1	0.783	12B1910-57 (upper longeron)	462477	2000344	6.86E-1	4.77E-5
CPLT II						
1	0.340	12B4912 (lower beam)	463527	2000308	6.12E-1	3.80E-3
2	0.401	12B4912 (transition mesh)	2009978	2000305	2.37E-1	1.06E-3
3	0.506	12B4912	463449	2000305	7.33E-1	6.16E-3
4	0.528	"	463520	2000309	9.36E-1	7.68E-3
5	0.581	"	463541	2000303	5.15E-1	4.15E-3
6	0.661	"	463443	2000304	8.05E-1	8.04E-3
7	0.724	12B1910-53 (Upper longeron)	462236	2000361	5.88E-1	5.85E-3
8	0.747	12B4912 (transition mesh)	2009973	2000308	2.93E-1	2.31E-3
9	0.783	12B4912	463449	2007264	1.00E+0	1.37E-3
10	0.784	Panel I – S1 (lower)	2007264	2007264	3.76E-1	3.76E-1
11	0.822	Panel I – S2	2007254	2007254	5.05E-1	5.05E-1
12	0.843	12B1910-57	462477	2000345	6.65E-1	4.38E-5
13	0.892	Panel I – S2	2007244	2007244	3.68E-1	3.68E-1
14	0.947	12B1910-53 (Upper longeron)	463449	2000308	7.63E-1	9.57E-3
15	0.956	Panel I - S1	2007274	20007274	5.06E-1	5.06E-1
16	1.014	Panel I – S3	2007234	2007234	5.04E-1	5.04E-1
17	1.032	Panel I – S11	2007992	2007992	3.70E-1	3.70E-1
18	1.068	Panel I – S10	2008002	2008002	4.92E-1	4.92E-1
19	1.072	Panel I – S9	2008032	2008032	3.72E-1	3.72E-1
20	1.077	Panel I – S11	2007064	2007064	4.84E-1	4.84E-1
21	1.096	"	2007074	2007074	3.74E-1	3.74E-1
22	1.102	Panel I – S12 (upper)	2007054	2007054	3.95E-1	3.95E-1
23	1.108	Panel I – S9	2008022	2008022	4.93E-1	4.93E-1
24	1.112	Panel I – S1	2007265	2007265	3.01E-1	3.01E-1
25	1.115	Panel I – S12	2007972	2007972	4.00E-1	4.00E-1
26	1.134	Panel I – S10	2008012	2008012	3.49E-1	3.49E-1
27	1.143	Panel I – S2	2007255	2007255	4.02E-1	4.02E-1
28	1.185	Panel I – S10	2007094	2007094	4.91E-1	4.91E-1
CPLT III						
1	0.785	12B1910-57	462477	2000344	6.94E-1	4.83E-5
CPLT IV						
1	0.607	12B4912	463527	2000308	6.08E-1	3.76E-3
2	0.719	"	2009979	2000305	2.36E-1	1.14E-3
3	0.778	12B1910-57	462477	2000346	6.63E-1	4.37E-5
4	0.789	"	462236	2000361	5.85E-1	5.82E-3
5	0.905	"	463449	2000305	7.71E-1	5.73E-3
6	0.947	"	463520	2000309	9.96E-1	7.71E-3

...continued

...continued

Table 18 Comparison of instabilities predicted in the sub-model and Panel I at -40 °C

Mode	Eigen -value	Part number containing buckled element	Element number		Max. Defection (")	
			Sub-model	Panel I	Sub-model	Panel I
CPLT IV						
7	0.977	Panel I - S11	2007992	2007992	3.71E-1	3.71E-3
8	0.991	Panel I - S1	2007264	2007264	3.75E-1	3.75E-3
9	1.023	Panel I - S12	2007972	2007972	4.00E-1	4.00E-1
10	1.024	Panel I - S10	2008002	2008002	4.93E-1	4.93E-1
11	1.036	12B4912	463541	2000303	5.00E-1	3.97E-3
12	1.051	Panel I - S2	2007254	2007254	5.04E-1	5.04E-1
13	1.053	Panel I - S9	2008032	2008032	3.72E-1	3.72E-1
14	1.090	"	2008022	2008022	4.94E-1	4.94E-1
15	1.092	Panel I - S10	2008012	2008012	3.50E-1	3.50E-1
16	1.117	Panel I - S11	2007064	2007064	4.79E-1	4.97E-1
17	1.137	Panel I - S11	2007074	2007074	3.75E-1	3.75E-1
18	1.146	Panel I - S2	2007244	2007244	3.68E-1	3.68E-1
19	1.148	Panel I - S12	2007054	2007054	3.95E-1	3.95E-1
20	1.190	12B1910-57	463443	2007274	7.56E-1	3.53E-2
21	1.196	Panel I - S1	2007274	2007274	5.05E-1	5.05E-1

as applied to the CRPSS. AC 20-107A is an acceptable means for composite aircraft structure to demonstrate compliance with FAR 25 [5]. Therefore it is argued that this report demonstrates that the structural aspects of the CRPSS have been satisfactorily addressed.

6. Conclusions

A demonstrator composite replacement panel, denoted Panel I, has been designed and manufactured for F-111C Panel 3208. It is planned that the Composite Replacement Panel Strain Survey (CRPSS) be conducted. Here, Panel I shall be instrumented and installed on an F-111 during a Cold Proof Load Test (CPLT). The experimental and predicted strains would be correlated, thereby validating the finite element modelling used to design Panel I. This report describes the detailed finite element analyses of Panel 3208 and Panel I that was conducted to predict that the structural integrity issues for the CRPSS have been addressed satisfactorily. It concludes that the test will not adversely impact the structural integrity of Panel I, or the F-111C aircraft onto which it is installed, during a CPLT.

Structural integrity was demonstrated by analysis supported by test. Design data for Panel I was established by test at the coupon and design detail level. The analysis was conducted using the F-111C Aircraft Internal Loads Finite Element Model (ILM) Revision 1 (current in December 2002). Although Revision 2 of the ILM was released in October 2003 the analysis was not repeated because it was judged that the results would not change significantly with the revised ILM.

The stiffness of Panel I was designed to match, as closely as possible, that of Panel 3208. Given that the panels were manufactured using different materials and configurations this was only partly achieved. Grid point displacement results for both panels were very close, indicating there was little difference predicted between the panels and their effect on the sub-structure.

An assessment of ply strains in Panel I found that a large margin-of-safety (MOS) was predicted for all CPLT loadcases. Some parts of the surrounding sub-structure was predicted to be close to yield. In these regions the effect of replacing Panel 3208 with Panel I was negligible. In some areas where the stresses were well below yield, there was some degradation predicted in the MOS. However, as the MOS in these regions were predicted to be very high, this was not expected to adversely impact their structural integrity.

Two methods were used to assess the fastener loading. One method calculated the total load that each edge of the panel could carry and the other calculated a MOS for each fastener. The former method suggested ample load carrying capacity. The latter approach predicted a negative MOS (= -0.13) for one fastener in one CPLT load case with Panel 3208 installed. The minimum MOS predicted for any fasteners when Panel I was installed was +0.25. In reality all fasteners survive the CPLT with Panel 3208 installed. This suggested that the approach used to model the panel/sub-structure joint was still excessively stiff and transferred too much load through the fasteners. Although this was a source of error that will need to be addressed when analysing the CRPSS, it also provides confidence that the ILM was conservative and that the positive MOS predicted with Panel I installed will be likewise conservative. It was therefore concluded that the fasteners attaching Panel I to the surrounding sub-structure have a sufficient MOS.

An assessment of the panel and surrounding structure stability found that all global instability modes were predicted at loads much higher than the applied loads. Although some local instabilities were predicted in the stiffener run outs, no correlation exists between these modes and the onset of global instabilities. They were therefore not expected to affect the structural integrity of the panel.

This document has been reviewed by an Australian Defence Force endorsed Authorised Engineering Organisation for the design of composite airframe structure, AeroStructures®, and accepted as addressing satisfactorily the structural requirements for the CRPSS.

7. Acknowledgements

R. Thomson is thanked for preparing Appendix A, and his substantial contribution to the analysis. The valuable comments of the reviewers; T. Cooper (AeroStructures®), J. Wang (DSTO), C. Wang (DSTO) and R. Chester (DSTO) are greatly appreciated. The patience of M. McDonald (DSTO) and S. Maan, V. Sridhar and N. Freund (AeroStructures®) in providing the ILM to the authors and assisting them to understand it are greatly appreciated.

8. References

1. Baker, A. A., Callus, P. J., Georgiadis, S., Falzon, P. J., Dutton S. E. and Leong, K. H., *An affordable methodology for replacing metallic aircraft panels with advanced composite"*, Composites A, Vol. 35, No. 5, May 2002, pp. 687-696.
2. Georgiadis, S., *Structural analysis of composite replacement panel 3208 in 60 % CPLT part of F-111C Strain Survey*, CRC-ACS-RF-511B-008, August, 2001, 33pp.
3. Cooper, T., *F-111 composite replacement panel Phase II – Engineering review*, ER-F111-51-ASM337, AeroStructures, Level 14, 222 Kingsway, South Melbourne, Victoria, Australia, 3205, 19 April 2004.
4. Federal Aviation Administration, *Composite aircraft structure*, Advisory Circular No: 20-107A, U.S. Department of Transportation, April 1984, 11 pp.
5. Federal Aviation Administration, *Federal Aviation Regulations, Part 25, Airworthiness standards: Transport category airplanes*, U.S. Department of Transportation, October 1994.
6. Per Cederqvist, et. al, *Version management with CVS for CVS 1.10.7*, Signum Support AB, 1992, 164 pp.
7. DSTO, Platform Sciences Laboratory, *Work Instruction F-111C ILM revision control*, AED-F111-W002, 24 September 2002.
8. Falzon, P. and Bitton, D., *Tooling and manufacture of a composite replacement panel*, CRC-ACS TM 02018, July 2002, 41 pp.
9. Watters, K. C., *F-111 aircraft structural integrity Sole Operator Program in AMRL – philosophy, objectives and work breakdown*, DSTO-DP-0511, 2000.
10. Lockheed Martin Corporation, FZS-12-38001, *F-111C airplane coarse grid finite element model for Royal Australian Air Force*, 2000.
11. Munoz, P., *XMTM49-3 fabric coupon tests – elastic and basic mechanical properties*, CRC-ACS-TR-511b-002, Issue 2, 14 April, 2003, 40 pp.
12. Advanced Composites Group, *Materials database MTM49-3/CF0304 fabric dated* 28 November 2003, Confidential Private Communication, 12 December 2003.

13. Sweeting, R. D. and Liu, X. L., *Cure distortion of XMTM49-3 prepreg parts*, CRC-ACS TM 01005, October, 2001, 27 pp.
14. United States of America, Department of Defense, *Composite materials handbook, Volume 2. Polymer matrix composites materials properties*, MIL-HDBK-17-2F, Vol 2 of 5, 17 June 2002.
15. Falzon, P., *The determination of the bearing properties in replacement panel edgebands*, CRC-ACS-TR-511b-003, December, 2001.
16. Thomson, R., McVilley, M. and Georgiadis, S., *Compression and shear sub-element testing for the panel replacement task*, CRC-ACS TM 02034, 2002, 38 pp.
17. Mills, T., *Review of F-111 structural materials*, DSTO-TR-1118, 2001.
18. MATWEB website - Material properties for Aluminium 2024-T851, http://www.matweb.com/index.asp?ckck=1, Last accessed 15/1/03.
19. General Dynamics, *F-111 design allowables*, FZS-12-141, 1 August 1966, 163 pp.
20. Thomson, R. *Compression testing and validation of a "quasi" full-scale curved panel for the panel replacement task*, CRC-ACS TM 02008, March, 2002, 33 pp.

Appendix A Sub-modelling approach for structures subjected to combined mechanical and thermal loading

A.1. Introduction

This Appendix describes the validation of a sub-modelling technique to analyse a structure where both mechanical and thermal loads are present.

A.2. Finite Element Models

A.2.1 Global Model

A model of a cylinder, shown in Figure 55, was created to simplify the fuselage structure of the F-111. The aluminium cylinder was 200 mm in length, 100 mm in diameter and had a thickness of 3 mm. The properties used are presented in Table 19. No frames or longerons were included.

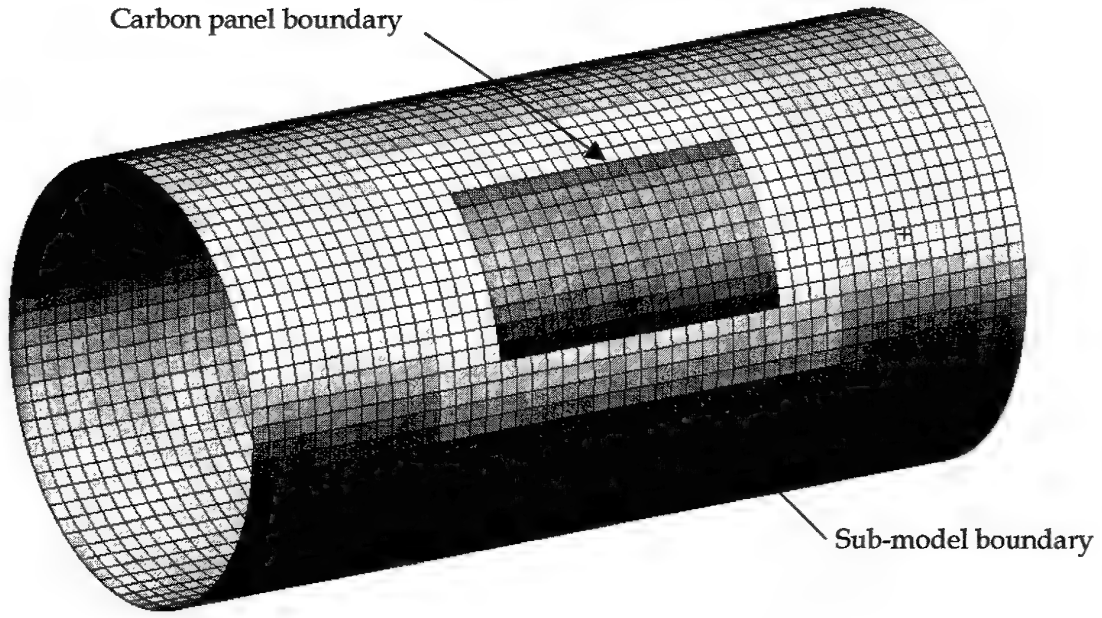

Figure 55 Global model of cylinder showing sub-model and carbon panel

Table 19 Properties used in the analysis

	Aluminium	Carbon Composite
Elastic Modulus (GPa)	72	48
Poisson's Ratio	0.3	0.3
Coefficient of Thermal Expansion ($°C^{-1}$)	23.0×10^{-6}	3.0×10^{-6}

A.2.2 Sub-Model

The sub-model, as shown in Figure 55, consisted of a curved rectangular region with the dimensions of 104 x 66 mm. Within this region was a carbon fibre reinforced composite panel with dimensions 72 x 39 mm. The properties of the carbon composite panel are listed in Table 19.

A.2.3 Global Model Loading and Boundary Conditions

A complex loading condition, representative of one of the F-111 CPLT's, was applied to the cylinder. The mechanical loading and boundary conditions were applied though rigid elements (RBE2) from a point at the centre of each end of the cylinder, as shown in Figure 56. This approach allowed the cylinder to expand or contract both longitudinally and radially, and also kept the two ends planar and parallel.

Loading applied to the cylinder was 50 kN compression, 1.0×10^{-6} N.mm torque and a temperature differential of –60 °C, which produced stresses in the cylinder in the order of 100 MPa.

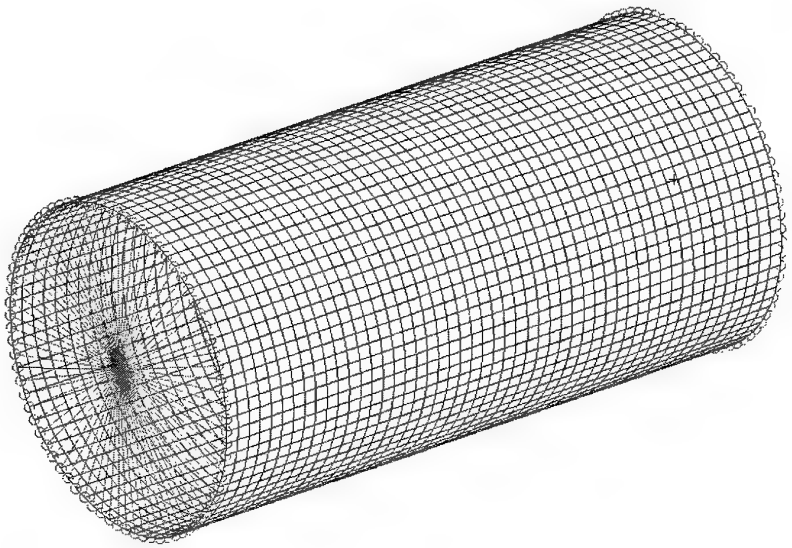

Figure 56 Global model of cylinder showing rigid bars elements, loads and boundary conditions

A.2.4 Local Model Loading and Boundary Conditions

The results of the global analysis were used to load the sub-model. In this work the sub-model did not have a refined mesh. This is in contrast to the approach described in the body of this report, however this refined mesh is not expected to influence the results.

A vector displacement field was created in MSC.Patran that was then applied to the outer two rows of nodes around the perimeter of the sub-model, as shown in Figure 57. The displacements were applied to the outer two rows to ensure that any bending was transferred to the sub-model as the vector displacement field contained only nodal translations, not rotations. It was also necessary to apply the thermal load to the sub-model, as this was an internal load not fully accounted for by the displacement field. Refer to Section A.5 for more information on the creation and application of the displacement field.

A.3. Results and Discussion

A.3.1 Global Model Analysis

The results from the global analysis of the cylinder are presented in Figure 58 to Figure 61 for the individual and combined load cases. The peak Von Mises stress for each load case, and the comparative value for an all aluminium cylinder, are presented in Table 20. It is clear that the presence of the carbon composite panel strongly influenced the stresses, and this is due to the mismatch in both stiffness and CTE. The stiffness mismatch increased the stresses by less than 10 MPa, while the CTE mismatch generated stresses of 73 MPa.

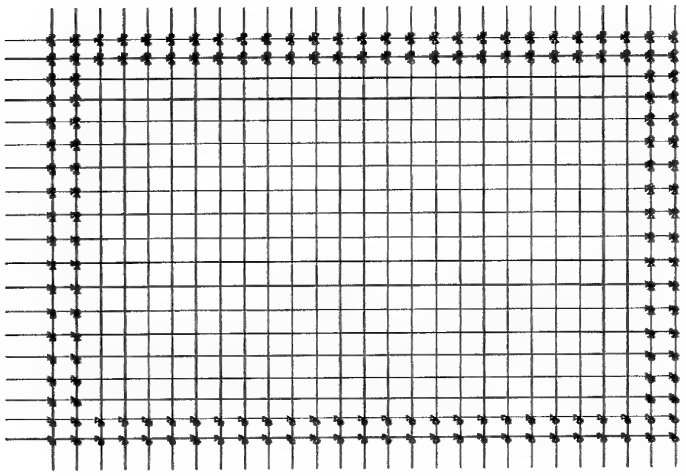

Figure 57 Local model showing applied displacement field

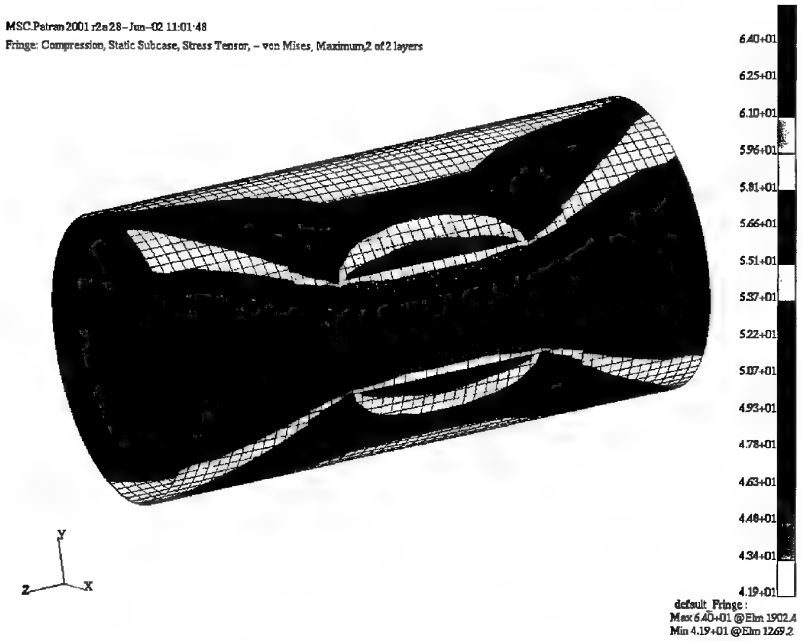

Figure 58 Von Mises stress for compression loading only

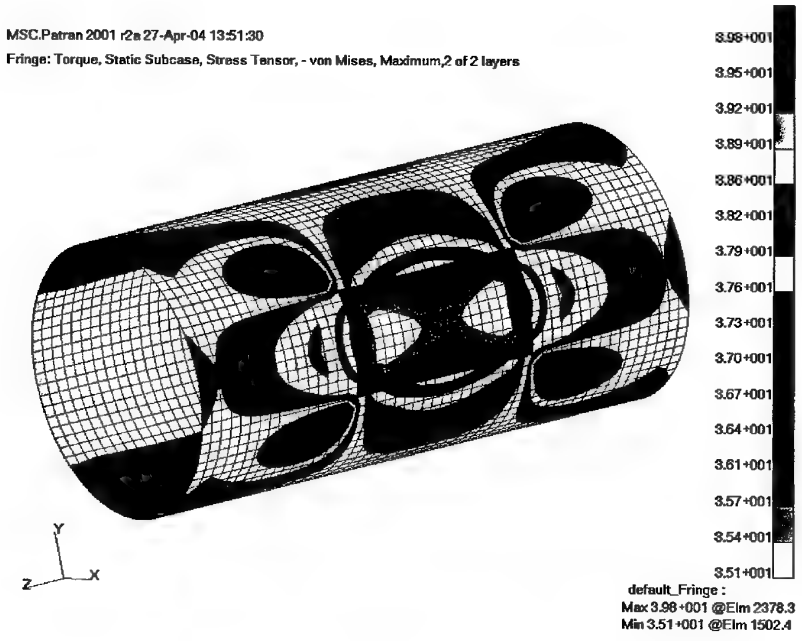

Figure 59 Von Mises stress for torsion loading only

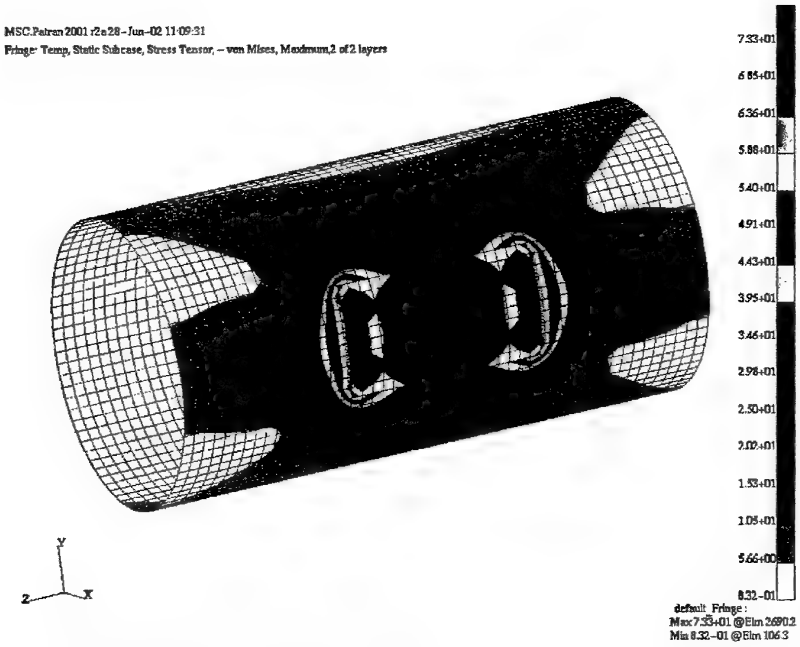

Figure 60 Von Mises stress for thermal loading only

Figure 61 Von Mises stress for combined loading

Table 20 Comparison of peak Von Mises stress in the cylinder for aluminium and composite panels

Load Case	Peak Von Mises Stress (MPa)	
	Aluminium Panel	Carbon Composite Panel
Compression Loading	53.1	64.0
Torsion Loading	38.1	39.8
Thermal Loading	0.0	73.3
Combined Loading	65.3	129.0

A.3.2 Sub-Model Analysis

Comparisons between the global cylinder model and the sub-model are presented in Figure 62 to Figure 65. In all cases the results were identical, validating the sub-modelling approach in the presence of combined mechanical and thermal loading.

A.4. Conclusions

A sub-modelling approach to analyse situations where both mechanical and thermal loads are applied has been validated. The basic steps are to:

- perform the analysis on the global model including all mechanical and thermal loads. This model must include the carbon composite panel,
- generate a displacement field from these results,
- apply the displacement field around the boundary of the sub-model (apply to two rows of nodes). The more detailed sub-model includes the carbon composite panel and the surrounding structure,
- apply the thermal load to the sub-model,
- run the sub-model analysis.

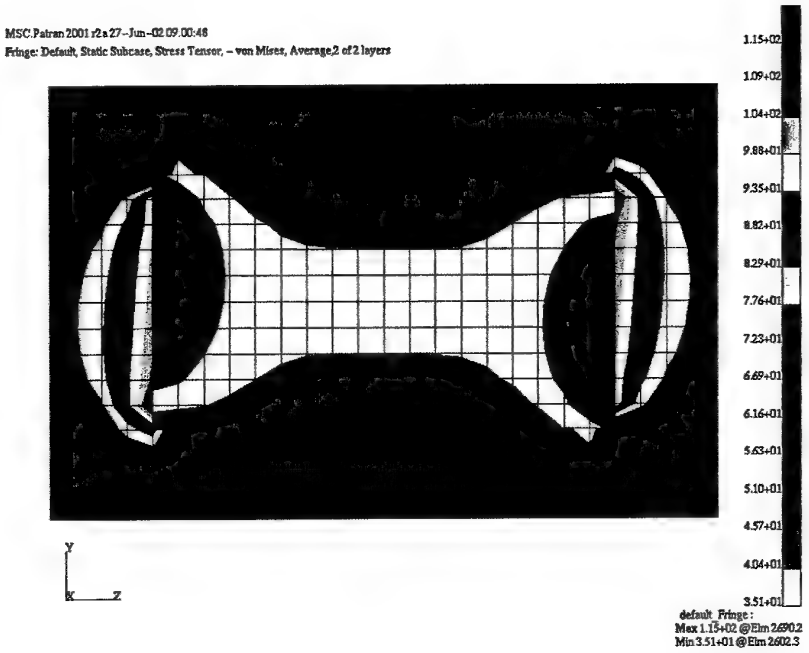

(a)

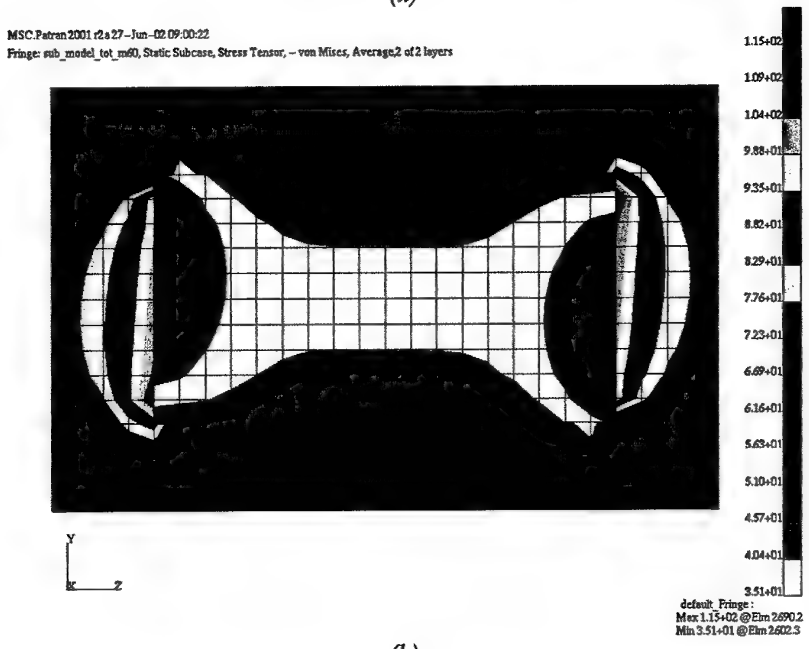

(b)

Figure 62 Von Mises stress for combined loading from (a) global model and (b) sub-model

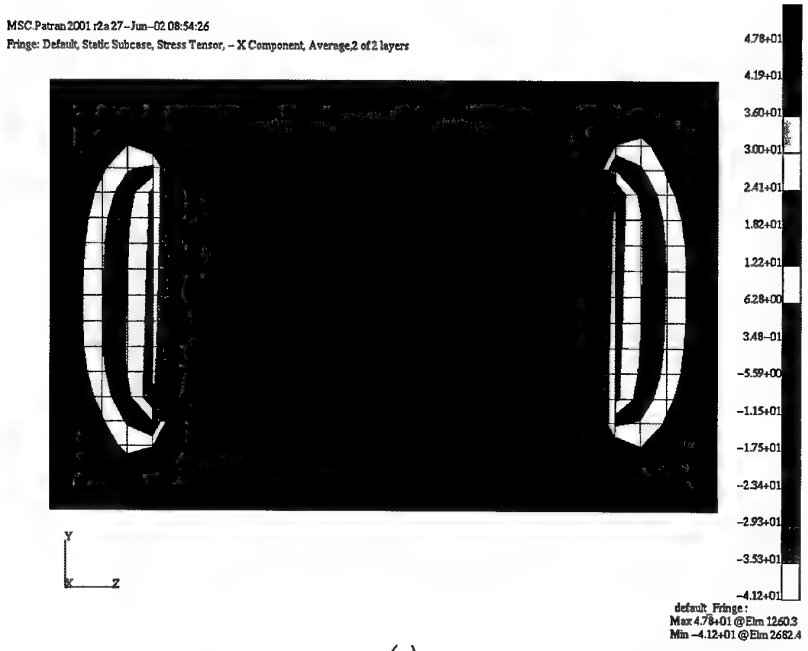

(a)

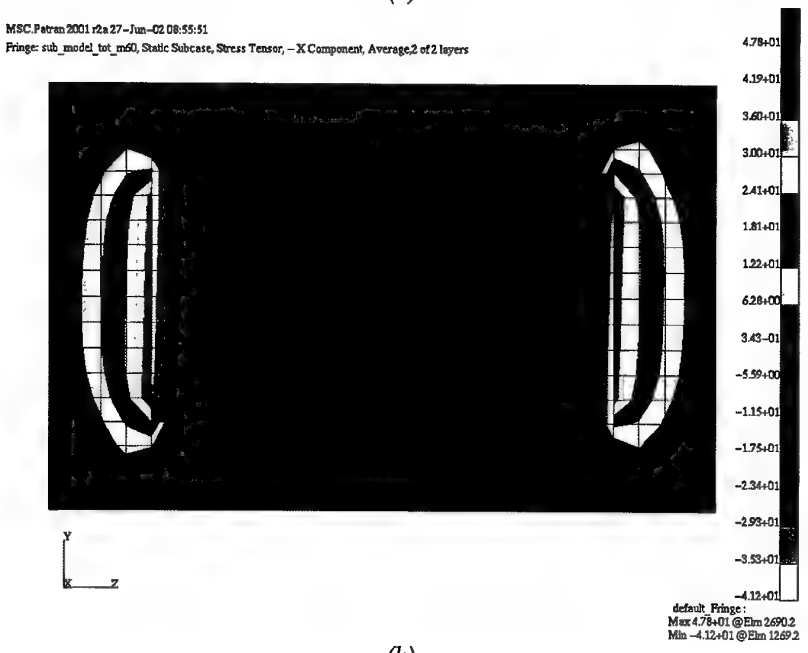

(b)

Figure 63 Longitudinal stress for combined loading from (a) global model and (b) sub-model

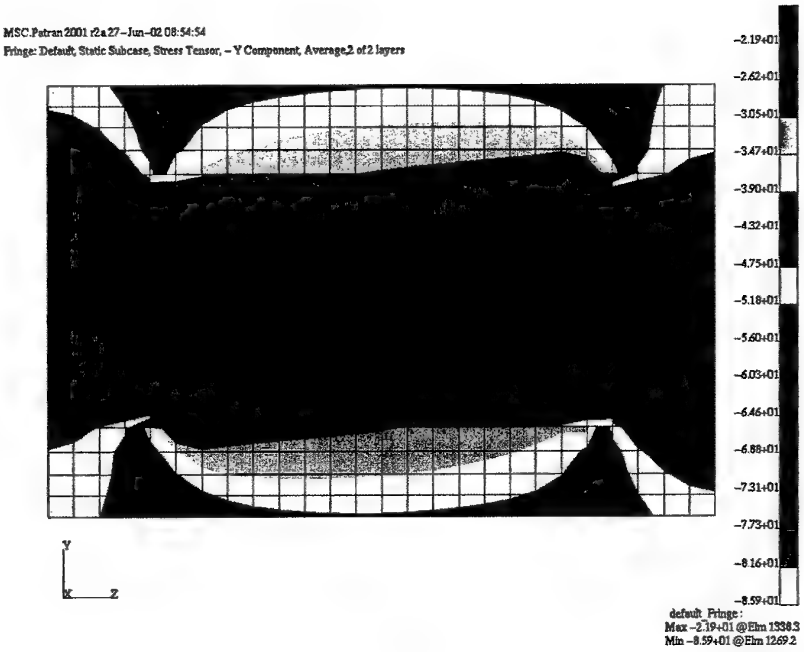

(a)

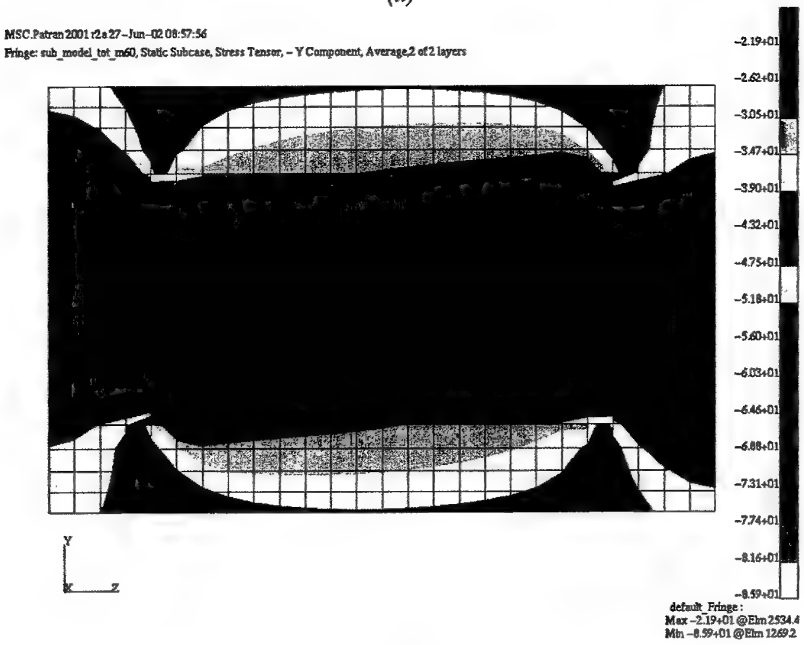

(b)

Figure 64 Hoop stress for combined loading from (a) global model and (b) sub-model

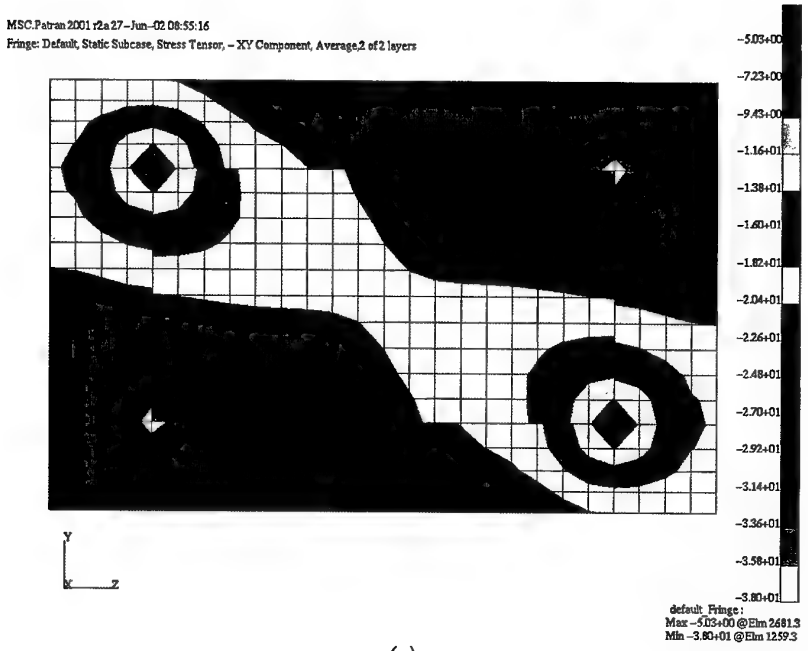

(a)

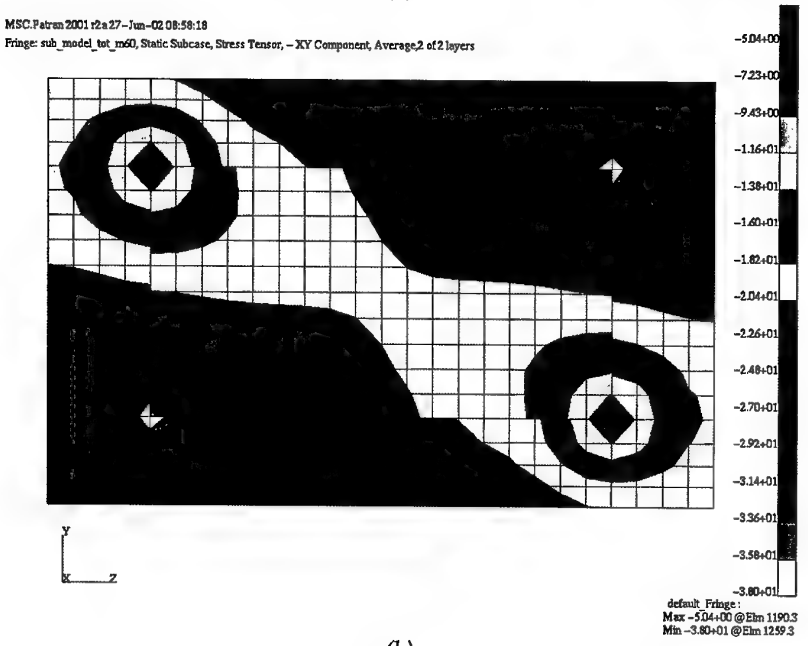

(b)

Figure 65 Shear stress for combined loading from (a) global model and (b) sub-model

A.5. Annex A to Appendix A: Sub-Modelling Procedure in MSC.PATRAN

In a global-local analysis, it may be desired to take the deformation obtained from the global model and apply it to the local model as an enforced displacement. This may be accomplished by the following procedure.

1 Run global model and import deformation results.

2 If the local model is in the same database, continue with step (3); if not, the global FEM & results MUST be imported into the local model database. The local model ids must not be the same as the global model ids.

3 Place the global & local model into two separate groups.

4 After posting only the global model group, select Results:Create:Marker:Vector and select the deformation result.

5 Once the marker plot appears in the viewport, go to Fields:Spatial:Fem & select Continuous:Vector. Since this field will be used to define the translation vector for the local model displacement loads and boundary conditions, it has to be a vector FEM field.

6 The name of the global model group should now be selectable because a valid vector plot is displayed on this group. If you had gone directly into the Fields form without generating a vector plot, no groups would appear in the listbox and you would not be able to create the field. Select the group and click Apply. This should create the field.

7 Post only the local model and go into Load/BCs:Create:Displacement. The name of the Spatial Field created in (6) should appear in the listbox of the Input Data form. Click in the translation databox and then select the field name.

8 Select the application region and then click Apply--this will create the LBC set defining the enforced displacement and a marker plot showing the 3 components of the displacement BC will appear in the viewport.

Appendix B Sub-model Boundary Nodes

Table 21 shows the identification numbers and locations of the sub-model boundary in the F-111 ILM global coordinate system of nodes. For all nodes GCID = ACID = 0. Displacements and rotations generated with the ILM were applied to these nodes in order to transfer load into the various sub-models. In total, 371 nodes were located on the sub-model boundary.

Table 21 Location of the boundary nodes for the sub-model

Entity ID	X Location	Y Location	Z Location
375218	487.230988	-33.771801	160.207993
375219	490.701996	-33.742802	160.018005
375223	487.164001	-33.859600	159.212997
375226	487.102997	-33.941200	158.287994
375233	487.036987	-34.028500	157.298996
375312	486.739990	-33.642700	152.912994
375315	486.864014	-33.478001	154.778000
375347	487.221008	-33.004799	160.141006
375349	487.153992	-33.092602	159.145996
375351	487.092987	-33.174198	158.220993
375353	487.027008	-33.261501	157.231995
455308	496.000000	-33.685101	159.889008
455315	496.600006	-33.666500	159.889008
455322	498.600006	-33.603001	159.889008
455330	495.398010	-33.692902	159.889008
455337	493.398010	-33.719002	159.889008
455428	496.000000	-38.176800	162.440002
455432	496.600006	-38.176800	162.440002
455437	495.398010	-38.176800	162.440002
455442	496.000000	-37.815102	162.014008
455447	496.600006	-37.815102	162.014008
455448	496.000000	-38.224602	161.667007
455455	495.398010	-38.224602	161.667007
455517	496.000000	-38.009602	164.139008
455518	495.398010	-38.009602	164.139008
455520	496.600006	-38.009602	164.139008
455522	496.000000	-38.626900	164.197006
455529	494.750000	-38.626900	164.197006
455539	497.643005	-38.464500	164.181000
455806	495.997009	-58.188301	186.498001
455808	497.247009	-56.854500	186.421005
455809	497.247009	-57.983002	186.488007
455812	494.750000	-58.387402	186.492004
455829	496.000000	-61.939301	189.949005
455833	497.250000	-61.939301	189.990005
455839	494.750000	-61.939301	189.949005
455850	495.997986	-61.780399	188.115005
455853	495.398010	-61.777500	188.113007
455859	496.597992	-61.783401	188.119003
456040	496.001007	-59.359001	187.272003
456042	496.808990	-59.359402	187.272003

Entity ID	X Location	Y Location	Z Location
456044	495.191010	-59.359501	187.272003
456237	495.375000	-38.626801	164.197006
456247	496.821014	-38.545700	164.188004
456329	531.679016	-59.664902	190.729004
456333	532.580017	-59.664902	190.737000
456348	530.778015	-59.664902	190.723007
456482	531.679016	-34.524700	164.311005
456486	530.429016	-34.772400	164.345001
456510	531.679016	-56.612202	186.641006
456513	530.429016	-56.611801	186.602005
456542	532.929016	-34.255600	164.281006
456557	532.929016	-56.610401	186.679001
457683	552.393005	-67.389900	190.145004
457690	552.393005	-68.943398	189.975006
457697	552.393005	-68.906197	188.235001
457712	496.000000	-61.939301	190.330002
457742	529.239014	-34.990200	164.371002
457756	529.239014	-56.610001	186.570007
457801	528.239014	-35.160000	164.391006
457816	528.239014	-56.609001	186.548004
457858	498.700012	-56.854500	186.425003
457891	498.699005	-38.360100	164.171005
458116	499.699005	-56.846100	186.425003
458117	503.199005	-56.817600	186.432007
458118	504.200012	-56.809700	186.434006
458119	506.239014	-56.791500	186.438004
458120	507.239014	-56.784500	186.440002
458121	509.903015	-56.762600	186.444000
458122	510.898010	-56.305000	186.423004
458123	511.854004	-56.322201	186.429001
458124	513.604004	-56.352600	186.436005
458125	517.098022	-56.414200	186.447006
458126	518.098022	-56.431900	186.451004
458127	520.650024	-56.478001	186.462006
458128	521.650024	-56.493500	186.468002
458129	524.348022	-56.540100	186.490005
458130	525.348022	-56.557800	186.503006
458341	525.348022	-35.597500	164.382004
458342	524.354004	-35.730301	164.380005
458343	521.648010	-36.049900	164.360001
458344	520.648010	-36.156300	164.354004

...continued

Table 21 (...continued) Location of the boundary nodes for the sub-model

Entity ID	X Location	Y Location	Z Location
458345	518.098022	-36.415600	164.332001
458346	517.098022	-36.514900	164.324005
458347	513.606018	-36.861000	164.294006
458348	511.855011	-37.037201	164.279007
458349	510.901001	-37.133301	164.272003
458350	509.898010	-37.234200	164.263000
458351	507.239014	-37.501400	164.242004
458352	506.239014	-37.601700	164.233002
458353	504.200012	-37.806900	164.216003
458354	503.200012	-37.907600	164.207001
458355	499.699005	-38.259102	164.184006
458804	534.179016	-33.873001	165.014008
458816	534.179016	-56.615200	186.714005
458840	552.179016	-50.029400	188.468002
458841	551.179016	-50.605400	188.307007
458842	547.679016	-51.846100	187.964005
458843	546.679016	-52.203800	187.869003
458844	543.179016	-53.437000	187.533005
458845	542.179016	-53.789200	187.434006
458846	539.179016	-54.845100	187.136002
458847	538.177002	-55.196602	187.044006
458848	535.179016	-56.257900	186.792007
458852	552.179016	-54.375000	186.557007
458869	552.179016	-57.226200	184.153000
458881	552.179016	-58.404400	182.677002
458888	552.179016	-58.875000	181.953003
458905	552.179016	-59.393700	181.020004
458912	552.179016	-59.948002	179.779007
458924	552.179016	-60.397301	178.429001
458936	552.179016	-60.820801	176.257004
458948	552.179016	-60.916500	174.597000
458960	552.179016	-60.750702	172.360001
458972	552.179016	-59.407902	167.186005
458989	552.179016	-58.335701	164.858002
459001	552.179016	-56.636002	162.195007
459013	552.177002	-53.443901	158.858002
459025	552.179016	-49.860100	156.539001
459037	552.179016	-45.780800	155.089005
459049	552.179016	-41.072300	154.641006
459061	552.179016	-38.554100	155.003006
459073	552.179016	-36.186600	155.800003
459085	552.179016	-30.878000	159.957001
459097	552.177002	-29.951700	161.287003
459109	552.179016	-28.895500	163.326004
459113	535.179016	-33.614601	165.085007
459114	538.179016	-32.775700	165.237000
459115	539.181030	-32.471100	165.296005
459116	542.179016	-31.508801	165.442001
459241	552.192017	-47.862900	155.695007
459253	552.190002	-43.543201	154.722000
459268	552.192017	-51.717400	157.598007
459282	552.179016	-60.231800	169.735001
459287	552.179016	-54.951302	160.238007
459302	552.179016	-32.466000	158.242004

Entity ID	X Location	Y Location	Z Location
459494	503.196014	-56.752102	187.630005
459495	504.196014	-56.745399	187.632004
459546	506.237000	-56.730499	187.636002
459547	507.237000	-56.725700	187.638000
459550	509.903015	-56.710800	187.643005
459551	510.898010	-56.247601	187.623001
459632	517.096008	-56.379700	187.647003
459635	518.096008	-56.402100	187.651001
459636	520.643005	-56.462200	187.662003
459639	521.643005	-56.484200	187.669006
459640	524.335022	-56.550499	187.690002
459643	525.335022	-56.577301	187.703003
459772	552.393005	-59.503300	182.302002
459873	534.156006	-56.712799	187.457001
459876	535.158997	-56.364700	187.533005
459895	538.153015	-55.319401	187.783005
459898	539.156006	-54.975300	187.876007
459903	542.158020	-53.936100	188.169006
459904	543.161011	-53.591400	188.268005
459952	499.696991	-56.807301	187.104004
459980	498.699005	-56.828899	186.863007
460018	528.226013	-56.637901	187.227005
460039	529.229004	-56.633400	187.009003
460047	513.601013	-56.306301	187.595001
460066	511.851013	-56.269100	187.628006
460493	546.674011	-52.382500	188.597000
460494	547.676025	-52.032700	188.692001
460496	552.174011	-50.214199	189.195007
460497	551.187012	-50.822399	189.024002
460629	510.782013	-35.946201	164.143005
460632	509.781006	-36.047001	164.134003
460633	507.121002	-36.313900	164.115005
460636	506.121002	-36.414200	164.110001
460637	504.079987	-36.619301	164.093002
460640	503.082001	-36.719700	164.087006
460740	525.192017	-34.416100	164.244003
460741	524.197021	-34.548599	164.242004
460742	521.523010	-34.864601	164.223007
460743	520.523010	-34.970901	164.216003
460744	517.981995	-35.229301	164.195007
460745	516.981995	-35.328400	164.188004
460848	533.999023	-33.150299	164.923004
460849	534.999023	-32.883499	165.067001
460850	537.968018	-32.061901	165.143005
460851	538.968018	-31.757900	165.201004
460852	541.947021	-30.803200	165.339005
460962	498.656006	-37.924301	164.128006
460978	499.631012	-37.585701	164.117004
460995	513.492004	-35.713902	164.166000
461010	511.734985	-35.850300	164.149002
461033	528.129028	-34.493900	164.309006
461047	529.163025	-34.560200	164.317001
461244	544.929016	-52.820801	187.703003
461293	549.429016	-51.225601	188.134003

...continued

Table 21 (...continued) Location of the boundary nodes for the sub-model

Entity ID	X Location	Y Location	Z Location
461312	523.000000	-56.516800	186.479004
461327	523.000000	-35.890202	164.371002
461368	515.351013	-56.383400	186.442001
461383	515.351013	-36.687401	164.309006
461426	508.569000	-56.773602	186.442001
461441	508.569000	-37.368000	164.253006
461489	501.450012	-56.832100	186.429001
461501	501.449005	-38.083401	164.197006
461560	526.794006	-56.583500	186.524002
461575	526.794006	-35.389000	164.388000
461731	552.179016	-52.390400	187.632004
461738	552.179016	-55.878300	185.447006
462059	552.179016	-59.999500	179.645004
462275	552.393005	-68.492203	180.496002
462277	552.393005	-68.408600	179.645004
462279	552.393005	-68.311897	178.845001
462280	552.393005	-67.097702	179.645004
462282	552.393005	-61.363400	181.645004
462284	552.393005	-61.363400	179.645004
462286	552.393005	-62.363400	181.645004
462289	552.393005	-62.149601	179.645004
462291	552.393005	-63.770500	179.645004
462293	552.393005	-65.391602	179.645004
462404	552.393005	-60.433300	180.973007
463620	550.866028	-42.090000	147.492004
463623	550.793030	-42.090000	146.457001
463626	550.718018	-42.089600	145.020004
463704	550.866028	-41.610100	147.492004
463719	550.866028	-42.750000	147.492004
463761	550.703979	-43.098999	145.248993
463792	550.718018	-40.989601	144.813004
463987	552.054016	-30.296101	159.501007
464100	552.179016	-31.283800	157.636002
464146	552.179016	-30.476999	157.565002
464187	552.179016	-27.372200	157.292999
464227	552.179016	-26.565500	157.223007
464275	552.182007	-26.101400	157.891006
465231	552.393005	-68.816002	185.656006
465249	552.393005	-68.693398	183.251007
465400	552.400024	-67.780296	175.753006
465401	552.405029	-67.318001	173.610001
465402	552.406006	-67.144096	172.889008
465403	552.408020	-66.895203	171.921005
465404	552.411011	-66.346199	169.998001
465405	552.419006	-65.245796	166.772003
465406	552.440002	-63.886398	163.546997
465407	552.437988	-62.697498	161.186005
465408	552.448975	-61.356998	158.901001
465409	552.434021	-60.088001	157.020004
465410	552.450012	-58.698700	155.216995
465411	552.450012	-57.259998	153.580002
465428	551.228027	-57.340900	153.623993
465429	551.213013	-55.419300	151.753998
465430	551.195984	-53.007198	149.811996

Entity ID	X Location	Y Location	Z Location
465431	551.182007	-50.559700	148.225006
465432	551.172974	-48.505199	147.145996
465433	551.158020	-45.573502	145.951996
465989	531.679016	-18.702200	160.701004
466111	531.679016	-18.344900	160.414001
466112	533.028015	-18.344900	160.414001
466151	531.679016	-28.735300	162.263000
466155	532.848022	-28.293100	162.248001
466159	531.679016	-27.537600	162.237000
466180	532.929016	-18.702200	160.701004
466403	486.750000	-34.409500	152.979004
466404	486.872009	-34.244900	154.845001
466449	486.678009	-34.494900	151.908005
466454	486.608002	-34.566101	150.835007
466459	486.536011	-34.568100	149.761002
466464	486.466003	-34.570000	148.690002
466470	486.463013	-32.989700	148.664001
466473	486.751007	-33.610100	152.981003
466569	550.718018	-30.926600	148.884003
466575	550.718018	-32.287800	148.869003
466581	550.718018	-32.284901	147.647003
466587	550.718018	-32.284901	146.136002
466593	550.736023	-32.284302	144.261993
466599	550.718018	-30.525101	144.457001
466686	501.587006	-61.657200	190.102005
466708	502.838013	-61.576500	190.132004
466731	503.334015	-61.544300	190.143997
466754	504.346008	-61.477200	190.169006
466776	505.596008	-61.393200	190.199997
466798	506.358002	-61.341400	190.218994
466819	507.355011	-61.272400	190.244995
466842	510.023010	-61.083900	190.313995
466864	511.026001	-61.011501	190.339996
466887	511.980011	-60.941601	190.365005
466909	513.726013	-60.812000	190.412003
466931	515.481018	-60.679600	190.460007
466954	517.239014	-60.544601	190.509995
466976	518.239014	-60.466900	190.537994
466999	520.801025	-60.265301	190.598999
467021	521.801025	-60.185101	190.613007
467044	524.518005	-59.964100	190.649994
467066	525.518005	-59.901402	190.662994
467089	528.348022	-59.731800	190.697998
467111	529.314026	-59.664200	190.710999
467143	498.734009	-61.842800	190.033997
467166	499.816010	-61.762100	190.059006
467268	534.252014	-59.542000	190.766998
467284	535.835999	-59.435699	190.807007
467301	537.247009	-59.320000	190.843994
467318	538.372009	-59.251400	190.871994
467334	539.369019	-59.183201	190.897003
467351	540.609009	-59.098301	190.927994
467367	541.747009	-59.010502	190.960007
467384	543.388000	-58.889500	191.007996

...continued

Table 21 (...continued) Location of the boundary nodes for the sub-model

Entity ID	X Location	Y Location	Z Location
467400	545.145020	-58.748600	191.065994
467417	546.692017	-58.597500	191.123001
467433	547.895020	-58.532200	191.164993
467450	548.950012	-58.431000	191.209000
467467	550.077026	-58.333900	191.257004
467483	551.205017	-58.238201	191.307007
467497	552.393005	-64.894600	190.473007
467498	552.393005	-62.791500	190.750000
467499	552.393005	-60.689800	191.026001
467500	552.393005	-58.186699	191.356003
467689	552.393005	-58.968300	191.253006
468462	550.716003	-33.933601	144.421005
468469	550.718018	-35.215801	144.412994
468481	550.718018	-36.377602	144.386002
468493	550.718018	-37.895100	144.451004
468503	550.718018	-39.910702	144.651001
468802	552.179016	-34.419300	156.748001
468811	543.179016	-31.173500	165.492004
468812	546.681030	-29.964800	165.677002
468813	547.682007	-29.616600	165.710007
468814	551.179016	-28.393801	165.871002
468815	552.177002	-28.049101	165.919006
468819	544.929016	-30.576000	165.576004
468820	549.429016	-29.003500	165.791000
468842	542.947998	-30.468300	165.386002
468844	550.945007	-27.698500	165.716003
468845	551.947021	-27.354401	165.757004
468854	546.440002	-29.265400	165.550003
468855	547.440002	-28.918800	165.576004
469208	529.250000	-29.601200	162.207001
469209	528.085022	-29.976200	162.117004
469210	526.697021	-30.391001	162.007004
469211	525.372009	-30.756300	161.903000
469212	524.372009	-31.012800	161.824005
469213	523.054016	-31.326200	161.720001
469214	521.669006	-31.627300	161.612000
469215	520.606018	-31.839100	161.529007
469216	518.080017	-32.279800	161.330002
469217	517.004028	-32.442200	161.246002
469218	515.317017	-32.667301	161.113007
469219	513.612000	-32.854801	160.979004
469220	511.834015	-32.977100	160.839005
469221	510.907013	-33.035801	160.766006
469222	509.933014	-33.094200	160.690002
469223	508.670013	-33.165401	160.591003
469224	507.346008	-33.234901	160.487000
469225	506.247009	-33.288700	160.399002
469226	504.174011	-33.383900	160.237000
469227	503.157013	-33.427700	160.156006
469228	501.459015	-33.496700	160.033005
469229	499.721008	-33.566601	159.888000
469260	530.437012	-29.189400	162.302002
469372	534.205017	-27.767700	162.296005
469394	535.299011	-27.347300	162.332001
469416	538.208008	-26.302000	162.434006
469438	539.210022	-25.971901	162.468002
469461	541.981018	-25.789101	160.794006
469483	543.202026	-25.494400	160.871002
469505	544.953003	-25.097900	160.981003
469527	546.601013	-24.748100	161.085007
469549	547.703003	-24.524000	161.154007
469571	549.458008	-24.180901	161.266006
469593	551.205017	-23.839500	161.376007
469615	552.205017	-23.643200	161.438004
469616	552.197021	-24.534800	160.153000
469617	552.190002	-25.262600	159.102005
469702	540.656006	-25.521000	162.520004
469703	540.663025	-26.126200	160.712006
469706	536.703003	-26.827400	162.382004
469883	550.487000	-31.497200	150.309006
470331	495.997009	-58.146400	187.218002
470341	496.026001	-61.939201	189.570007
470553	552.179016	-28.924601	157.429001

Appendix C Selected data from MIL-HDBK-17-2F

MIL-HDBK-17-2F was inspected and those carbon fibre/epoxy composites for which data in the room temperature ambient (RTA) and cold temperature ambient (CTA) condition existed were identified. The data at these conditions was extracted and is shown in Table 22 to Table 26. The following explanations apply to each of these tables:

Page The page number in MIL-HDBK-17-2F where the data for the material commences.

RTA Specimens manufactured then stored and tested in ambient laboratory air. Test temperature typically 24 °C (75 °F).

CTA Specimens manufactured and stored in ambient laboratory air. Test temperature typically -54 °C (-65 °F)

Factor CTA knockdown factor for that property = CTA property/RTA property

Table 22 Longitudinal tension data from MIL-HDBK-17-2F [13] for those carbon/epoxy composites where properties in the RTA and CTA condition are given

Material	Page	Tension, 1 axis								
		Mean Strength (ksi)			Mean strain to failure (με)			Mean Modulus (Msi)		
		RTA	CTA	Factor	RTA	CTA	Factor	RTA	CTA	Factor
T-500 12k/976 UD tape	1	295	213	0.722	13000	10700	0.823	21.9	19.0	0.868
Hitex 33 6k/E7K8 UD tape	6	313	296	0.946	15900	16100	1.013	18.2	18.5	1.016
AS4 12k/E7K8 UD tape	15	303	291	0.960	13900	13500	0.971	19.3	20.1	1.041
Celion 12k/E7K8 UD tape	24	293	281	0.959	14300	14800	1.035	20.0	19.2	0.960
AS4 12k/938 UD tape	33	314	296	0.943				22.4	19.5	0.871
T300 3k/934 plain weave	41	91	83	0.912	9780	8990	0.919	9.1	10.0	1.099
Celion 12k/938 UD tape	53	273	262	0.960	13100	12800	0.977	19.7	19.0	0.964
AS4 12k/3502 UD tape	63	258	231	0.895				19.3	19.2	0.995
Celion 3000/E7K8 plain weave	78	132	110	0.833	13700	11000	0.803	9.67	9.98	1.032
Hitex 33 6k/E7K8 plain weave fab.	93									
AS4/3501-6 (no bleed) UD tape	120	290	261	0.900				18.9	21.1	1.116
AS4 3k/3501-6 plain weave	129	124	112	0.903				9.8	10.5	1.071
AS4 6k/3502-6S 5-harness satin weave	144	114	105	0.921				9.6	9.7	1.006
T-300 15k/976 UD tape	152	211	199	0.943	10400	8600	0.827	19.6	20.8	1.061
AS4/3501-6 (no bleed) 5-harness satin weave fabric	164	134	125	0.933				9.67	10.2	1.055
AS4 6k/PR500 RTM 5-harness satin weave fabric	182									
T300 3k/EA 9396 8-harness satin weave fabric	205									
AS4 12k/997 UD tape	215	327	306	0.936	15300	14300	0.935	19.9	20.0	1.005
T650-35 12k/976 UD tape	227	231	170	0.736				22.0	20.7	0.941
T650-35 3k/976 8-harness satin weave fabric	235	99.2	82.0	0.827				10.3	10.3	1.000
T700S 12k/3900-2 plain weave fabric	243									
800HB 12k/3900-2 UD tape	249									
T650-35 3k 976 plain weave fabric	255	94.4	75.4	0.799				10.4	10.5	1.010
		Minimum		**0.722**	Minimum		**0.803**	Minimum		**0.868**
		Maximum		**0.960**	Maximum		**1.035**	Maximum		**1.116**
		Average		**0.890**	Average		**0.923**	Average		**1.006**
		Standard Dev.		**0.075**	Standard Dev.		**0.086**	Standard Dev.		**0.068**

Table 23 Transverse tension data from MIL-HDBK-17-2F [13] for those carbon/epoxy composites where properties in the RTA and CTA condition are given

Material	Page	Tension, 2 axis								
		Mean Strength (ksi)			Mean strain to failure (με)			Mean Modulus (Msi)		
		RTA	CTA	Factor	RTA	CTA	Factor	RTA	CTA	Factor
T-500 12k/976 UD tape	1	10.2	10.3	1.010	7750	7110	0.917	1.3	1.5	1.154
Hitex 33 6k/E7K8 UD tape	6									
AS4 12k/E7K8 UD tape	15									
Celion 12k/E7K8 UD tape	24									
AS4 12k/938 UD tape	33									
T300 3k/934 plain weave	41	88.0	80.0	0.909	9630	9100	0.945	9.0	9.1	1.011
Celion 12k/938 UD tape	53	9.6	9.5	0.990	7200	6700	0.931	1.35	1.35	1.000
AS4 12k/3502 UD tape	63	7.76	6.65	0.857				1.34	1.44	1.075
Celion 3000/E7K8 plain weave	78	128	113	0.883	13400	11700	0.873	9.50	9.51	1.001
Hitex 33 6k/E7K8 plain weave fab.	93	131	126	0.962	14300	15600	1.091	8.65	8.10	0.936
AS4/3501-6 (no bleed) UD tape	120									
AS4 3k/3501-6 plain weave	129									
AS4 6k/3502-6S 5-harness satin weave	144									
T-300 15k/976 UD tape	152	5.7	4.7	0.836	3900	2760	0.708	1.34	1.69	1.261
AS4/3501-6 (no bleed) 5-harness satin weave fabric	164									
AS4 6k/PR500 RTM 5-harness satin weave fabric	182									
T300 3k/EA 9396 8-harness satin weave fabric	205	100	93.6	0.936	10500	9580	0.912	9.10	9.60	1.055
AS4 12k/997 UD tape	215	11.3	12.7	1.124	8820	8700	0.986	1.36	1.53	1.125
T650-35 12k/976 UD tape	227	5.71	4.76	0.834				1.30	1.37	1.054
T650-35 3k/976 8-harness satin weave fabric	235	106	82.2	0.775				10.7	10.4	0.972
T700S 12k/3900-2 plain weave fabric	243									
800HB 12k/3900-2 UD tape	249									
T650-35 3k 976 plain weave fabric	255	93.7	74.0	0.790				10.0	9.91	0.991
		Minimum		**0.775**	Minimum		**0.708**	Minimum		**0.936**
		Maximum		**1.124**	Maximum		**1.091**	Maximum		**1.261**
		Average		**0.909**	Average		**0.920**	Average		**1.053**
		Standard Dev.		**0.101**	Standard Dev.		**0.108**	Standard Dev.		**0.091**

Table 24 Longitudinal compression data from MIL-HDBK-17-2F [13] for those carbon/epoxy composites where properties in the RTA and CTA condition are given

Material	Page	Compression, 1 axis								
		Mean Strength (ksi)			Mean strain to failure (με)			Mean Modulus (Msi)		
		RTA	CTA	Factor	RTA	CTA	Factor	RTA	CTA	Factor
T-500 12k/976 UD tape	1									
Hitex 33 6k/E7K8 UD tape	6	209	230	1.100	12600	13600	1.079	17.1	17.9	1.047
AS4 12k/E7K8 UD tape	15	245	276	1.127	11700	14400	1.231	19.0	17.6	0.926
Celion 12k/E7K8 UD tape	24	206	221	1.073	11200	9870	0.881	19.9	22.9	1.151
AS4 12k/938 UD tape	33									
T300 3k/934 plain weave	41	95	104	1.095				8.4	8.2	0.976
Celion 12k/938 UD tape	53	201	240	1.194				17.2	18.8	1.093
AS4 12k/3502 UD tape	63	204	233	1.142				18.0	18.8	1.044
Celion 3000/E7K8 plain weave	78	104	121	1.163	10900	12200	1.119	9.88	9.83	0.995
Hitex 33 6k/E7K8 plain weave fab.	93	136	155	1.140				9.11	10.10	1.109
AS4/3501-6 (no bleed) UD tape	120									
AS4 3k/3501-6 plain weave	129									
AS4 6k/3502-6S 5-harness satin weave	144	104	108	1.038				8.49	8.90	1.048
T-300 15k/976 UD tape	152	188	192	1.021	19	19	1.005	12500	14500	1.160
AS4/3501-6 (no bleed) 5-harness satin weave fabric	164									
AS4 6k/PR500 RTM 5-harness satin weave fabric	182							8.9	8.85	0.997
T300 3k/EA 9396 8-harness satin weave fabric	205									
AS4 12k/997 UD tape	215	229	233	1.017	15400	15600	1.013	17.8	18.1	1.017
T650-35 12k/976 UD tape	227									
T650-35 3k/976 8-harness satin weave fabric	235	86	93	1.074				8.8	9.38	1.065
T700S 12k/3900-2 plain weave fabric	243									
800HB 12k/3900-2 UD tape	249									
T650-35 3k 976 plain weave fabric	255	96.7	92.8	0.960				8.83	9.36	1.060
		Minimum		**0.960**	Minimum		**0.881**	Minimum		**0.926**
		Maximum		**1.194**	Maximum		**1.231**	Maximum		**1.160**
		Average		**1.088**	Average		**1.055**	Average		**1.049**
		Standard Dev.		**0.066**	Standard Dev.		**0.118**	Standard Dev.		**0.065**

Table 25 Transverse compression data from MIL-HDBK-17-2F [13] for those carbon/epoxy composites where properties in the RTA and CTA condition are given

Material	Page	Compression, 2 axis								
		Mean Strength (ksi)			Mean strain to failure (με)			Mean Modulus (Msi)		
		RTA	CTA	Factor	RTA	CTA	Factor	RTA	CTA	Factor
T-500 12k/976 UD tape	1									
Hitex 33 6k/E7K8 UD tape	6									
AS4 12k/E7K8 UD tape	15									
Celion 12k/E7K8 UD tape	24									
AS4 12k/938 UD tape	33									
T300 3k/934 plain weave	41	90	103	1.144				8.3	8.4	1.012
Celion 12k/938 UD tape	53									
AS4 12k/3502 UD tape	63	35	50	1.439				1.41	1.68	1.191
Celion 3000/E7K8 plain weave	78									
Hitex 33 6k/E7K8 plain weave fab.	93	104	128	1.231				8.9	9.49	1.064
AS4/3501-6 (no bleed) UD tape	120									
AS4 3k/3501-6 plain weave	129									
AS4 6k/3502-6S 5-harness satin weave	144									
T-300 15k/976 UD tape	152	30	35	1.170	32300	22100	0.684	1.46	1.84	1.260
AS4/3501-6 (no bleed) 5-harness satin weave fabric	164									
AS4 6k/PR500 RTM 5-harness satin weave fabric	182									
T300 3k/EA 9396 8-harness satin weave fabric	205	63.7	86.4	1.356	8260	11700	1.416	8.21	8.79	1.071
AS4 12k/997 UD tape	215	37.0	39.0	1.054	30600	24700	0.807	1.45	1.55	1.069
T650-35 12k/976 UD tape	227	33.6	39.5	1.176				1.38	1.55	1.123
T650-35 3k/976 8-harness satin weave fabric	235	90.1	97.4	1.081				8.98	9.21	1.026
T700S 12k/3900-2 plain weave fabric	243									
800HB 12k/3900-2 UD tape	249									
T650-35 3k 976 plain weave fabric	255	92.6	88.0	0.950				8.82	8.95	1.015
		Minimum		**0.950**	Minimum		**0.684**	Minimum		**1.012**
		Maximum		**1.439**	Maximum		**1.416**	Maximum		**1.260**
		Average		**1.178**	Average		**0.969**	Average		**1.092**
		Standard Dev.		**0.150**	Standard Dev.		**0.392**	Standard Dev.		**0.085**

Table 26 Shear data from MIL-HDBK-17-2F [13] for those carbon/epoxy composites where properties in the RTA and CTA condition are given

Material	Page	Short Beam Shear, 31 plane			Shear, 12 plane					
		Mean Strength (ksi)			Mean Strength (ksi)			Mean Modulus (Msi)		
		RTA	CTA	Factor	RTA	CTA	Factor	RTA	CTA	Factor
T-500 12k/976 UD tape	1									
Hitex 33 6k/E7K8 UD tape	6									
AS4 12k/E7K8 UD tape	15									
Celion 12k/E7K8 UD tape	24									
AS4 12k/938 UD tape	33									
T300 3k/934 plain weave	41	12.0	11.9	0.992						
Celion 12k/938 UD tape	53				14	16	1.143			
AS4 12k/3502 UD tape	63				14.8	15.3	1.034	0.543	0.769	1.416
Celion 3000/E7K8 plain weave	78	10.3	11.6	1.126						
Hitex 33 6k/E7K8 plain weave fab.	93	8.67	8.83	1.018						
AS4/3501-6 (no bleed) UD tape	120									
AS4 3k/3501-6 plain weave	129									
AS4 6k/3502-6S 5-harness satin weave	144				12.6	14.0	1.111	0.514	0.682	1.327
T-300 15k/976 UD tape	152	12.9	16.6	1.287	11.1	13.7	1.234	0.91	1.00	1.099
AS4/3501-6 (no bleed) 5-harness satin weave fabric	164									
AS4 6k/PR500 RTM 5-harness satin weave fabric	182				14.8	15.4	1.041	0.639	0.838	1.311
T300 3k/EA 9396 8-harness satin weave fabric	205				12.8	18.4	1.438	0.634	0.829	1.308
AS4 12k/997 UD tape	215	18.3	23.1	1.262						
T650-35 12k/976 UD tape	227				14.9	17.4	1.168	0.745	0.919	1.234
T650-35 3k/976 8-harness satin weave fabric	235				12.8	14.5	1.133	0.9	1.1	1.235
T700S 12k/3900-2 plain weave fabric	243	10.3	12.4	1.204						
800HB 12k/3900-2 UD tape	249	12.7	16.7	1.315						
T650-35 3k 976 plain weave fabric	255				15.0	17.2	1.147	0.80	1.01	1.263
		Minimum		**0.992**	Minimum		**1.034**	Minimum		**1.099**
		Maximum		**1.315**	Maximum		**1.438**	Maximum		**1.416**
		Average		**1.172**	Average		**1.161**	Average		**1.274**
		Standard Dev.		**0.130**	Standard Dev.		**0.121**	Standard Dev.		**0.092**

Appendix D Equivalent Panel Property Definitions

This appendix contains the material properties, lay-up and resulting PSHELL and MAT2 cards used to define the equivalent Panel I properties that were used in the relevant ILM analyses. These properties have been derived using the method described in Section 3.5.3.

D.1. Central Section

Materials:	XMTM49_3_fabric	XLTA245_adhesive (a)
E_{11} (psi)	8770000	725000
E_{22} (psi)	8770000	72500
ν_{12}	0.05999999	0.30000001
G_{12} (psi)	570000	279000
G_{23} (psi)	570000	279000
G_{13} (psi)	570000	279000
ρ	0.055	
α_{11} ($°F^{-1}$)	1.66E-6	1.25E-5
α_{22} ($°F^{-1}$)	1.66E-6	1.25E-5
T_{ref} (°F)	68	68
Thickness (inch)	0.0085	0.0050

Lay-up: $[45_2\ 0\ 45_3\ 0\ 45_3\ 0\ 45_2\ a\ 45\ 45_3]_T$

Notes: Lay-up produced by smearing top-hat stiffener lay-up [a 45 45_x] onto skin
- x = 3 in region of webs and flanges, x = 4 on top hat stiffener caps
The additional 45° ply on top-hat stiffener cap was ignored

```
PSHELL * 1               100000001       1.49500012E-01  200000001
*        1.00000000E+00  300000001       1.00000000E+00  0.00000000E+00
*        -7.47500062E-02 7.47500062E-02  400000001

MAT2 *   100000001       5.69484150E+06  3.35755125E+06  -1.00862645E-01
*        5.69484150E+06  -1.00862645E-01 3.39938625E+06  5.31605333E-02
*        1.70147939E-06  1.70147939E-06  -1.18195299E-14 6.80000000E+01
*        0.00000000E+00  0.00000000E+00  0.00000000E+00  0.00000000E+00
*        0

MAT2 *   200000001       5.49603500E+06  3.61554025E+06  -1.09954685E-01
*        5.49603500E+06  -1.09954685E-01 3.65738875E+06  5.31605333E-02
*        1.69241775E-06  1.69241775E-06  -1.25208918E-14 6.80000000E+01
*        0.00000000E+00  0.00000000E+00  0.00000000E+00  0.00000000E+00
*        0
```

```
MAT2 *   300000001       4.58043688E+05  -8.33000056E-03  0.00000000E+00
*        4.58043688E+05  0.00000000E+00  0.00000000E+00  5.31605333E-02
*        0.00000000E+00  0.00000000E+00  0.00000000E+00  6.80000000E+01
*        0.00000000E+00  0.00000000E+00  0.00000000E+00  0.00000000E+00
*        0

MAT2 *   400000001       1.17331641E+05  -4.63596563E+04  1.73485675E-03
*        1.17331641E+05  1.73485675E-03  -4.63433125E+04  5.31605333E-02
*        2.17434019E-02  2.17434019E-02  1.31894708E-08  6.80000000E+01
*        0.00000000E+00  0.00000000E+00  0.00000000E+00  0.00000000E+00
*        0
```

D.2. Edge Section

Materials: XMTM49_3_fabric
Properties as per section D.1.

Lay-up: $[(45\ 0)_{4s}]_T$
Notes: Lay-up is same as on Panel I

```
PSHELL * 1               100000001       1.36000007E-01  200000001
*        1.00000000E+00  300000001       1.00000000E+00  0.00000000E+00
*        -6.80000037E-02 6.80000037E-02  0

MAT2 *   100000001       7.01828950E+06  2.31149700E+06  -6.33569956E-02
*        7.01828950E+06  -6.33569956E-02 2.35339600E+06  5.49999997E-02
*        1.65999995E-06  1.65999995E-06  -1.29577101E-14 6.80000000E+01
*        0.00000000E+00  0.00000000E+00  0.00000000E+00  0.00000000E+00
*        0

MAT2 *   200000001       6.68390250E+06  2.64588375E+06  -7.52364323E-02
*        6.68390250E+06  -7.52364323E-02 2.68778275E+06  5.49999997E-02
*        1.65999995E-06  1.65999995E-06  -1.34729501E-14 6.80000000E+01
*        0.00000000E+00  0.00000000E+00  0.00000000E+00  0.00000000E+00
*        0

MAT2 *   300000001       4.67223469E+05  -5.14793862E-03  0.00000000E+00
*        4.67223469E+05  0.00000000E+00  0.00000000E+00  5.49999997E-02
*        0.00000000E+00  0.00000000E+00  0.00000000E+00  6.80000000E+01
*        0.00000000E+00  0.00000000E+00  0.00000000E+00  0.00000000E+00
*        0
```

DISTRIBUTION LIST

Structural analyses of a demonstrator composite replacement panel in a F-111C Cold Proof Load Test

Alex Harman and Paul J. Callus

AUSTRALIA

DEFENCE ORGANISATION

Task Sponsor	
DGTA	1
S&T Program	
Chief Defence Scientist	shared copy
FAS Science Policy	
AS Science Corporate Management	
Director General Science Policy Development	
Counsellor Defence Science, London	Doc Data Sheet
Counsellor Defence Science, Washington	Doc Data Sheet
Scientific Adviser to MRDC, Thailand	Doc Data Sheet
Scientific Adviser Joint	1
Navy Scientific Adviser	Doc Data Sht & Dist List
Scientific Adviser - Army	Doc Data Sht & Dist List
Air Force Scientific Adviser	1
Scientific Adviser to the DMO M&A	1
Scientific Adviser to the DMO ELL	Doc Data Sht & Dist List
Director of Trials	1
Platforms Sciences Laboratory	
Chief of Air Vehicles Division	Doc Data Sht & Dist List
Research Leader	Doc Data Sht & Dist List
Head	1
Task Manager	1
Author(s):	2
DSTO Library and Archives	
Library Fishermans Bend	Doc Data Sheet
Library Edinburgh	1
Australian Archives	1
Capability Systems Division	
Director General Maritime Development	Doc Data Sheet
Director General Aerospace Development	1
Director General Information Capability Development	Doc Data Sheet
Office of the Chief Information Officer	
Deputy CIO	Doc Data
SheetDirector General Information Policy and Plans	Doc Data SheetAS
Information Structures and Futures	Doc Data SheetAS

Information Architecture and Management — Doc Data
SheetDirector General Australian Defence Simulation Office — Doc Data Sheet

Strategy Group

Director General Military Strategy — Doc Data
SheetDirector General Preparedness — Doc Data Sheet

HQAST

SO (Science) (ASJIC) — Doc Data Sheet

Navy

SO (SCIENCE), COMAUSNAVSURFGRP, NSW — Doc Data Sht & Dist
ListDirector General Navy Capability, Performance and Plans, Navy Headquarters — Doc Data Sheet
Director General Navy Strategic Policy and Futures, Navy Headquarters — Doc Data Sheet

Air Force

SO (Science) - Headquarters Air Combat Group, RAAF Base, Williamtown NSW 2314 — Doc Data Sht & Exec Summ
ASI4 — 1

Army

ABCA National Standardisation Officer, Land Warfare Development Sector, Puckapunyal — e-mailed Doc Data Sheet
SO (Science), Deployable Joint Force Headquarters (DJFHQ) (L), Enoggera QLD — Doc Data Sheet
SO (Science) - Land Headquarters (LHQ), Victoria Barracks NSW — Doc Data & Exec Summ

Intelligence Program

DGSTA Defence Intelligence Organisation — 1
Manager, Information Centre, Defence Intelligence Organisation — 1 (PDF version)
Assistant Secretary Corporate, Defence Imagery and Geospatial Organisation — Doc Data Sheet

Defence Materiel Organisation

Head Airborne Surveillance and Control — Doc Data Sheet
Head Aerospace Systems Division — Doc Data Sheet
Head Electronic Systems Division — Doc Data Sheet
Head Maritime Systems Division — Doc Data Sheet
Head Land Systems Division — Doc Data Sheet
Head Industry Division — Doc Data Sheet
Chief Joint Logistics Command — Doc Data Sheet
Management Information Systems Division — Doc Data Sheet
Head Materiel Finance — Doc Data Sheet

Defence Libraries

Library Manager, DLS-Canberra — Doc Data Sheet

Library Manager, DLS - Sydney West	Doc Data Sheet

OTHER ORGANISATIONS

National Library of Australia	1
NASA (Canberra)	1

UNIVERSITIES AND COLLEGES

Australian Defence Force Academy	
Library	1
Head of Aerospace and Mechanical Engineering	1
Hargrave Library, Monash University	Doc Data Sheet
Librarian, Flinders University	1

OUTSIDE AUSTRALIA

INTERNATIONAL DEFENCE INFORMATION CENTRES

US Defense Technical Information Center	2
UK Defence Research Information Centre	2
Canada Defence Scientific Information Service	e-mail link to pdf
NZ Defence Information Centre	1

ABSTRACTING AND INFORMATION ORGANISATIONS

Library, Chemical Abstracts Reference Service	1
Engineering Societies Library, US	1
Materials Information, Cambridge Scientific Abstracts, US	1
Documents Librarian, The Center for Research Libraries, US	1

INFORMATION EXCHANGE AGREEMENT PARTNERS

National Aerospace Laboratory, Japan	1
National Aerospace Laboratory, Netherlands	1

SPARES	5
Total number of copies:	**36**

DEFENCE SCIENCE AND TECHNOLOGY ORGANISATION
DOCUMENT CONTROL DATA

1. PRIVACY MARKING/CAVEAT (OF DOCUMENT)

2. TITLE

Structural Analyses of a Demonstrator Composite Replacement Panel in a F-111C Cold Proof Load Test

3. SECURITY CLASSIFICATION (FOR UNCLASSIFIED REPORTS THAT ARE LIMITED RELEASE USE (L) NEXT TO DOCUMENT CLASSIFICATION)

Document	(U)
Title	(U)
Abstract	(U)

4. AUTHOR(S)

Alex B. Harman and Paul J. Callus

5. CORPORATE AUTHOR

Platforms Sciences Laboratory
506 Lorimer St
Fishermans Bend Victoria 3207 Australia

6a. DSTO NUMBER	6b. AR NUMBER	6c. TYPE OF REPORT	7. DOCUMENT DATE
DSTO-TN-0546	AR-013-071	Technical Note	March 2004

8. FILE NUMBER	9. TASK NUMBER	10. TASK SPONSOR	11. NO. OF PAGES	12. NO. OF REFERENCES
2003/3428/1	AIR 03/188	DGTA	91	20

13. URL on the World Wide Web

http://www.dsto.defence.gov.au/corporate/reports/DSTO-TN-0546.pdf

14. RELEASE AUTHORITY

Chief, Air Vehicles Division

15. SECONDARY RELEASE STATEMENT OF THIS DOCUMENT

Approved for Public Release

OVERSEAS ENQUIRIES OUTSIDE STATED LIMITATIONS SHOULD BE REFERRED THROUGH DOCUMENT EXCHANGE, PO BOX 1500, EDINBURGH, SA 5111

16. DELIBERATE ANNOUNCEMENT

No Limitations

17. CITATION IN OTHER DOCUMENTS Yes

18. DEFTEST DESCRIPTORS

F-111C aircraft, Aircraft panels, Replacement, Composite materials, Structural analysis, Airworthiness, Finite element analysis, F-111C Internal Loads Model

19. ABSTRACT

The Defence Science and Technology Organisation, in collaboration with the Cooperative Research Centre for Advanced Composite Structures, is developing the Composite Replacement Panel Technology (CRPT). The aim of this technology is to replace metallic aircraft structure with that manufactured from advanced composites, thereby reducing support costs and/or increasing capability. The CRPT is being developed through the production of a demonstrator replacement for F-111C Panel 3208, denoted Panel I. It is planned that the design methodology for Panel I (and the analysis described in this report) be validated through the Composite Replacement Panel Strain Survey (CRPSS). In the CRPSS, Panel I will be installed on an F-111C aircraft undergoing a Cold Proof Load Test (CPLT). The CPLT is a static ground test conducted at -40 °C that imparts design limit load to critical airframe structure. This report describes the analysis, based on the F-111 Internal Loads Model Revision 1 (December 2002), and tests that predict positive margins-of-safety and no buckling for Panel I, the fasteners and local sub-structure during CPLT loading. It has been accepted by an Australian Defence Force Authorised Engineering Organisation (AeroStructures®) as satisfactorily addressing the structural requirements for the CRPSS.